

**STUDY OF CURRENT TRANSPORT IN  
NONHOMOGENEOUS RECTIFYING  
METAL-SEMICONDUCTOR CONTACTS**

**A Thesis Submitted  
in Partial Fulfilment of the Requirements  
for the Degree of  
DOCTOR OF PHILOSOPHY**

**By  
G. S. VISWESWARAN**

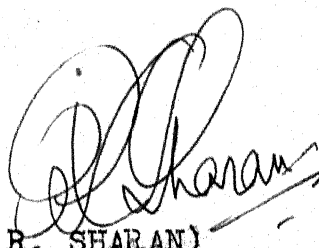
**to the  
DEPARTMENT OF ELECTRICAL ENGINEERING  
INDIAN INSTITUTE OF TECHNOLOGY, KANPUR  
JUNE, 1979**

8.6.1979

BZ.

## CERTIFICATE

Certified that this work 'Study of Current Transport in Nonhomogeneous Rectifying Metal-Semiconductor Contacts' by G. S. Visweswaran has been carried out under my supervision and that it has not been submitted elsewhere for a degree.



(R. SHARAN)

Professor

Department of Electrical Engineering,  
Indian Institute of Technology  
Kanpur

This work has been approved  
for the award of the degree of  
Doctor of Philosophy  
in accordance with the  
regulations of the Indian  
Institute of Technology Kanpur  
Dated: 21.1.1980 BZ.



EE-1979-D-VIS-STU

I.I.T. KANPUR  
CENTRAL LIBRARY  
62242,  
Acc. No. A

13 MAY 1980

## ACKNOWLEDGEMENTS

I am grateful to Dr. R. Sharan for his patient guidance, help, and cooperation, which have been largely responsible for the successful completion of this work.

I would like to thank the others working in the field of Semiconductor Devices at IIT Kanpur, for the help rendered during the course of this work.

Finally, I would like to thank Nihal Ahmad, who typed the manuscript, for his uncanny instinct in unravelling my much amended handwriting, and above all, to my friends for their cheerful forbearance in putting up with my idiosyncrasies.

G. S. Visweswaran

## CONTENTS

	Page
LIST OF FIGURES	vii
LIST OF TABLES	xii
LIST OF SYMBOLS	xiii
SYNOPSIS	xvi
CHAPTER 1 INTRODUCTION	1
1.1 Current Transport	2
1.1.1 Transport by tunneling across the barrier	2
1.1.2 Transport by emission over the barrier	2
1.1.3 Methods to distinguish between transport by tunneling and by emission	5
1.2 Barrier Height	6
1.3 The Experimental Method to Identify the Mechanism of Current Transport in a Schottky Barrier Diode	9
1.4 $T_0$ Effect	12
1.4.1 Evaluation of surface state charge	13
1.4.2 Evaluation of $T_0$	16
1.5 The Present Work	18
1.5.1 Current transport in large area Schottky barrier diodes	19
CHAPTER 2 THEORETICAL STUDIES ON THE EFFECT OF FLUCTUATION ON THE IDENTIFICATION OF THE MECHANISM OF CURRENT TRANSPORT	26
2.1 MIS Model	28
2.1.1 Identification of the fluctuating parameter	29
2.1.2 Effect of fluctuations in $\delta$	31
2.2 Effect of fluctuations in $E_0$	34
2.2.1 Calculation of $T_1$ and $T_u$	38
2.3 Summary	50

	Page
CHAPTER 3	
EXPERIMENTAL STUDY OF THE EFFECT OF FLUCTUATIONS IN $E_0$	54
3.1 Guard ring Structures	56
3.1.1 Design guidelines for an auxiliary Schottky barrier diode guard ring structure	60
3.2 Details of Fabrication and the Experimental Setup	69
3.2.1 Details of fabrication	69
3.2.2 Details of the measurement setup	71
3.3 Characterisation of a Schottky Barrier Diode Showing $T_0$ Effect	75
3.3.1 Determination of $E_0$	75
3.3.2 Determination of $\phi_{BO}$	78
3.3.3 Determination of $\phi^*$ and $D_{so}$	80
3.4 Results and Discussions	83
3.5 Summary	103
CHAPTER 4	
$T_0$ AS AN EFFECT OF TUNNELING OF METAL ELECTRONS INTO THE FORBIDDEN BANDGAP OF THE SEMICONDUCTOR	112
4.1 Generalised Approach to the Surface State Models	116
4.2 Existing Models for $T_0$ Effect	120
4.2.1 Workfunction model	120
4.2.2 Surface state model	121
4.2.3 Doped interface model	128
4.3 $T_0$ as an Effect of Tunneling of Metal Electrons into the Forbidden Bandgap of the Semiconductor	129
4.3.1 Pellegrini's calculations for Heine's Model	131
4.3.2 Results and Discussions	139
CHAPTER 5	
DETERMINATION OF DOPING DENSITY FROM THE FORWARD CURRENT-VOLTAGE CHARACTERISTICS	151
5.1 Evaluation of Doping Density from the C-V Characteristics	153
5.2 Determination of Doping Density from the Forward I-V Characteristics	157
5.3 Results and Discussion	159

	vi
	Page
CHAPTER 6 SUMMARY AND CONCLUSIONS	163
REFERENCES	168
APPENDIX A	174
APPENDIX B	179
APPENDIX C	182
APPENDIX D	190
APPENDIX E	196

## LIST OF FIGURES

Fig.		Page
1.1	A flow diagram of major developments in the study of metal-semiconductor contacts.	2
1.2	Plot of $V_T$ versus $(kT/q)$ to determine the mechanism of current transport in Schottky barriers.	11
1.3	Schematic relationship between barrier height $\phi_B$ and charge in interface states for (a) forward-bias, (b) zero bias, (c) reverse bias conditions. The amount of charge in each case is supposed to be proportional to the dark area.	14
1.4	Plot of $V_T$ versus $(kT/q)$ with $\sigma$ as a parameter for $\bar{E}_0 = 0.075$ eV. The donor density is $2.5 \times 10^{15}/\text{cm}^3$ .	23
2.1	Plot of $V_T$ versus $kT/q$ with $\sigma$ as a parameter for $\delta = 15 \text{ \AA}$ . The donor density is $N_D = 2.5 \times 10^{15}/\text{cm}^3$ .	33
2.2a	Plot of $V_T$ versus $kT/q$ with $\sigma$ as a parameter for $\bar{E}_0 = 0.070$ eV. The donor density is $2.5 \times 10^{15}/\text{cm}^3$ .	35
2.2b	Plot of $V_T$ versus $kT/q$ with $\sigma$ as a parameter for $\bar{E}_0 = 0.065$ eV. The donor density is $2.5 \times 10^{15}/\text{cm}^3$ .	36
2.3a	Plot of $(1 + (Q_{\text{sci}}/Q_{\text{fi}}))^{E_{\text{oi}}/kT}$ versus $E_{\text{oi}}$ at different temperatures for $\bar{E}_0 = 0.075$ eV and $\sigma = 0.045$ eV.	41
2.3b	Plot of $(1 + (Q_{\text{sci}}/Q_{\text{fi}}))^{E_{\text{oi}}/kT}$ versus $E_{\text{oi}}$ at different temperatures for $\bar{E}_0 = 0.075$ eV and $\sigma = 0.025$ eV.	42
2.3c	Plot of $(1 + (Q_{\text{sci}}/Q_{\text{fi}}))^{E_{\text{oi}}/kT}$ versus $E_{\text{oi}}$ at different temperatures for $\bar{E}_0 = .065$ eV and $\sigma = 0.025$ eV	43

Fig.		Page
2.4a	A plot of $u$ , $w$ and $t$ versus $\sigma$ for $\bar{E}_0 = 0.075$ eV.	46
2.4b	A plot of $u$ , $w$ and $t$ versus $\sigma$ for $\bar{E}_0 = 0.070$ eV.	47
2.4c	A plot of $u$ , $w$ and $t$ versus $\sigma$ for $\bar{E}_0 = 0.065$ eV.	48
2.5	A plot of $V_T$ versus $kT/q$ for a large area diode with $N_D = 2.5 \times 10^{15}/\text{cm}^3$ .	51
3.1	The three kinds of guard ring structures used in literature. (a) MOS guard ring (b) p-n junction guard ring (c) Auxiliary Schottky barrier guard ring.	57
3.2	A cross-sectional elevation of a Schottky barrier diode with an auxiliary Schottky barrier guard ring structure. The rectangle abcd marks the boundary of the region over which the Poisson's equation is solved.	57
3.3	Constant field profile near the edge of a Schottky barrier diode without a guard ring.	64
3.4a	Constant field profile near the edge of a Schottky barrier diode with a guard ring at a distance of 3.2 W.	66
3.4b	Constant field profile near the edge of a Schottky barrier diode with a guard ring at a distance of 2.5 W.	67
3.4c	Constant field profile near the edge of a Schottky barrier diodes with a guard ring at a distance of 1.8 W.	68
3.5	Flow diagram showing the device fabrication process.	70
3.6a	Block diagram of the I-V measurement set up.	72

Fig.		Page
3.6b	Block diagram for the C-V measurement set up.	72
3.7	A cross-sectional elevation of the arrangement used to obtain controlled temperatures from 80°K onwards.	73
3.8	ln I-V Plot at different temperatures for the diode EAU 110.	84
3.9	ln I-V plot at different temperatures for the diode EAU 120.	85
3.10	ln I-V plot at different temperatures for the diode EAU 130.	86
3.11	ln I-V plot at different temperatures for the diode EAU 410.	87
3.12	ln I-V plot at different temperatures for the diode CD 123.	88
3.13	A plot of $V_{\text{q}}$ versus $kT/q$ for different small area Au-nSi Schottky barrier diodes.	89
3.14	A plot of $V_{\text{T}}$ versus $kT/q$ for the large area diode EAU 410 and combined diode CD 123.	90
3.15	Plot of $1/T_0$ versus $V$ at different temperatures for EAU 110.	93
3.16	Plot of $1/T_0$ versus $V$ at different temperatures for EAU 120.	94
3.17	Plot of $1/T_0$ versus $V$ at different temperatures for EAU 130.	95
3.18	A plot of $\phi_{\text{BO}}(T)$ versus $E_{\text{g}}(T)$ for the three small area diodes EAU 110, EAU 120 and EAU 130.	96
3.19	A plot of $\ln I_{\text{R}}$ versus $\ln (-V+0.4)$ at room temperature for the three small area diodes EAU 110, EAU 120, EAU 130.	97



Fig.		Page
3.20	Plot of $1/T_0$ versus $\ln I$ for the three small area diodes.	98
3.21	$1/C^2$ versus $V$ plot at different temperatures for EAU 110.	104
3.22	$1/C^2$ versus $V$ plot at different temperatures for EAU 120.	105
3.23	$1/C^2$ versus $V$ plot at different temperatures for EAU 130.	106
3.24	$1/C^2$ versus $V$ plot at different temperatures for EAU 410.	107
3.25	$1/C^2$ versus $V$ plot at different temperatures for CD 123.	108
4.1	(a) Energy band diagram for a Schottky barrier with conversion of semiconductor near the surface, (b) Schematic doping profile for the energy band diagram in (a). (c) Electrical field distribution.	115
4.2	A schematic of the various barrier height models with the corresponding energy band diagram and charge profile.	119
4.3	Comparison of the electric field dependence of the barrier height in terms of $E_0/q$ according to the exponential interface state model and two parabolic interface state models, one of which matches value, slope and curvature at $\mathcal{E} = \mathcal{E}_0$ and the other which features a three point match.	126
4.4	Electron energy diagram in the semiconductor as a function of $k_{xsb}^2$ and $E_T'$ .	134
4.5	(a) Plot of $\ln W$ versus $\phi_B$ for $E_T' = 0.073$ eV. (b) Plot of $\ln W$ versus $\phi_B$ for $E_T' = 0.065$ eV.	141

Fig.		Page
4.5	(c) Plot of $\ln W$ versus $\phi_B$ for $E_T' = 0.0452$ eV. (d) Plot of $\ln W$ versus $\phi_B$ for $E_T' = 0.028$ eV.	142
4.6	Plot of $V_T$ versus $kT/q$ for different $E_T'$ .	143
5.1	Plot of $1/I_0$ versus $\ln I$ for the three diodes EAU 110, EAU 120, EAU 130.	160
A.1	Energy band diagram of a Schottky barrier (MIS) contact under (a) forward bias (b) zero bias (c) reverse bias.	175
C.1	Cross-sectional elevation of a Schottky barrier diode with an auxiliary Schottky barrier guard ring.	183
C.2	Schematic drawing of the mesh used in the numerical computation.	183
E.1	Schematic showing the dc circuit with a four-point probe method.	196
E.2	A sample of arbitrary shape used with the Van der Pauw method.	198

## LIST OF TABLES

	Page
Table 2.1    Functional relationship between $X$ , $D_{ss}$ , and $D'_{sb}$ and the oxide thickness $\delta$ .	30
Table 3.1    Normalization factors used in the solution of two dimensional Poisson's equation.	63
Table 3.2    Values of $E_o$ , $\phi^*$ , $D_{so}$ and $\phi_{BO}$ (at dif- ferent temperatures) for three sets of diodes showing $T_o$ effect.	100
Table 4.1    Table showing a correlation between $E_T'$ and $E_o$ for different values of the doping density.	148
Table 5.1    Values of doping densities calculated using different methods for three sets of diodes showing $T_o$ effect.	161

## LIST OF SYMBOLS

$A^*$	Effective Richardson constant ( $\text{Amp. cm}^{-2} \text{ } ^\circ\text{K}^{-2}$ )
$C$	Capacitance (Farad)
$D_{so}$	Density of surface states at the neutral level in the exponential surface state model ( $\text{cm}^{-2} \text{ eV}^{-1}$ )
$D_{sa}$	Density of surface states readily communicating with the metal in a MIS diode ( $\text{cm}^{-2} \text{ eV}^{-1}$ )
$D_{sb}$	Density of surface states readily communicating with the semiconductor in a MIS diode ( $\text{cm}^{-2} \text{ eV}^{-1}$ )
$E_g$	Semiconductor bandgap (eV)
$E_o$	Characteristic energy characterising the exponential distribution of surface states
$\mathcal{E}_s$	Maximum field in a Schottky barrier diode ( $\text{V.cm}^{-1}$ )
$h$	Plank's constant (Joules-sec.)
$I$	Current (Amp)
$k$	Boltzmann's constant ( $\text{eV } ^\circ\text{K}^{-1}$ )
$n$	Ideality factor
$N_A$	Acceptor impurity density ( $\text{cm}^{-3}$ )
$N_D$	Donor impurity density ( $\text{cm}^{-3}$ )
$N_C$	Effective density of states in the semiconductor conduction band ( $\text{cm}^{-3}$ )
$N_c$	Effective density of surface states due to the metal electrons tunneling close to the conduction band ( $\text{cm}^{-3}$ )

$N_v$	Effective density of surface states due to the metal electrons tunneling close to the valence band ( $\text{cm}^{-3}$ )
$N_m$	Density of electrons in the metal conduction band ( $\text{cm}^{-3}$ )
$q$	Charge of the electron (Coulomb)
$Q_{sc}$	Total space charge in the semiconductor ( $\text{cm}^{-2}$ )
$Q_{ss}$	Total surface state charge ( $\text{cm}^{-2}$ )
$Q_m$	Total charge on the metal ( $\text{cm}^{-3}$ )
$S$	Area of the diode ( $\text{cm}^2$ )
$T$	Absolute temperature ( $^{\circ}\text{K}$ )
$T_0$	A constant defining the temperature dependence of the ideality factor ( $^{\circ}\text{K}$ )
$V$	Applied bias (V)
$V_T$	Reciprocal of the slope of the $\ln I$ - $V$ plot (V)
$v_0$	The potential at the metal-semiconductor interface in the Heine-Pellegrini model (V)
$v_m$	The maximum value of the potential in the Heine-Pellegrini model (V)
$v_c$	Contact potential (V)
$v_q$	Contribution to the potential profile due to the metal-electrons tunneling with the forbidden bandgap of the semiconductor (V)
$W$	Depletion width ( $\mu\text{m}$ )
$x_m$	The distance from the metal-semiconductor junction to the point where the potential maximum occurs in the Heine-Pellegrini model ( $\text{\AA}$ )

$\delta$	Oxide thickness ( $\text{\AA}$ )
$\epsilon_m$	Permittivity of the metal (Farad/cm)
$\epsilon_i$	Permittivity of the oxide layer (Farad/cm)
$\epsilon_s$	Permittivity of the semiconductor (Farad/cm)
$q\phi_m$	Work function of metal (eV)
$q\chi_s$	Electron affinity of the semiconductor (eV)
$\phi_B$	Barrier height (V)
$\phi_{B0}$	Barrier height at zero bias (V)
$\phi^{\#}$	Neutral level at the surface measured from the bottom of the conduction band in the exponential surface state model
$q\phi_f$	Fermi level in the semiconductor measured from the bottom of the conduction band
$q\chi_{ox}$	Electron affinity of the oxide (eV)
$q\chi_s$	Electron affinity of the semiconductor (eV)
$\chi$	Mean barrier height in the insulator (eV)
$\Delta$	Potential across the oxide (V)
$\lambda_c$	Mean penetration depth for electrons tunneling close to the conduction band ( $\text{\AA}$ )
$\lambda_v$	Mean penetration depth for electrons tunneling close to the valence band ( $\text{\AA}$ )
$\lambda_{TF}$	Thomas-Fermi screening length in the metal ( $\text{\AA}$ )
$\rho$	Space charge density ( $\text{cm}^{-3}$ ).
$\phi_o$	Neutral level at the surface measured from the top of the valence band for an MIS diode.

## SYNOPSIS

### STUDY OF CURRENT TRANSPORT IN NONHOMOGENEOUS RECTIFYING METAL-SEMICONDUCTOR CONTACTS

By

G.S. VISWESWARAN

Department of Electrical Engineering  
Indian Institute of Technology, Kanpur

May 1979

The study of metal-semiconductor junctions started in 1874 with the work of Braun [1]. Although more than a century has elapsed since then, the understanding of the metal-semiconductor junction is still far from complete. Perhaps the main reason for this is the fact that the performance of semiconductor junctions is strongly dependent on processing, which in turn controls the condition of the metal semiconductor interface. For example, it is commonly found that depending upon the condition at the interface, the rectifying metal-semiconductor junctions (Schottky barrier diodes) made on low-doped silicon, GaAs etc. show either a temperature independent or a temperature dependent ideality factor. The study in the present thesis has been mainly directed towards the understanding and clarification of some of the ambiguities in those cases where the ideality factor is temperature dependent. Such ambiguities have been detected in the published literature concerning the assignment of the mechanism of current transport in some specific metal-semiconductor diodes. The clarification of these ambiguities

has been brought out in the present work by incorporating the fluctuation of geometrical and material parameters at the metal-semiconductor interface [2].

A description of the ambiguities under consideration here would become easier if we first consider the commonly used method for assignment of the mechanism of current transport in 'homogeneous' Schottky barrier diodes; the term 'homogeneous' implies that there is no fluctuation of geometrical and material parameters across the metal-semiconductor interface. The method of assignment of the mechanism of current transport for homogeneous Schottky-barrier diodes is well known and was developed by Saxena [3]. This method consists of obtaining the current voltage (I-V) characteristics in the forward region at different temperature (T), and thereby plotting  $nT$  versus T from the slope of the  $\ln I-V$  plot, where  $n$  is the ideality factor of the diode. Different mechanisms of current transport are identified by their characteristic  $nT$  versus T plot given in Fig. 1, 2 where the curves I, II and III represent the cases where the thermionic emission (TE) is the mechanism of current transport with unity ideality factor, with ideality factor greater than unity and with  $T_0$  effect respectively. Curves IV and V correspond to thermionic field emission (TFE) and field emission (FE) respectively.

This method of assignment of the mechanism of current transport has been used by many workers. Some [4] have found



that in the case of metal- (low doped) silicon diodes operating above room temperature the experimentally obtained  $nT$  is independent of temperature. Thus the assignment of transport is made to be by field emission. This however is contrary to the common experience [5,6] that Schottky barriers made on low-doped silicon and operating at temperatures higher than room temperature have thermionic emission as the mechanism of current transport. In the present work we have demonstrated that in the presence of fluctuations in geometrical and material parameters (transverse to the metal-semiconductor interface) there is a definite possibility of obtaining a temperature independent plot of  $nT$  even in some of those cases where thermionic emission is the dominant mechanism of current transport. Thus one concludes that the correspondence of field emission with temperature independent value of  $nT$  is not unambiguous. The repercussions of this conclusion are obvious - the nature of the  $nT$  versus  $T$  plot is not uniquely relatable to a specific mechanism of current transport.

The role of fluctuations mentioned above in current transport has been incorporated in the present work in an intuitive fashion [2]. We have observed that the fluctuations of  $E_0$ , which is a characteristic energy characterising the interface distribution for a diode showing  $T_0$  effect (see Levine [7]), can play a dominant role in current transport. Furthermore, we have assumed that the different areas of Schottky barriers have different  $E_0$ 's and the distribution is Gaussian such that

$$\frac{\Delta S_i}{S} = \frac{1}{\sqrt{2\pi}\sigma} \exp\left\{-\frac{(\bar{E}_0 - E_{oi})^2}{2\sigma^2}\right\} \Delta E_{oi} \quad (1)$$

where  $\Delta S_i$  is the area of a patch with  $E_0$  between  $E_{oi}$  and  $E_{oi} + \Delta E_{oi}$ ,  $\bar{E}_0$  is the mean value of the  $E_{oi}$ 's,  $\sigma$  is the standard deviation and  $S$  is the total area of the diode. Under these assumptions the expression for the total current using thermionic emission model is given by

$$I = \sum_i S \frac{1}{\sqrt{2\pi}\sigma} \exp\left\{-\frac{(\bar{E}_0 - E_{oi})^2}{2\sigma^2}\right\} A^* T^2 \exp\left(-\frac{q\phi_{Bi}}{kT}\right) \times \exp\left(\frac{qV}{kT}\right) \Delta E_{oi} \quad (2)$$

where  $\phi_{Bi}$  is the barrier height of the  $i$ th patch for an applied voltage  $V$ . Using equations (1) and (2) the I-V characteristics and hence  $(\frac{\partial \ln I}{\partial V})^{-1}$  were evaluated at different temperatures. Then using the relation,

$$\left(\frac{\partial \ln I}{\partial V}\right)^{-1} = \frac{n k T}{q} \quad (3)$$

the  $nT$  versus  $T$  plot was obtained. Depending on the values of  $\bar{E}_0$  and  $\sigma$ , it has been possible to get temperature independent  $nT$  for some temperature ranges, although the mechanism of current transport in equations (1) - (3) is only thermionic emission.

Similar calculations have been carried out for Schottky barriers with a thin oxide layer between the metal and the semiconductor. Fluctuations in the interfacial oxide thickness have been incorporated in this calculation. It has been observed

that the fluctuations in oxide thickness do not appreciably change the nature of the  $nT$  versus  $T$  plot. This and the previous calculations considering the fluctuations in  $E_0$  are the subject matter of the first and the second chapters of this thesis.

An experiment has been designed to verify the theoretical model mentioned above. For this a large number of isolated small area (homogeneous) diodes have been prepared and the  $nT$  versus  $T$  plot of each has been obtained. These show a straight-line plot with an intercept  $T_0$ , where there is a scatter in the values of  $T_0$  for different diodes. This has been true even in the case of diodes made on the same wafer. We have selected three or four diodes of different values of  $T_0$  and connected them in parallel. Then the  $nT$  versus  $T$  plot of the combination has been obtained and it has been found that over certain range of temperature  $nT$  becomes independent of  $T$ . The condition under which these observations have been made and other details of the experiment are given in Chapter III.

Having noted that the fluctuations in physical parameters could cause the ambiguities in the determination of the mechanism of current transport we have proceeded further to determine some phenomenological parameters which would correlate  $T_0$  with geometrical and material parameters of the interface. One such parameter,  $E_0$ , which is the characteristic energy describing the assumed exponential

distribution of interface states has already been introduced earlier. Regarding  $E_0$ , we note that the  $T_0$  effect is not unique to an exponentially distributed surface states as predicted by Levine [7] but to the constancy of the slope of  $\ln Q_{SG} - \phi_B$  plot at all temperatures and bias, as noted by Crowell [8]. Here  $Q_{SG}$  is the total depletion charge in the semiconductor and  $\phi_B$  is the barrier height. Crowell [8] has also noted that the potential profile of metal-P(thin)-N diodes for a certain doping profile in the P-layer is such that one can obtain a linear  $\ln Q_{SG} - \phi_B$  plot leading to  $T_0$  effect.

It is interesting to note here that a similar potential profile as in the case of M-P (thin)-N-diodes, is also obtained in the case of Heine's model [9] of a Schottky barrier. It is well known that Heine's model starts on a very different premise from Bardeen's model [10] of Schottky barrier and primarily considers that the surface-states are due to the tunneling of metal electrons into the forbidden bandgap of the semiconductor. A direct consequence of Heine's assumption is that in this case the surface state charges are not localised in space. This non-localization of space-charge makes the potential profile similar to that of M-P(thin)-N-diodes. Hence we attempted to correlate the  $T_0$  effect with the parameters of tunneling in Heine's model as developed in Pellegrini's calculations[11]. The details of this correlation are given in the fourth chapter.

In the penultimate chapter, a novel method to determine the doping density of a semiconductor wafer using the dependence of  $T_0$  on the current at which  $T_0$  is measured has been described. This method requires the measurement of only the forward I-V characteristics of a Schottky barrier diodes. A concluding discussion of the various observations made in the present work is given in the last chapter.

#### REFERENCES:

1. F. Braun, "Über die stromleitung durch Schwefelmetalle", Ann. Physik. Chem., Vol.153, p.556, 1874.
2. G.S.Visweswaran, and R. Sharan, "Current transport in large area Schottky barrier diodes", Proc. IEEE, Vol.67, No.3, Mar. 1979.
3. A.N. Saxena, "Forward current-voltage characteristics of Schottky barriers on n-type silicon", Surface Sci., Vol.13, pp. 151-171, 1969.
4. S.M. Vernon and W.A. Anderson, "Temperature effect in Schottky barrier silicon solar cells", App. Phys. Lett., Vol.26, pp. 707-709, 1975.
5. F.A. Padovani, Semiconductors and Semimetals, Vol.7A, R.K. Willardson and A.J.Beer, Eds. New York: Academic Press, 1971, pp. 75-146.
6. B. Bhaumik and R. Sharan, "Temperature effects in Schottky barrier solar cells", App. Phys., Lett., Vol.29, pp.257-259 1976.
7. J.D. Levine, "Schottky barrier anomalies and interface states", J. of App. Phys., Vol.42, pp. 3991-3999, 1971.
8. J.R. Jrowell, "The physical significance of  $T_0$  anomalies in Schottky barriers", Solid State Electron., Vol. 20, pp. 171-175, 1977.
9. V. Heine, "Theory of surface States", Phys. Rev., Vol.138, No.6A, pp. A1689-A1696, 1965.

10. J. Bardeen, "Surface states and rectification at a metal-semiconductor contact", Phys., Rev., Vol.71, pp. 717-727, 1947.
11. B. Pellegrini, "A detailed analysis of the metal-semiconductor contact", Solid State Electron., Vol.17, pp. 217-237, 1974.

## CHAPTER 1

### INTRODUCTION

The present study is aimed at the investigation of current transport in nonhomogeneous rectifying metal-semiconductor contacts. The nonhomogenities that have been considered are due to the fluctuation of geometrical and material parameters transverse to the metal-semiconductor interface.

To put this work in its proper perspective a flow-diagram of major developments in the study of metal-semiconductor contacts has been given in Fig. 1.1. It is worth noting that the first reported work [1] in this area was done in 1874 by Braun, who made point-contacts to semiconductors like copper sulphide and iron sulphide. It is generally considered, for example see [2], that the next significant step in this study was the recognition by Schottky et al. [3] of a 'potential barrier' as the cause of the asymmetry in the current-voltage characteristics. Developments from this point onwards were rather fast and various classifications regarding the order of development are possible. We have arbitrarily decided to classify these developments under two heads, (i) the 'study of current transport' and (ii) the 'study of barrier heights',

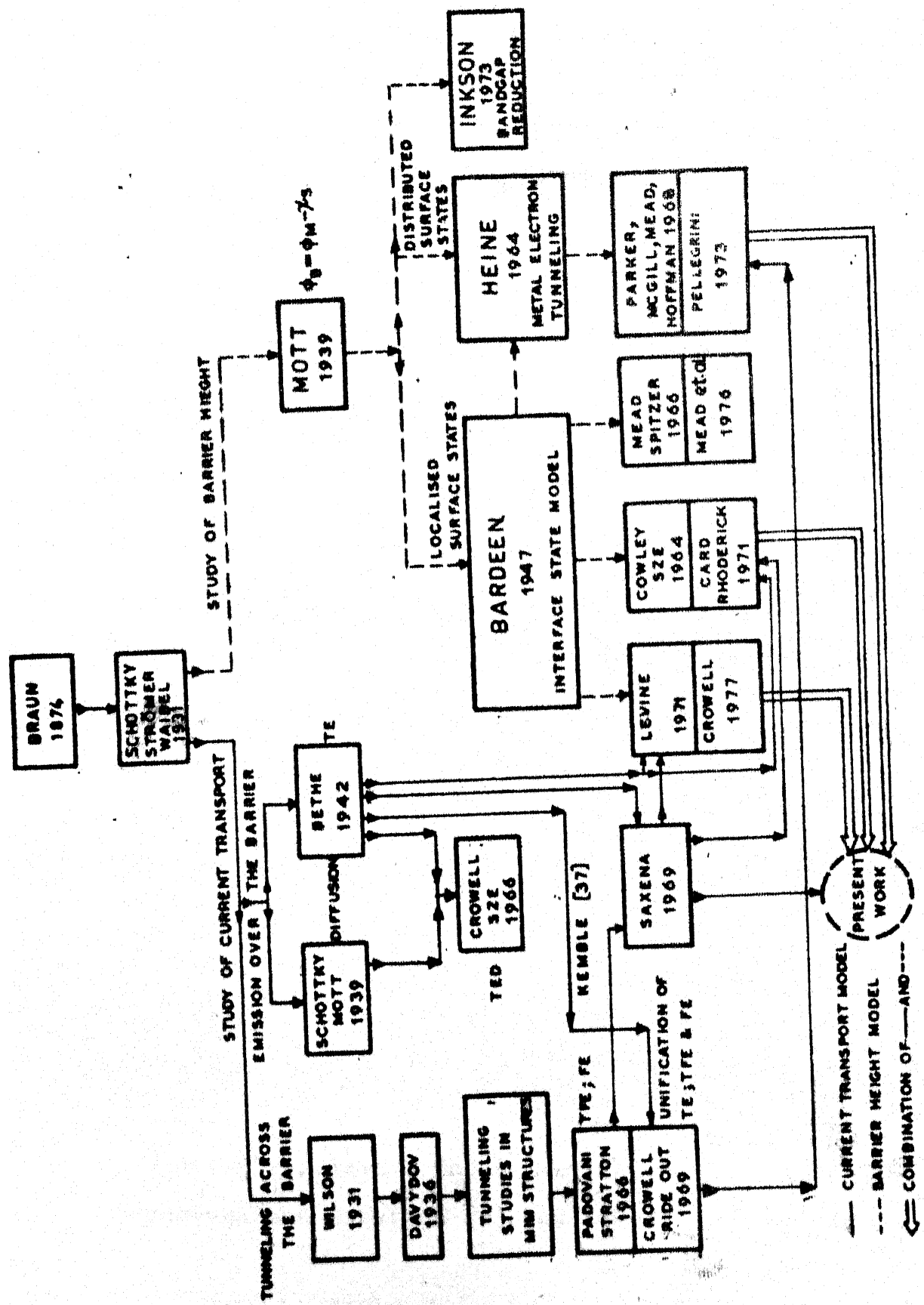


Fig. 1.1 A flow diagram of major developments in the study of metal-semiconductor contacts.



it is obvious, however, that both of these studies are highly interrelated and a conceptual separation between them can only be artificial. To rectify this situation several cross-connecting links have been shown in Fig. 1.1.

## 1.1 Current Transport

The current transport in a metal-semiconductor contact can be either (i) due to tunneling of carriers across the potential barrier or (ii) due to the transport of carriers over the barrier. The tunneling mechanism was the first one to be suggested and then was rejected as ambiguous; it was later rehabilitated as a valid mechanism in some cases, as would become clear from the discussion below.

### 1.1.1 Transport by tunneling across the barrier

Wilson [4] in 1932, tried to explain the rectifying action in terms of quantum mechanical tunneling of electrons across the barrier. However, it was shown by Davydov [5] in 1938 that for the Schottky barrier diodes made in that period, the direction of rectification was opposite to the direction of rectification predicted by the tunneling theory of Wilson. This observation of Davydov [5] led to tunneling being completely ruled out as a mode of current transport in Schottky barriers. The situation, however, changed when Padovani and Stratton [6] and later Crowell and Rideout [7]

showed that in the case of diodes made with highly doped semiconductors, the current transport is due to tunneling, thus giving rise to two additional modes of current transport, viz. Field Emission (FE), wherein the current flow is dominated by carriers tunneling close to Fermi level and Thermionic Field Emission (TFE), where the current flow is due to temperature aided tunneling, away from the Fermi-level. In Fig. 1.1, the block representing the works of Padovani and Stratton [6] and Crowell and Rideout [7], is separated from that representing Wilson's [5] work by a block representing the work done on tunneling in Metal-Insulator Metal (M-I-M) structures. Though the study in MIM structure is not explicitly related to the study of Schottky barriers, the tunneling theory used to study the Schottky barrier with highly doped semiconductor was developed in the context of MIM devices only [8,9]. Having traced the development in the current transport model for tunneling across the barrier, we move over to look into the development in the models describing the current transport by 'emission over the barrier'.

#### 1.1.2 Transport by emission over the barrier

As is shown in Fig. 1.1 there are two distinct models to explain current transport by emission over the barrier. The first model for transport of carriers over the barrier was

advanced by Schottky [10] and independently by Mott [11], when they pointed out that the current-voltage relationship can be explained assuming that the carriers passed over the barrier by the normal process of diffusion and drift. The next model of current transport was proposed by Bethe, in 1942 [12], who assumed the transport of electrons over the barrier to be by the process of thermionic emission. The models proposed by Schottky and Mott [10,11], and Bethe [12] are respectively the 'Diffusion theory' and 'Thermionic emission (TE) theory'. A generalized transport model called thermionic emission diffusion (TED) theory was developed by Crowell and Sze in 1966 [13]. A good treatment of these developments has been recently given by Rhoderick [2].

### 1.1.3 Methods to distinguish between transport by tunneling and by emission

It is obvious that an experimental method which in a fabricated Schottky barrier diode can determine whether the current transport in it is dominated by tunneling through the barrier or by emission over the barrier would be of great importance. A search for this technique in 1950's and 1960's, culminated in the experiments suggested by Saxena in 1969 [14]. These experiments of Saxena are of central importance to our work and are discussed in detail in Sec. 1.3. Here we only want to reiterate that Saxena's work provides a way to distinguish between the TE, TFE and FE mechanisms of transport.

## 1.2 Barrier Height

The first model to evaluate the barrier height was proposed by Mott in 1938 [11]. According to Mott the barrier  $\phi_B$  seen from the metal would be given by the difference between the work-function  $\phi_m$  of the metal and the electron affinity  $\chi_s$  of the semiconductor. However, the experimental measurements [15] of  $\phi_B$  brought to notice that there were metal-semiconductor systems in which Mott's conclusions were not valid; actually there were systems where the barrier height was almost independent of the work function of the metal used. This, in a way led to the work of Bardeen, Heine and Inkson as shown in Fig. 1.1.

The first model to explain the weak dependence of  $\phi_B$  on  $\phi_m$  recognised the importance of the existence of surface states on the semiconductor and was proposed by Bardeen in 1947 [16]. The Bardeen model assumes the existence of a thin insulating layer between the metal and the semiconductor and identifies a neutral level ' $\phi_o$ ' in the forbidden energy gap of the semiconductor, to characterise the surface states. It has been further demonstrated by Bardeen that in the case of large surface state densities, the semiconductor Fermi-level at the surface gets pinned to the neutral level ' $\phi_o$ '.

Two of the important extensions of Bardeen's model are the study of Metal-Insulator-Semiconductor Structure (MIS) (by Cowley and Sze [17], and by Card and Rhoderick [18]) and

the exponential surface state model (by Levine [19])). The details of these two models are given in Sections 1.4 and 2.1 respectively. The other interesting extension of Bardeen's work, shown in Fig. 1.1 is that of Mead and Spitzer [20], who experimentally evaluated the value of  $\phi_0$  for various semiconductors and enunciated their famous  $2/3 E_g$  law for the barrier height in n-type semiconductor of Group IV and Group III-V compound semiconductors. In a recent publication, Mead et al. [21], have shown that the covalent compound semiconductors do not follow the  $2/3 E_g$  law and that ' $\phi_0$ ' in these cases is directly dependent on the 'anion' electronegativity of the semiconducting material. Since we are mainly interested in Group IV semiconductors, this point would not be pursued any further.

In the Bardeen's model discussed above the surface states have been taken to be localised in space. In 1964, Heine [22] proposed a model in which the surface states are distributed in space near the metal-semiconductor interface. These surface states arise due to the tunneling of metal-electron into the forbidden bandgap of the semiconductor. Though an empirical formulation of Heine's model was used by some authors to study the field dependence of the barrier height [23], a detailed study of Heine's model was first carried out in 1973 by Pellegrini [24]. The details of Pellegrini's calculations are given in Chapter IV. The

horizontal line in Fig. 1.1, connecting Bardeen's model and Heine's model shows that both these models are derived under the same premise, that it is the presence of surface states which causes the weak dependence of  $\phi_B$  on  $\phi_m$ .

Another model to explain the weak dependence of  $\phi_B$  on  $\phi_m$  has been proposed by Inkson [25]. The basis of this model is the reduction in the bandgap of the semiconductor near the metal-semiconductor interface. The reduction in bandgap of the semiconductor at the surface arises due to the opposite effect of the image forces on the conduction and valence bands. According to Inkson, the bandgap actually disappears at the interface, so that the semiconductor behaves like a semi-metal, and the barrier height is determined by the energy level at which the top of the valence band and the bottom of the conduction band coalesce [2].

This brings us to the end of the description of the flow diagram given in Fig. 1.1 excepting the small dotted block, named the present work, which concerns itself with certain ambiguities, to be shortly described, which have been observed in metal-semiconductor junctions. These ambiguities have been discovered by us in the experimental work done by some workers [26] to distinguish between the TE, TFE or FE mode of current transport in their fabricated diodes. In order to describe these ambiguities and methods (as developed in the present work) to resolve them, it becomes

necessary to describe the nomenclature and methodology developed by Saxena to distinguish between TE, TFE and FE modes of current transport and those developed by Levine [19] and Crowell [27] to describe the ' $T_0$ ' effect. Hence, in the following two sections we present brief descriptions of these works and then elaborate on the ambiguities and methods of resolving them.

### 1.3 The Experimental Method to Identify the Mechanism of Current Transport in a Fabricated Schottky Barrier diode [14]

The method proposed by Saxena [14] is based on the following observations:

(i) While the TE theory predicts a forward I-V relationship for  $V > \frac{3kT}{q}$  of the form [12],

$$I = I_s \exp (qV/kT), \quad (1.1)$$

most of the practical diodes follow the relation,

$$I = I_s \exp (qV/nkT) \quad (1.2)$$

where 'n' is called the ideality factor. In eqn. (1.1) and eqn. (1.2)  $I_s$  represents the reverse saturation current, given by

$$I_s = SA^*T^2 \exp(-\frac{q\phi_B}{kT}) \quad (1.3)$$

(ii) In some cases the ideality factor 'n' is temperature independent whereas in some other cases it is temperature dependent. Moreover, in the latter cases it is commonly found that

$$n = \left(1 + \frac{T_0}{T}\right) \quad (1.4)$$

where  $T_0$  is independent of temperature [28],

and (iii) It was shown by Padovani and Stratton [6] that for a forward bias ( $V \geq \frac{3kT}{q}$ ), the current by both TFE and FE theories can be represented as

$$I = I_S \exp(V/V_T) \quad (1.5)$$

$$\text{where } V_T = V_{00} \coth(V_{00}/kT) \text{ for TFE} \quad (1.6)$$

$$= V_{00} \quad \text{for FE}$$

$$V_{00} = \frac{1}{2}(N_D/m^* \epsilon_S) \quad (1.7)$$

From the above observations, it is seen that the I-V relationship under forward bias can in general be written in the form,

$$I = I_S \exp(V/V_T) \quad (1.8)$$

where  $V_T$  is the inverse of the slope of the  $\ln I$ -V plot. The method suggested by Saxena [14] consists of obtaining I-V characteristics in the forward region at different temperatures (T) and plotting  $V_T$  versus T,  $V_T$  measured at a constant current. The typical nature of the resulting plot is shown in Fig. 1.2, where the curves I, II and III represent the cases where the TE is the mechanism of transport with unity ideality factor, with ideality factor greater than unity and with  $T_0$  effect respectively. Curves IV and V correspond to TFE and FE respectively.



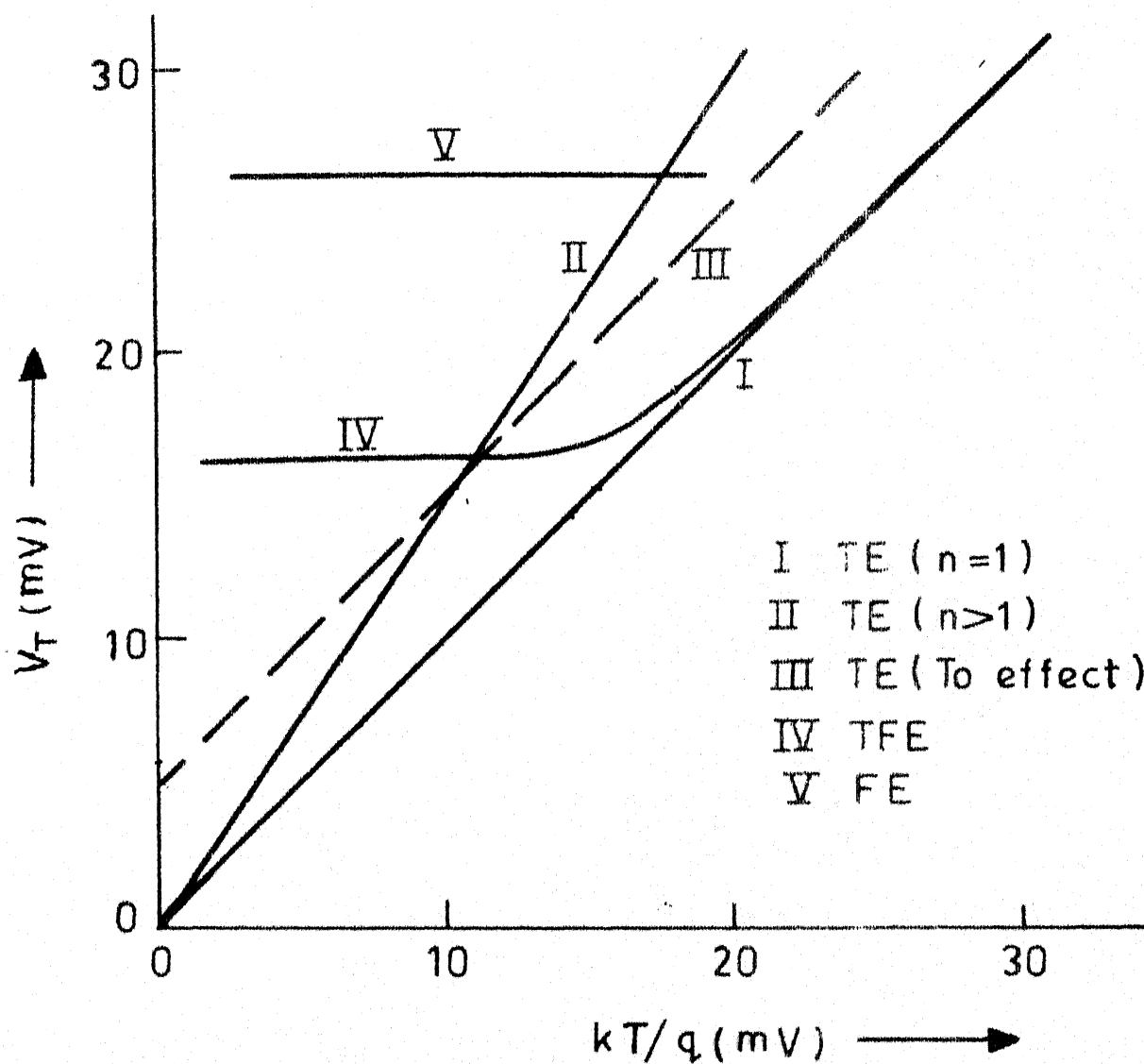


Fig.1.2 Plot of  $V_T$  Versus( $kT/q$ ) to determine the mechanism of current transport in Schottky barriers ( see Text ).

Before concluding, the following points regarding Saxena's work are worth noticing,

(i) The experimental method suggested by Saxena [14] considers only thermionic emission and not diffusion as the transport for emission over the barrier. This was later confirmed by the observations of Crowell and Beguwala [20], and Rhoderick [31], that Schottky diodes made from fairly high mobility semiconductors like Germanium, Silicon and Gallium Arsenide etc., should confirm to thermionic theory for emission over the barrier rather than to diffusion theory. and (ii) the validity of the experimental methods suggested by Saxena [14] should only be tested in very small area diodes - this is mainly because of the technological limitation in getting a large area semiconducting crystal of uniform properties.

#### 1.4 $T_0$ Effect

In the previous section on the experimental method to identify the mechanism of current transport in a Schottky barrier diode, we have already mentioned that many metal semiconductor junctions show a temperature dependent ideality factor. Moreover, in some cases this temperature dependence has been found to obey the relation

$$n = (1 + T_0/T) \quad (1.9)$$

These diodes are said to exhibit  $T_0$  anomaly, mainly because the physical mechanisms responsible for this behaviour were not identified in the beginning. It was with the work of Levine [19] in 1971, that the first successful model to explain this  $T_0$  effect was available. Later in 1977, Crowell [27] has emphasized that the choice of parameters in the model of Levine is not unique, rather several other choices are possible. To start with, we would consider only the model of Levine which assumes an exponential energy distribution, characterized by a characteristic energy  $E_0$ , of the interface states.

Note, however, that the original work of Levine had some physical discrepancies, regarding the vanishing of charge in the semiconductor and consequently in the surface state, at the flat band condition, as highlighted by Crowell. It is interesting to note that this physical discrepancy is identical to missing a constant of integration in Levine's work. Realization of this fact has allowed us to view the models of Levine and Crowell in a novel perspective which is presented below.

#### 1.4.1 Evaluation of the surface state charge

Fig. 1.3 shows the energy band diagram for a Schottky barrier made on an n-type semiconductor under (a) forward bias, (b) zero bias and (c) reverse bias, with an exponential

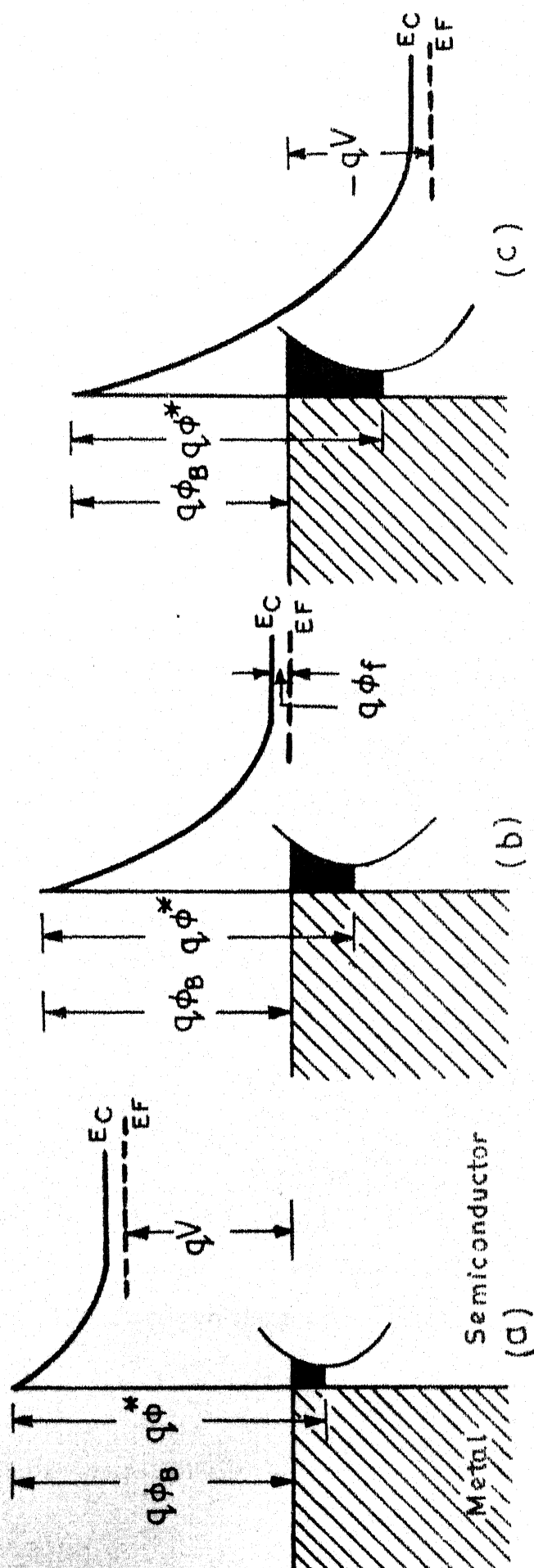


Fig. 1.3 Schematic relationship between barrier height  $\phi_B$  and change in interface states for (a) forward-bias (b) zero-bias (c) reverse-bias conditions. The amount of charge in each case is supposed to be proportional to the dark area [19].

surface state distribution incorporated in it. The negative charges will be located in the acceptor like surface states which lie above the neutral level [19] and lie below the Fermi-level. The negative charges in the surface state can be derived under the following assumptions:

(i) The surface states distribution in the forbidden bandgap of the semiconductor is of the form,

$$D_{ss}(E) = D_{so} \exp (|E|/E_0) \quad (1.10)$$

where  $E$  is the energy measured from the neutral level and is positive in the direction towards the Fermi-level,  $E_0$  is the characteristic energy and  $D_{so}$  is the density of the surface states at the neutral level, and

(ii) the occupation of surface states follows Fermi statistics with zero degree approximation of abrupt transition of occupation probability from unity to zero at the metal Fermi level. This fixes the integration limits for the evaluation of the surface state charge to be 0 and  $\phi^{\#} - \phi_B$ , where  $\phi^{\#}$  is the neutral level at the surface and  $\phi_B$  is the barrier height (see Fig. 1.3). We can write the surface charge  $Q_{ss}$  as,

$$Q_{ss} = qD_{so} \int_0^{q(\phi^{\#} - \phi_B)} \exp (|E|/E_0) dE \quad (1.11)$$

where  $|E| = E$ , since we are interested only in the positive values of  $E$ . Integrating eqn. (1.11), we obtain,

$$\begin{aligned}
 Q_{ss} &= qD_{so} E_o [\exp(q(\phi^{\infty} - \phi_B)/E_o) - 1] \\
 &= Q_f [\exp(q(\phi^{\infty} - \phi_B)/E_o) - 1]
 \end{aligned}
 \tag{1.12}$$

Here  $Q_f$  is the interface charge that neutralises the surface state charge at flat band. We note that the expression for  $Q_{sc}$  given in eqn. (1.12) is the same as that used by Crowell to modify Levine's formulation and which marks the starting point for Crowell's model [27].

#### 1.4.2 Evaluation of $T_o$

It is well known that the ideality factor ( $n$ ) of a Schottky barrier diode is given by the relation [32],

$$n = \left(1 - \frac{\partial \phi_B}{\partial V}\right)^{-1} \tag{1.13}$$

The evaluation of  $n$  requires the knowledge of the voltage dependence of the barrier height  $\phi_B$ . From eqn. (1.12) one can write the barrier height  $\phi_B$  as,

$$\phi_B = \phi^{\infty} - \frac{E_o}{q} \ln \left( \frac{Q_{ss} + Q_f}{Q_f} \right) \tag{1.14}$$

To obtain the voltage dependence of  $\phi_B$ , one requires the voltage dependence of  $Q_{ss}$ . The voltage dependence of  $Q_{ss}$  and hence  $\phi_B$  can be obtained from the charge neutrality at the surface as follows. Invoking charge neutrality at the surface, one has,

$$Q_{ss} = Q_{sc} \tag{1.15}$$

where  $Q_{sc}$  is the total space charge in the semiconductor and the charge on the metal is taken to be zero. Using eqn. (1.14) and (1.15) we have,

$$\phi_B = \phi^* - \frac{E_o}{q} \ln \left( \frac{Q_{sc} + Q_f}{Q_f} \right) \quad (1.16)$$

where  $Q_{sc}$  is given by [31],

$$Q_{sc} = \sqrt{2q\epsilon_s N_d (\phi_B - V - \phi_f - (kT/q))} \quad (1.17a)$$

$$f = \frac{kT}{q} \ln (N_C/N_D) = \frac{kT}{q} b \quad (1.17b)$$

Eqn. (1.16) along with eqns. (1.17a) and (1.17b) gives us the barrier height as a function of voltage. Differentiating eqn. (1.16) with respect to  $V$  we have,

$$\frac{\partial \phi_B}{\partial V} = - \frac{E_o}{2q} \left[ (\phi_B - V - \phi_f - \frac{kT}{q})^{-1} \right] \left( \frac{\partial \phi_B}{\partial V} - 1 \right) \cdot \frac{1}{f(Q_{sc})} \quad (1.18)$$

where  $f(Q_{sc}) = 1/(1 + Q_f/Q_{sc})$ .

From eqn. (1.18) one obtains the value of  $(1 - \partial \phi_B / \partial V)$  required for the evaluation of the ideality factor as,

$$\left( 1 - \frac{\partial \phi_B}{\partial V} \right) = 1 / \left[ 1 + \frac{E_o}{2q} (\phi_B - V - \phi_f - \frac{kT}{q})^{-1} \cdot \frac{1}{f(Q_{sc})} \right] \quad (1.19)$$

Using eqns. (1.9), (1.13) and (1.19) one obtains

$$\frac{1}{T_o} = \frac{2q}{E_o T} (\phi_B - V - \phi_f - \frac{kT}{q}) \cdot f(Q_{sc}) \quad (1.20)$$

For barrier height  $\phi_B < \phi^* - \frac{2E_o}{q}$ , when  $Q_{sc} \gg Q_f$ ,

eqn. (1.20) reduces to the following expressions obtained by Levine [19]:

$$\frac{1}{T_0} = \frac{2q}{E_0 T} (\phi_B - V - \phi_f - \frac{kT}{q}) \quad (1.21a)$$

$$= \frac{2k}{E_0} (\ln (J/A^{\frac{1}{2}} T^2) - (b+1)) \quad (1.21b)$$

where  $\phi_B - V = \frac{kT}{q} \ln (J/A^{\frac{1}{2}} T^2)$

Under constant current conditions, ignoring the slowly varying  $\ln T$  term one observes from eqn. (1.21b) that  $T_0$  is independent of temperature and is proportional to  $E_0$ .

It is important to note here that the inconsistency in the evaluation of surface state charge in Levine's model has arisen due to the use of eqn. (1.21a) for  $T_0$ , rather than the more general expression given in eqn. (1.20).

So far we have looked into the model of Levine and of Crowell to explain the  $T_0$  effect and the experimental methods of Saxena to identify the mechanism of current transport in Schottky barrier diodes. In the following section we present a brief outline of the work done in the present thesis.

## 1.5 The Present Work

In recent years, due to their applications in photovoltaic [33] and power devices [34], it has become necessary to fabricate large area Schottky barrier diodes. To identify



the mechanism of current transport in these cases also the method suggested by Saxena [14] has been utilized by some workers [26] leading to an ambiguity in this identification [35]. The ambiguity is that the experimental plot of  $V_T$  versus  $T$  has shown the mechanism of current transport to be field emission for Schottky barrier diodes made of semiconductor substrates of low doping [26], when the operation is at a high temperature. It seems obvious that in diodes of low doping, field emission should not be a mechanism of current transport at high temperatures [35]. One of the purposes of the present work is to demonstrate that even though the mechanism of the current transport in a large area Schottky diode may be TE, the fluctuation of parameters can create a situation so that the experimental plot of  $V_T$  versus  $T$  would show FE to be the mechanism of current transport. In our study of current transport in large area Schottky barrier diodes, we have considered a diode with the mechanism of current transport defined by TE with  $T_0$  effect and with a fluctuation in  $E_0$ . The choice of the fluctuating parameter would be clear from the following discussions.

#### 1.5.1 Current transport in large area Schottky barrier diodes [36]

The choice of fluctuating parameter in a large area Schottky barrier diode was based on two important observations regarding diodes showing  $T_0$  effect and are given below:

(i) The first observation is due to Padovani [32], who noted that the different Au-n-GaAs Schottky barrier diodes made on the same wafer showed different values  $T_0$ . We have also noted a similar trend in different Au-nSi Schottky barrier diodes made on the same wafer.

(ii) One observes from the discussions in the previous section that  $T_0$  is a function of  $E_0$ ,  $\phi^*$  and  $D_{s0}$  and that the fluctuations in  $T_0$  could be due to the fluctuations in any of the three parameters. To identify the fluctuating parameter, the values of  $E_0$ ,  $\phi^*$  and  $D_{s0}$  are evaluated using the method given in Chapter III, for each diode. It is found that while  $E_0$  is different for diodes with different  $T_0$ , the values of  $\phi^*$  and  $D_{s0}$  are nearly the same for all the diodes.

Guided by these observations, we have considered that the value of  $E_0$  fluctuates for a large area diode. It is further assumed that the variation of areas,  $\Delta S_i$ , of patches with values of  $E_0$  between  $E_0$  and  $E_{oi} + \Delta E_{oi}$  has a Gaussian distribution [36], i.e.

$$\frac{\Delta S_i}{S} = \frac{1}{\sqrt{2\pi}\sigma} \exp \left[ -\frac{(\bar{E}_0 - E_{oi})^2}{2\sigma^2} \right] \Delta E_{oi} \quad (1.22)$$

where  $\bar{E}_0$  is the mean value of  $E_{oi}$ 's and  $\sigma$  is the standard deviation and  $S$  is the total area of the diode. The total current flowing in the diode can then be written as,

$$\begin{aligned}
I &= SJ = \int_{E_0} J_i \cdot \frac{dS_i}{dE_{oi}} dE_{oi} \\
&= \int_{E_{oi1}}^{E_{oi2}} (dS_i/dE_{oi}) A^* T^2 \exp\left(\frac{-q\phi_{Bi}}{kT}\right) \left[\exp\left(\frac{qV}{kT}\right) - 1\right] dE_{oi}
\end{aligned} \tag{1.23}$$

where  $\phi_{Bi}$  = the barrier height of the  $i$ th path and  $dS_i/dE_{oi}$  is obtained from eqn. (1.22) in the limits  $\Delta E_{oi} \rightarrow 0$  as

$$\frac{dS_i}{dE_{oi}} = \frac{S}{\sqrt{2\pi}\sigma^2} \exp\left[-\frac{(\bar{E}_0 - E_{oi})^2}{2\sigma^2}\right] \tag{1.24}$$

To evaluate the value of current using eqns. (1.23), (1.24), (1.12) and (1.14), we need the values of  $\bar{E}_0$ ,  $\phi^*$ ,  $D_{so}$ ,  $E_{oi1}$  and  $E_{oi2}$ . The area  $S$  taken to be  $1 \text{ cm}^2$  and the method of choosing the values of the other parameters is discussed below.

Keeping in mind that the choice of  $\bar{E}_0$ ,  $\phi^*$  and  $D_{so}$  should be close to the realistic values, a preliminary experimental investigation has been carried out to choose the values of these parameters. The experimental investigation consisted of preparing a number of homogeneous Au-nSi diodes on a single wafer and evaluating  $\bar{E}_0$ ,  $\phi^*$  and  $D_{so}$  in each diode. The diodes made in the same wafer showed a scatter in  $T_0$  (measured at the same current density in all the diodes) and hence in the corresponding values of  $\bar{E}_0$ . The average of these  $\bar{E}_0$ 's has been chosen to be  $\bar{E}_0$ . The limits

of integration  $E_{oi1}$  and  $E_{oi2}$  are taken to be the values of  $E_{oi}$  where the integrand falls to less than 10% of the maximum value. Regarding the evaluation of  $\phi^*$  and  $D_{so}$ , we observed that there is no method available in literature to evaluate these parameters. We have developed a method to determine  $\phi^*$  and  $D_{so}$  from the temperature dependence of the barrier height at zero bias (see Chapter III). From the values of  $\phi^*$  and  $D_{so}$  obtained for different diodes we observed that these values were nearly the same for all diodes and are  $0.78 E_g$  and  $1.48 \times 10^{11}/\text{cm}^2$  eV respectively. Here  $E_g$  represents the band gap of the semiconductor. The experimentally measured values of  $\phi^*$  and  $D_{so}$  are then used in our theoretical calculations. Using these values and eqns. (1.23) and (1.24), the forward I-V characteristic has been obtained at different temperatures and the corresponding  $V_T$  has been calculated from the relation,

$$V_T = \left( \frac{\partial \ln I}{\partial V} \right)^{-1} \quad (1.25)$$

at each temperature.

A plot of  $V_T$  vs.  $kT/q$  is given in Fig. 1.4 for  $\bar{E}_0 = 0.75\text{eV}$  with  $\sigma$  as a parameter. The following feature of the plot should be noted.

For a given  $\bar{E}_0$  when  $\sigma = 0$ , one gets a plot of  $V_T$  vs.  $kT/q$  which is typical of  $T_0$  effect, i.e. a straight line parallel to unity ideality factor line but not passing through

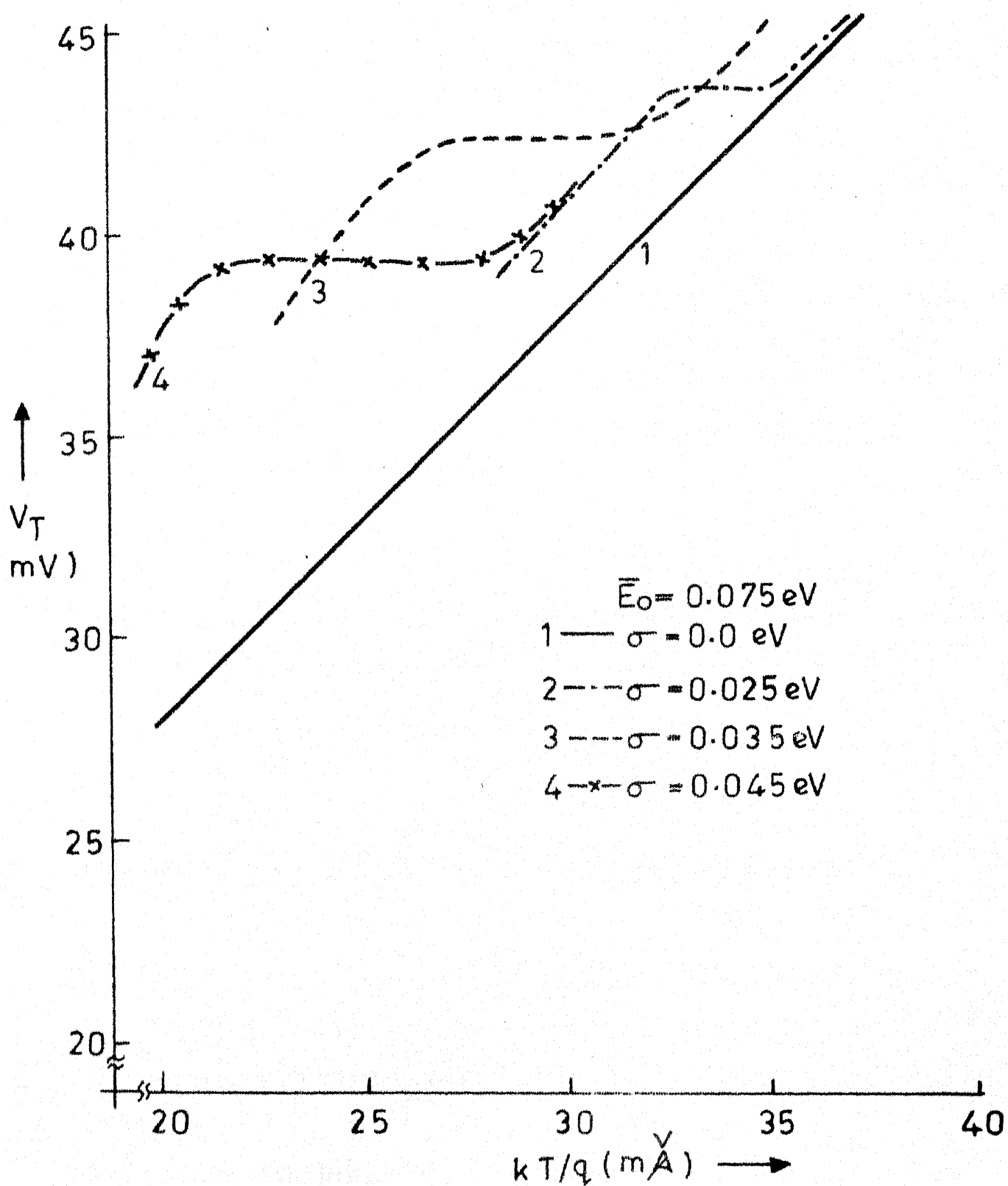


Fig.1.4 Plot of  $V_T$  versus  $\frac{kT}{q}$  with  $\sigma$  as a parameter for  $\bar{E}_0 = 0.075$  eV. The donor density is  $2.5 \times 10^{15} \text{ cm}^{-3}$ .

the origin. As the value of  $\sigma$  becomes finite a flat region appears which is typical of field emission in the conventional interpretation. Thus although the mechanism of current transport in the diode is thermionic emission, the fluctuation of parameters have brought in the characteristics of field emission, if attention is restricted to a limited range of temperature. This suggests that caution must be exercised while inferring the mechanisms of current transport in Schottky diodes from  $V_T$  vs.  $T$  plots. The analytical detail of the calculations of  $V_T$  vs  $T$  plot for large area diodes showing fluctuations in  $T_0$ , is given in Chapter II, where we also present a calculation of the effect of fluctuation in interfacial layer (oxide layer) thickness in devices with a thin interfacial oxide layer.

An experimental verification of the theoretical calculations carried out for large area diodes with fluctuations in  $T_0$  is presented in Chapter III, where we also present a method to characterise the surface state distribution leading to  $T_0$  effect, and a numerical calculation to establish the function of a guard ring in a Schottky barrier diode.

In Chapter IV we present an analysis to establish the  $T_0$  effect as an effect of metal-electron tunneling into the forbidden bandgap of the semiconductor and establish an equivalence with Levine's model for  $T_0$  effect.

In Chapter V we present a novel method to determine the doping density of the semiconductor in Schottky barrier diodes showing  $T_0$  effect. A few concluding remarks are made in Chapter VI.

## CHAPTER 2

### THEORETICAL STUDIES ON THE EFFECT OF FLUCTUATION ON THE IDENTIFICATION OF THE MECHANISM OF CURRENT TRANSPORT

It has been mentioned in Chapter I that the manifestation of the mechanism of current transport in the nature of the  $V_T$  versus  $\frac{kT}{q}$  plot in a nonhomogeneous Schottky barrier diode is different from that in a homogeneous Schottky barrier diode. It should be noted, however, that to demonstrate the differences, we have considered only the fluctuations in ' $E_0$ '. It is clear that there would be many other parameters which also can fluctuate in a nonhomogeneous diode and affect the identification of the mechanism of current transport. The purpose of the study in this chapter is to systematically search for the parameters which can fluctuate and affect the identification of the mechanism of current transport. To do this, first of all, we consider the current-voltage equation for a Schottky barrier diode, under a forward bias  $V$ , (with  $V \geq \frac{3kT}{q}$ ) [1]:

$$I = SA^*T^2 \exp(-\chi^{\frac{1}{2}}\delta) \exp\left(\frac{-q\phi_{B0}}{kT}\right) \exp\left(\frac{qV}{nkT}\right) \quad (2.1)$$

Here the term  $\exp(-\chi^{\frac{1}{2}}\delta)$  represents the transmission coefficient of the interfacial oxide layer of thickness  $\delta$  and of mean barrier height  $\chi$ , and other terms are defined in the list of nomenclatures.



Our aim now is to locate, from a perusal of eqn. (2.1), the parameters which may fluctuate and affect the mechanism of current transport in nonhomogeneous Schottky barrier diodes. Before proceeding further, let us point out the difference between the calculations of current-voltage characteristic in a nonhomogeneous diode and a homogeneous diode. In the case of a homogeneous diode the calculation is one dimensional, whereas for a nonhomogeneous diode it is basically two dimensional. The two dimensional nature of the calculation in a nonhomogeneous diode arises primarily because of the fluctuation of material and geometrical parameters transverse to the metal-semiconductor interface. These fluctuations may also lead to the flow of a transverse current in the nonhomogeneous diodes. To simplify the situation, we have incorporated the fluctuations, but have ignored the flow of transverse current while building the model here. It is worth mentioning here that an experiment has been designed (see Chapter III) to check the validity of the assumption mentioned above and has shown that under practical conditions the neglect of the transverse current does not introduce noticeable errors. Hence, the nonhomogeneous diode has in effect been treated as composed of several homogeneous diodes, but with varying values of  $\chi$ ,  $\phi_{BO}$ ,  $n$  and  $\delta$  in eqn. (2.1), in parallel. Furthermore, the system has been taken to be isothermal and  $A^{\#}$  has been assumed to be constant.

To look into the possible nature of variation and to identify a parameter which would uniquely define the fluctuations in  $\chi$ ,  $\phi_{BO}$ ,  $n$  and  $\delta$  it is necessary to consider the various barrier height models. From a description of the development in the study of metal-semiconductor contacts, given in Chapter I, we see that the barrier height models can be classified as (i) Work function model (ii) Localised surface state models or (iii) Distributed surface state models. A study of the effect of fluctuations in diodes governed by the work function model has already been carried out by Johnson et al. [2], hence is not discussed here. The effect of fluctuations in localised and distributed surface state models is treated in the present work, the former in this chapter and the latter in Chapter IV.

In the next two sections we present the study of fluctuations in MIS model (sec 2.1) and exponential surface state model of Levine (sec 2.2).

## 2.1 MIS Model

The study of the effect of fluctuation of parameters on the determination of the mechanism of current transport in a MIS diode is divided into two parts. The first part deals with the identification of a parameter which uniquely defines  $\phi_{BO}$ ,  $n$  and  $\chi$ . The second part deals with the study of the effect of fluctuation of this parameter on the  $V_T$  versus  $\frac{kT}{q}$  plot.

### 2.1.1 Identification of the fluctuating parameter

For an MIS diode, using the methodology outlined by Cowley and Sze [3], and the identification of two kinds of surface states by Card and Rhoderick [1] the expressions for the barrier height ( $\phi_{BO}$ ) at zero bias and the ideality factor ( $n$ ) can be written as (see Appendix B)

$$\begin{aligned} \phi_{BO} = & [C_2(\phi_M - \chi_s) + (1-C_2) \left( \frac{E_g}{q} - \phi_o \right)] \\ & + \frac{C_2^2 C_1}{2} - C_2^{3/2} [C_1(\phi_M - \chi_s) + (1-C_2) \left( \frac{E_g}{q} - \phi_o \right) \frac{C_1}{C_2} \\ & - \frac{C_1}{C_2} \left( \phi_f + \frac{kT}{q} \right) + \frac{C_2 C_1^2}{4}]^{\frac{1}{2}} \end{aligned} \quad (2.3)$$

$$\text{and } n = 1 + \frac{(\delta/\epsilon_i)qD_{sb}}{1+(q\delta D_{sa}/\epsilon_i)} = 1 + (\delta/\epsilon_i)q D'_{sb} \quad (2.4)$$

where  $\phi_o$  = Neutral level at the surface measured from the valence band ( $=0.27 E_g$ ).

$$C_2 = \epsilon_i / [\epsilon_i + q^2 \delta (D_{ss})]$$

$$C_1 = 2q\epsilon_s N_D \delta^2 / \epsilon_i^2$$

$$D_{ss} = D_{sa} + D_{sb}$$

$D_{sa}$  = Density of surface states communicating with the metal

$D_{sb}$  = Density of surface states communicating with the semiconductor;

and  $D'_{sb}$  = Effective density of surface states communicating with the semiconductor.

From equations (2.3) and (2.4) we see that both  $\phi_{B0}$  and  $n$  are functions of  $D_{sa}$ ,  $D_{sb}$  and  $\delta$ . It is seen from literature [1,4] that  $\delta$  is the only independent variable and that  $D_{sa}$  and  $D_{sb}$  are both functions of  $\delta$ . Regarding the mean barrier height  $\chi$  of the interfacial layer we see that [1,4] this is also a function of the oxide thickness  $\delta$ . From the above observations we note that  $\delta$  is the only independent variable and hence the fluctuating parameter in the MIS model.

In table 2.1 we present the  $\delta$  dependence of  $D_{ss}$ ,  $D'_{sb}$  and  $\chi$ , for  $0 < \delta \leq 30 \text{ \AA}$ , evaluated from the data of Card [4] and Card and Rhoderick [1].\* Note that we have considered the  $\delta$  dependence of  $D_{ss}$  and  $D'_{sb}$  rather than the more fundamental quantities  $D_{sa}$  and  $D_{sb}$  because for the calculation of  $\phi_{B0}$  and  $n$  we do not need the individual values of  $D_{sa}$  and  $D_{sb}$  but only those of  $D_{ss}$  and  $D'_{sb}$ .

Table 2.1. Functional relationship between  $\chi$ ,  $D_{ss}$  and  $D'_{sb}$  and the oxide thickness  $\delta$ .

Parameter	Function of oxide thickness ' $\delta$ '
$\chi$	$\chi^{\frac{1}{2}} = a\delta^2 + b$ ; $a = 7.10^{20} \text{ eV}^{\frac{1}{2}}/\text{cm}^2$ , $b = 1.11 \times 10^7 \text{ eV}^{\frac{1}{2}}$
$D_{ss}$	$D_{ss} = c\delta + d$ ; $c = -2.04 \times 10^{20}/\text{eV cm}^3$ $d = 6.68 \times 10^{13}/\text{eV cm}^2$
$D'_{sb}$	$D'_{sb} = e\delta^3 + f$ ; $e = 1.46 \times 10^{32}/\text{eV cm}^5$ $f = 1.28 \times 10^{12}/\text{eV cm}^2$ .

\*The value of  $D_{ss}$  at different oxide thicknesses has been evaluated by using eqn. (2.3) and a plot of  $\phi_{B0}$  versus  $\delta$  given in Ref. [4].

Having identified the oxide thickness ( $\delta$ ) as the fluctuating parameter and defined the relationship of the other relevant parameter with  $\delta$ , let us now look into the effect of fluctuations in  $\delta$  on the determination of the mechanism of current transport in a MIS diode. Before proceeding further it should be mentioned that our study is restricted to oxide thickness  $\delta \leq 30 \text{ \AA}$ .

### 2.1.2 Effect of fluctuations in ' $\delta$ '

The aim in this section is to evaluate the I-V characteristic of a nonhomogeneous diode, with a fluctuation in the oxide thickness, at different temperatures and hence obtain the  $V_T$  versus  $\frac{kT}{q}$  plot. To calculate the I-V characteristic we need to know: (i) the area of the individual diodes which make up the large area diode and (ii) the temperature dependence of the various parameters, viz.  $\phi_m$ ,  $\chi_s$ ,  $\chi$ ,  $D_{ss}$ ,  $D'_{sb}$  and  $E_g$ . Let us look into these one by one.

In this study we assume that the sub-area  $\Delta S_i$  of patches with oxide thickness between  $\delta_i$  and  $\delta_i + \Delta\delta_i$  has a gaussian distribution, and is given by,

$$\frac{\Delta S_i}{S} = \frac{1}{\sqrt{2\pi}\sigma} \exp\left(-\frac{(\bar{\delta} - \delta_i)^2}{2\sigma^2}\right) \Delta\delta_i \quad (2.5)$$

where  $\bar{\delta}$  is the mean oxide thickness,  $\sigma$  is the standard deviation and  $S$  is the total area of the diode and is taken to be  $1 \text{ cm}^2$ .

The parameters  $D_{ss}$ ,  $D'_{sb}$  and  $\chi$  are all considered to be temperature invariant and the temperature dependence of  $E_g$  [5],  $\phi_m$ , and  $\chi_s$  [3] are given by the equations

$$E_g(T) = E_g(0) - \alpha T^2 / (\beta + T) \quad (2.6)$$

$$\alpha = 7.2 \times 10^{-4} \text{ eV/}^\circ\text{K}; \quad \beta = 1108^\circ\text{K}$$

$$\phi_m(T) = \phi_{m0} - aT \quad (2.7)$$

$$\phi_{m0} = 4.698 \text{ eV}; \quad a = 1.3 \times 10^{-4} \text{ eV/}^\circ\text{K}$$

$$\chi_s(T) = \chi_{s0} + bT \quad (2.8)$$

$$\chi_{s0} = 4.02 \text{ eV}; \quad b = 10^{-4} \text{ eV/}^\circ\text{K}.$$

The total current  $I$  flowing in the diode can be written analogous to eq. (1.23) as,

$$I = \frac{SA \pi T^2}{\sqrt{2\pi\sigma^2}} \int_{\delta_1}^{\delta_2} \exp(-\chi \frac{1}{2}\delta) \exp(-\frac{q\phi_{Boi}}{kT}) \exp(\frac{qV}{nkT}) \exp\left(\frac{(\bar{\delta} - \delta)^2}{2\sigma^2}\right) d\delta \quad (2.9)$$

where  $\delta_1$  and  $\delta_2$  are the values of  $\delta$  at which the integrand drops down to less than 10% of the maximum value. Using eqn. (2.3) to (2.9) and eqn. (1.24), the  $I$ - $V$  characteristic and  $V_T$  under constant current condition is evaluated at different temperatures. In Fig. (2.1) we present a plot of  $V_T$  versus  $\frac{kT}{q}$  for a fixed value of  $\bar{\delta}$  for different values of  $\sigma$ . The following feature of Fig. 2.1 is to be noted.

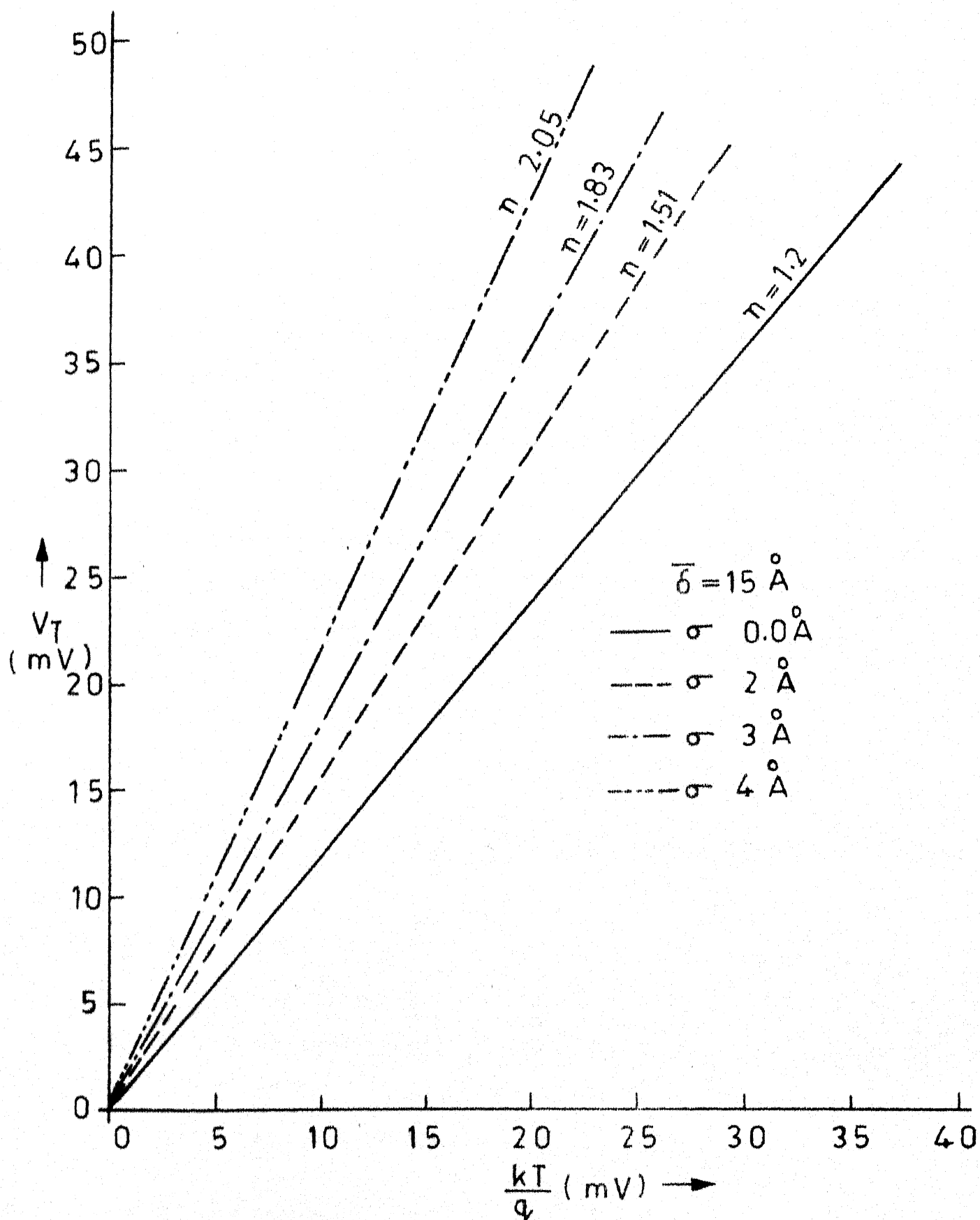


Fig.2.1 Plot of  $V_T$  versus  $\frac{kT}{q}$  with  $\sigma$  as a parameter for  $\bar{\delta} = 15 \text{ Å}$ . The donor density is  $N_D = 2.5 \times 10^{15} / \text{cm}^3$ .

The plot of  $V_T$  versus  $\frac{kT}{q}$  is a straight line passing through the origin with a slope greater than unity. The slope of the straight line increases with an increase in  $\sigma$ . Thus we see that the fluctuations in  $\delta$  does not alter the qualitative nature of the  $V_T$  versus  $\frac{kT}{q}$  plot.

From a preliminary study of the effect of fluctuations on the nature of the  $V_T$  versus  $\frac{kT}{q}$  plot in the two localised surface state models we see that fluctuation in  $E_0$  brings about a qualitative change in the  $V_T$  versus  $\frac{kT}{q}$  plot whereas fluctuations in oxide thickness does not cause any qualitative change in the nature of the  $V_T$  versus  $\frac{kT}{q}$  plot. Since our interest is in the study of nonhomogeneous diodes which do not have a unique relationship between the mechanism of current transport and the  $V_T$  versus  $\frac{kT}{q}$  plots, in the next section we shall look into the effect of fluctuations of  $E_0$  in greater detail.

## 2.2 Effect of Fluctuations in $E_0$

A brief account of the effect of fluctuations in  $E_0$  has already been presented in Chapter I. In this section we present further details of the  $V_T$  versus  $\frac{kT}{q}$  plot and present a semi-analytical calculation to identify the temperature range where  $V_T$  remains independent of temperature. In Fig. 2.2 we present  $V_T$  versus  $\frac{kT}{q}$  plots for



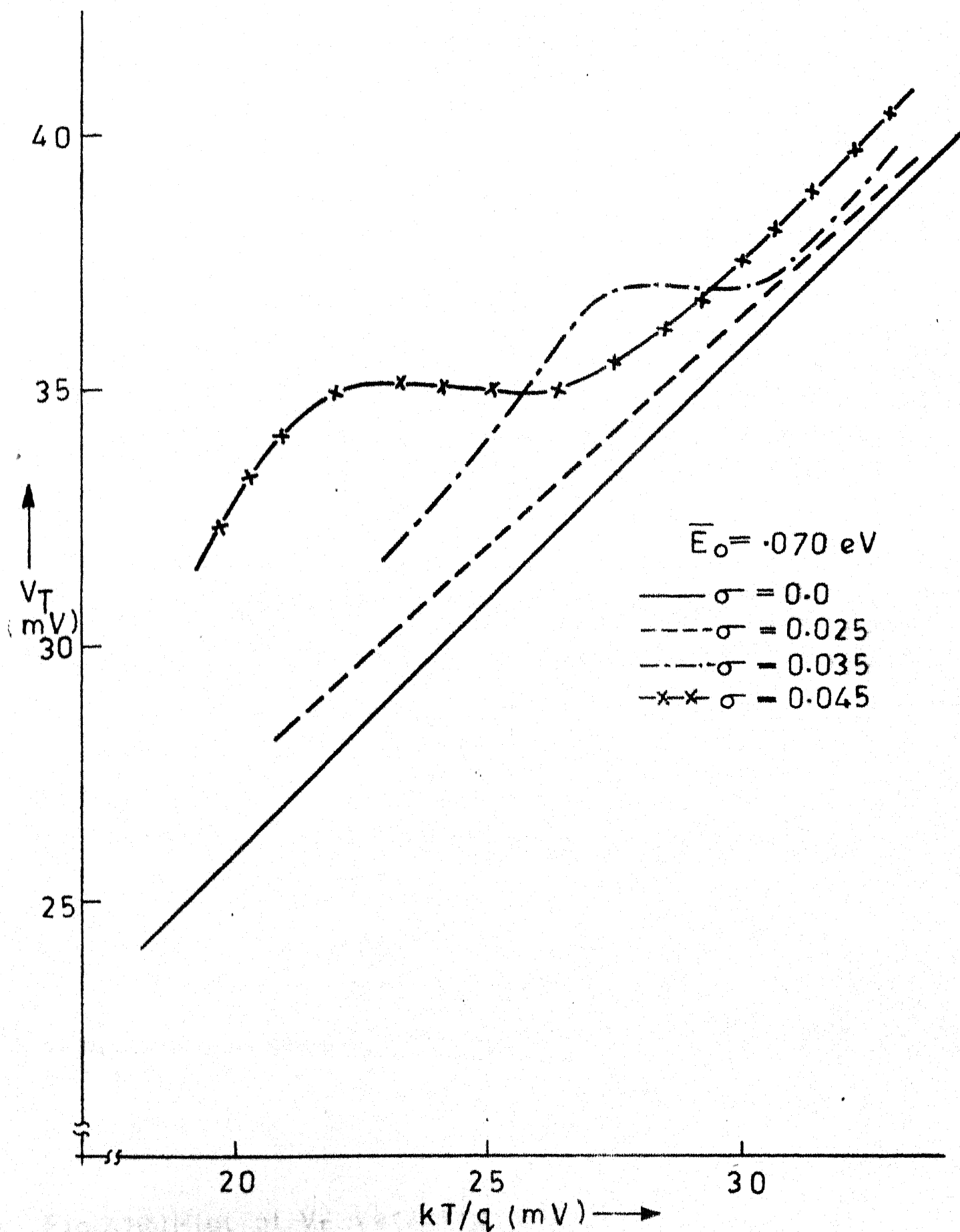


Fig.2.2(a) Plot of  $V_T$  versus  $kT/q$  with  $\sigma$  as a parameter for  $\bar{E}_0 = 0.070$  eV. The donor density is  $2.5 \times 10^{15} \text{ cm}^{-3}$

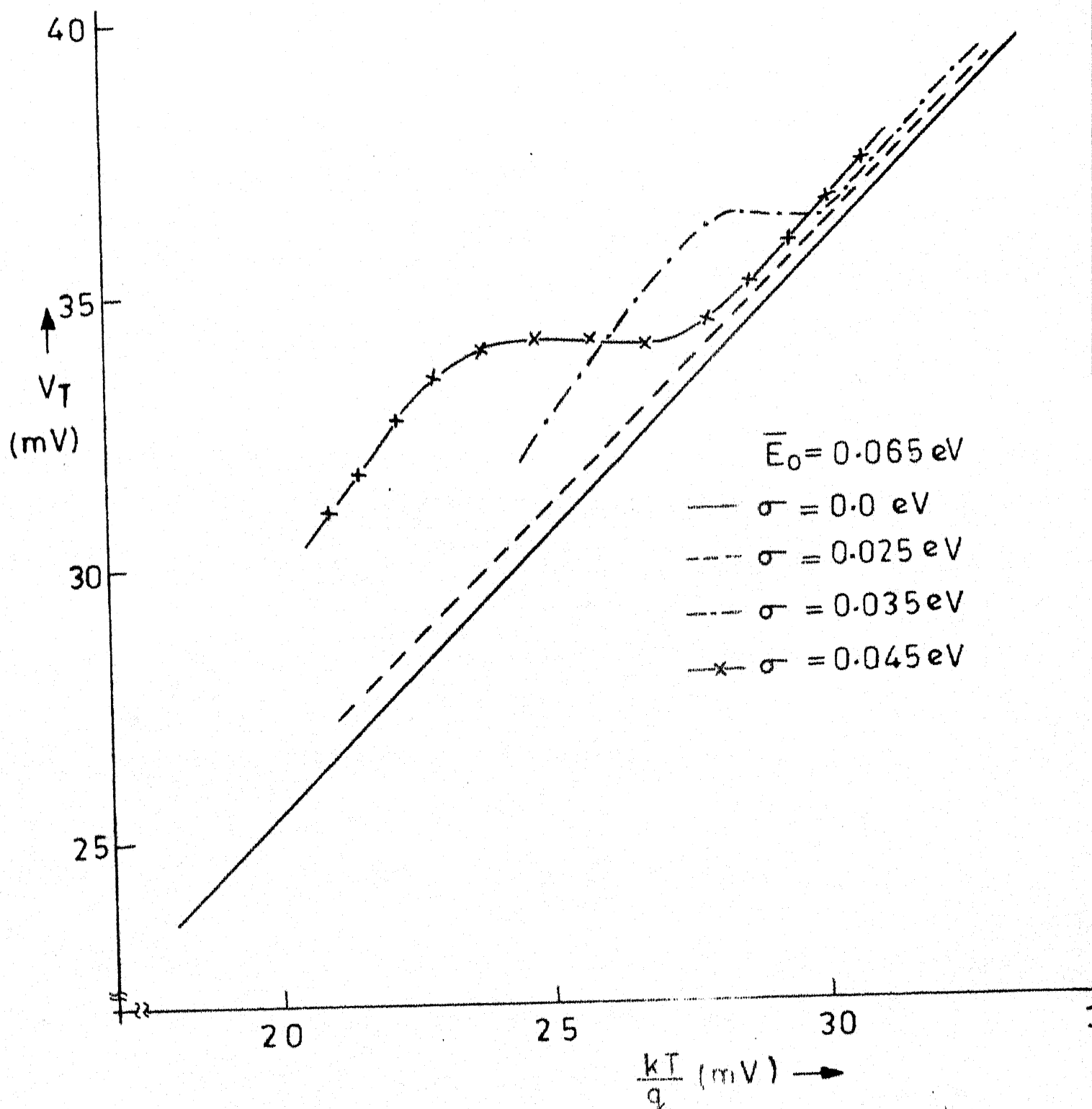


Fig.2.2(b) Plot of  $V_T$  versus  $\frac{kT}{q}$  with  $\sigma$  as a parameter for  $\bar{E}_0 = 0.065$  eV. The donor density is  $N_D = 2.5 \times 10^{15} / \text{cm}^3$

different  $\bar{E}_0$  with  $\sigma$  as a parameter. Apart from the trend explained in Chapter I, the following trends are also worth noting.

(i) The range of temperature over which the value of  $V_T$  remains to be independent of temperature reduces with the reduction in  $\sigma$  for the same value of  $\bar{E}_0$ . We also see that for the same value of  $\sigma$ , the mid point of the temperature range over which  $V_T$  is constant increases with a decrease in  $\bar{E}_0$ .

(ii) For a given value of  $\bar{E}_0$ , there is a threshold value of  $\sigma$ , below which the  $V_T$  versus  $\frac{kT}{q}$  plot is still a straight line not passing through the origin. It should be noted however that in the presence of fluctuations in  $E_0$ , the slope of the  $V_T$  versus  $\frac{kT}{q}$  plot remains to be less than unity, as compared to the unity slope in the homogeneous case.

Having looked into the nature of the  $V_T$  versus  $\frac{kT}{q}$  plot for devices with fluctuations in  $E_0$ , the next logical step is to look for a relationship between  $V_T'$  (the value of  $V_T$  when independent of temperature)  $T_l$  and  $T_u$  (where  $T_l \leq T \leq T_u$  is the temperature range over which  $V_T$  remains to be independent of temperature) and  $\bar{E}_0$  and  $\sigma$ , to identify the nature of fluctuation in a nonhomogeneous diode. In the next section we present a semi-analytical calculation to evaluate  $V_T$ ,  $T_l$  and  $T_u$  as a function of  $\bar{E}_0$  and  $\sigma$ .

### 2.2.1 Calculation of $T_l$ and $T_u$

From Chapter I, we see that the total current in a non-homogeneous diode with a Gaussian area distribution in  $E_o$  is given by,

$$I = SJ = \int_{E_{oi1}}^{E_{oi2}} S'_i \exp\left(\frac{-q\phi_{Bi}}{kT}\right) \exp\left(\frac{qV}{kT}\right) dE_{oi} \quad (2.11)$$

$$\text{where } S'_i = \frac{dS_i}{dE_{oi}} = \frac{S}{\sqrt{2\pi}\sigma^2} \exp \frac{-(\bar{E}_o - E_{oi})^2}{2\sigma^2} \quad (2.12)$$

Differentiating  $\ln I$  with respect to  $V$  to obtain  $V_T$ , we have,

$$\frac{1}{V_T} = \frac{\partial \ln I}{\partial V} = \frac{\partial}{\partial V} \left[ \frac{qV}{kT} + \ln \int_{E_{oi1}}^{E_{oi2}} S'_i \exp\left(\frac{-q\phi_{Bi}}{kT}\right) dE_{oi} \right] \quad (2.13)$$

$$= \frac{q}{kT} - \frac{q}{kT} \frac{\int_{E_{oi1}}^{E_{oi2}} S'_i \exp\left(-\frac{q\phi_{Bi}}{kT}\right) \frac{\partial \phi_{Bi}}{\partial V} dE_{oi}}{\int_{E_{oi1}}^{E_{oi2}} S'_i \exp\left(\frac{-q\phi_{Bi}}{kT}\right) dE_{oi}} \quad (2.14)$$

In eqn. (2.14), we can obtain  $\phi_{Bi}$  and  $(\partial \phi_{Bi} / \partial V)$  as a function of  $E_{oi}$  from eqn. (1.14) and eqn. (1.18) of Chapter I, as,

$$\exp\left(\frac{-q\phi_{Bi}}{kT}\right) = \exp\left(\frac{-q\phi^*}{kT}\right) \left(\frac{Q_{sci}}{Q_{fi}} + 1\right)^{\frac{E_{oi}}{kT}} \quad (2.15)$$

and  $\frac{\partial \phi_{Bi}}{\partial V} = \frac{T_{oi}}{(T + T_{oi})}$

Substituting eqn. (2.15) in eqn. (2.14) we get,

$$\frac{\partial \ln I}{\partial V} = \frac{q}{kT} \left\{ 1 - \frac{1}{T} \frac{\int_{E_{oi1}}^{E_{oi2}} S'_i \left( 1 + \frac{Q_{sci}}{Q_{fi}} \frac{E_{oi}}{kT} \frac{T_{oi}}{(T+T_{oi})} dE_{oi} \right)}{\int_{E_{oi1}}^{E_{oi2}} S'_i \left( 1 + \frac{Q_{sci}}{Q_{fi}} \right) \frac{E_{oi}}{kT} dE_{oi}} \right\} \quad (2.16)$$

$$= \frac{q}{kT} [1 - \mu(T)] \quad (2.17)$$

where

$$\mu(T) = \frac{1}{T} \frac{\int_{E_{oi1}}^{E_{oi2}} S'_i \left( 1 + \frac{Q_{sci}}{Q_{fi}} \frac{E_{oi}}{kT} \frac{T_{oi}}{(T+T_{oi})} dE_{oi} \right)}{\int_{E_{oi1}}^{E_{oi2}} S'_i \left( 1 + \frac{Q_{sci}}{Q_{fi}} \right) \frac{E_{oi}}{kT} dE_{oi}} \quad (2.18)$$

Our interest now is in finding out the temperature range over which  $V_T$  remains a constant. This means the evaluation of the temperature range over which  $\frac{\partial V_T}{\partial T}$  or  $\frac{\partial (1/V_T)}{\partial T}$  is equal to zero. So differentiating eq. (2.18) with respect to temperature and equating it to zero we have,

$$\frac{\partial (1/V_T)}{\partial T} = 0 = \frac{\partial}{\partial T} \left[ \frac{q}{kT} (1 - \mu(T)) \right] \quad (2.19a)$$

$$\text{i.e.} \quad \frac{q}{kT} \left[ (1 - \mu(T)) \frac{1}{T} + \frac{\partial \mu(T)}{\partial T} \right] = 0 \quad (2.19b)$$

$$\text{i.e.} \quad 1 - \mu(T) = -T \frac{\partial \mu(T)}{\partial T} \quad (2.20a)$$

Taking  $\mu(T) \ll 1$ , we have  $(1 - \mu(T)) \approx 1$  and the equation (2.20a) reduces to

$$\frac{\partial \mu(T)}{\partial T} + \frac{1}{T} = 0 \quad (2.20b)$$

It is obvious from eqn. (1.14), which gives  $\phi_{Bi}$  as the solution of a transcendental equation and the expression for  $Q_{sci}$ , (eqn. (1.15)), that a completely analytical solution of eqn. (2.20b) is not feasible. To overcome this we have explored to find out a mathematical fit to the dependence of  $(1 + \frac{Q_{sci}}{Q_{fi}}) E_{oi}/kT$  on  $E_{oi}$ . From a plot of  $(1 + \frac{Q_{sci}}{Q_{fi}}) E_{oi}/kT$  versus  $E_{oi}$  given in Fig. (2.3) for a constant current at different temperatures, we note that  $(1 + \frac{Q_{sci}}{Q_{fi}}) E_{oi}/kT$  can be represented by a three piece linear approximation:

$$(1 + \frac{Q_{sci}}{Q_{fi}}) E_{oi}/kT = \exp[a_j E_{oi} + b_j(T)] \quad 1 \leq j \leq 3 \quad (2.21)$$

$$\text{with} \quad \exp(b_1(T) - b_2(T)) = AT + B \quad (2.22)$$

$$\text{and} \quad \exp(b_3(T) - b_2(T)) = CT + D$$

Using eqn (2.21) and (2.22) in eqn. (2.20a) we obtain,

$$\mu(T) = \frac{1}{T} \cdot \frac{(AT+B) x_1 + x_2 + (CT+D) x_3}{(AT+B) x_4 + x_5 + (CT+D) x_6} \quad (2.25)$$

$$\text{where} \quad x_j = \int_{I_k} \exp \left( - \frac{(\bar{E}_o - E_{oi})^2}{2\sigma^2} \right) \frac{T_{oi}}{(1 + T_{oi}/T)} \exp(a_j E_{oi}) dE_{oi}$$

$$1 \leq j \leq 3$$

$$1 \leq k \leq 3$$

$$= \int_{I_k} \exp \left( - \frac{(\bar{E}_o - E_{oi})^2}{2\sigma^2} \right) \exp(a_j E_{oi}) dE_{oi}$$

$$1 \leq k \leq 3$$

$$4 \leq j \leq 6$$

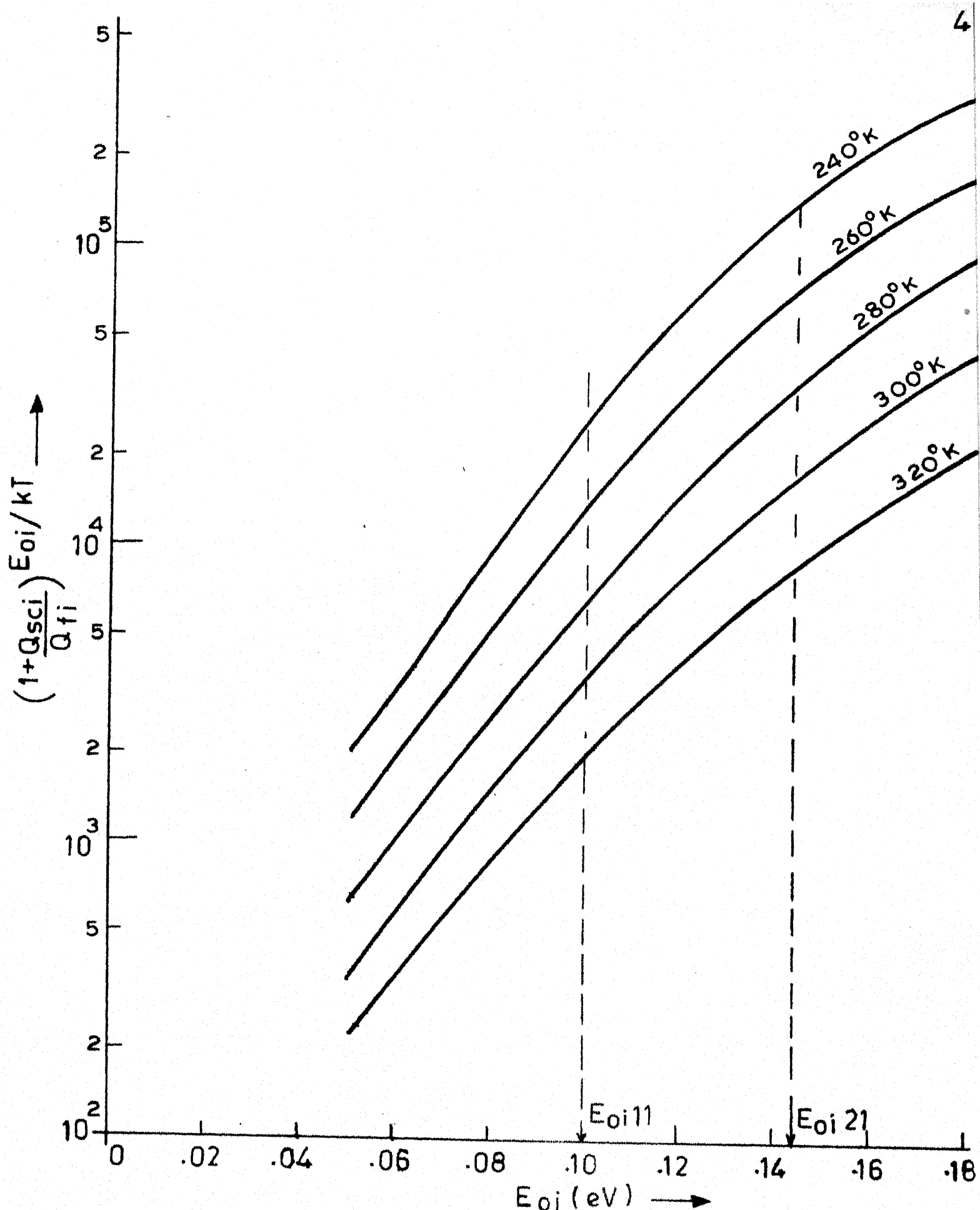


Fig.23a Plot of  $(1 + \frac{Q_{sci}}{Q_{fi}}) \frac{E_{oi}}{kT}$  versus  $E_{oi}$  at different temperatures for  $\bar{E}_0 = 0.075 \text{ eV}$  and  $\sigma = 0.045 \text{ eV}$ .

Fig.2.3(b) Plot of  $\left(1 + \frac{Q_{sci}}{Q_{fl}}\right) \frac{E_{oi}}{kT}$  versus  $E_{oi}$  at different temperatures for  $\bar{E}_0 = 0.075 \text{ eV}$  and  $\sigma = 0.025 \text{ eV}$ .



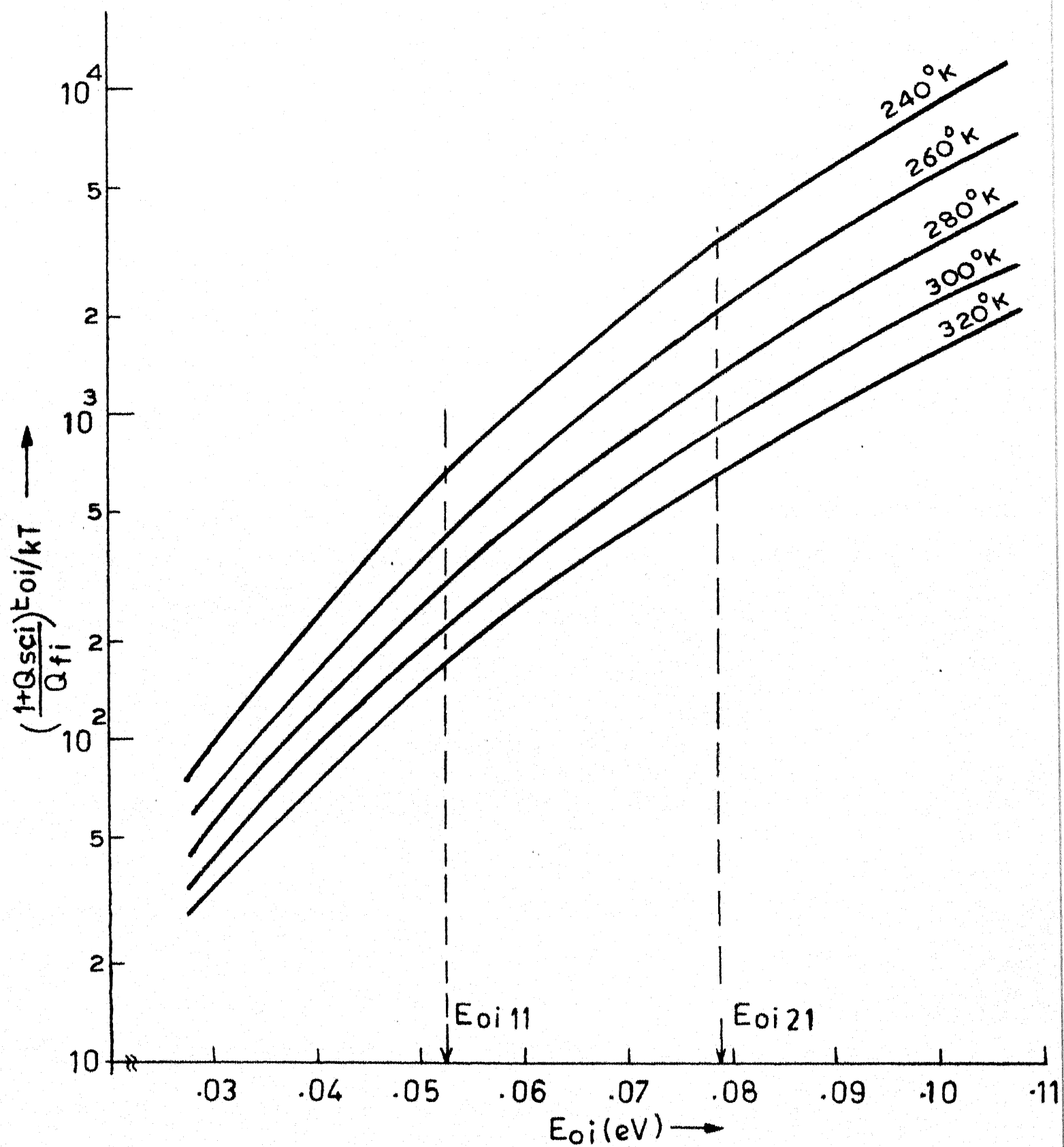


Fig.2.3 c Plot of  $\left(\frac{1+Q_{sci}}{Q_{fi}}\right) \frac{E_{oi}}{kT}$  versus  $E_{oi}$  at different temperatures for  $\bar{E}_0 = 0.065 \text{ eV}$  and  $\sigma = 0.025 \text{ eV}$

$$\begin{aligned}
\text{where } I_1 &= [E_{oi1}, E_{oi11}], \\
I_2 &= [E_{oi11}, E_{oi21}], \\
\text{and } I_3 &= [E_{oi21}, E_{oi2}]
\end{aligned}$$

are the three intervals over which the three piece linear approximation is made.

$$\begin{aligned}
\text{Putting, } q &= Ax_1 + Cx_3 \\
p &= Bx_1 + x_2 + Dx_3 \\
s &= Ax_4 + Cx_6 \\
r &= Bx_4 + x_5 + Dx_6
\end{aligned} \tag{2.24}$$

and differentiating eqn. (2.23) with respect to temperature and using eqn. (2.20b), we have,

$$T^3 + \frac{2rs - qs}{s^2} T^2 + \frac{r^2 - 2ps}{s^2} T - pr = 0 \tag{2.25}$$

$$\text{i.e. } T^3 + u'T^2 + v'T - w' = 0$$

$$\text{with } u' = \frac{2rs - qs}{s^2}, \quad v' = r^2 - 2ps/s^2 \quad \text{and} \quad w' = pr$$

Normalising the temperature  $T$  with respect to  $100^\circ\text{K}$ , we have the normalised form,

$$T'^3 + uT'^2 + vT' - w = 0. \tag{2.26}$$

$$\text{where } T' = T/100^\circ\text{K}.$$

A perusal of eqn. (2.26) with the values of  $u, v$  and  $w$  obtained from our numerical calculation shows the presence of a root close to the origin, which can be evaluated using the expression, [6], (Appendix C),

$$t = -(v^2 - uw)w/(v^3 - uvw + w^2) \quad (2.27)$$

It is, however, seen that the temperature corresponding to this root falls close to the transition region between thermionic emission and thermionic field emission. Based on this observation, the cubic equation was reduced to a quadratic equation, after eliminating the root ' $t$ '. The solutions  $T_l$  and  $T_u$  of the quadratic equation is obtained from,

$$T_l + T_u = u - t \quad (2.28)$$

$$\text{and } T_l T_u = w/t .$$

In Fig. 2.4 we present a plot of  $u, t$  and  $w$  as a function of  $\sigma$  for three different values of  $\bar{E}_0$ . For the cases where a flatness in  $V_T$  versus  $\frac{kT}{q}$  is seen, the values of  $T_l$  and  $T_u$  obtained from eqn. (2.27) and eqn. (2.28) was found to be well matched with the values obtained from the  $V_T$  versus  $\frac{kT}{q}$  plot. For the cases where in  $V_T$  vs  $\frac{kT}{q}$  did not show a flat region, the roots  $T_l$  and  $T_u$  obtained from eqn. (2.28) were found to be complex.

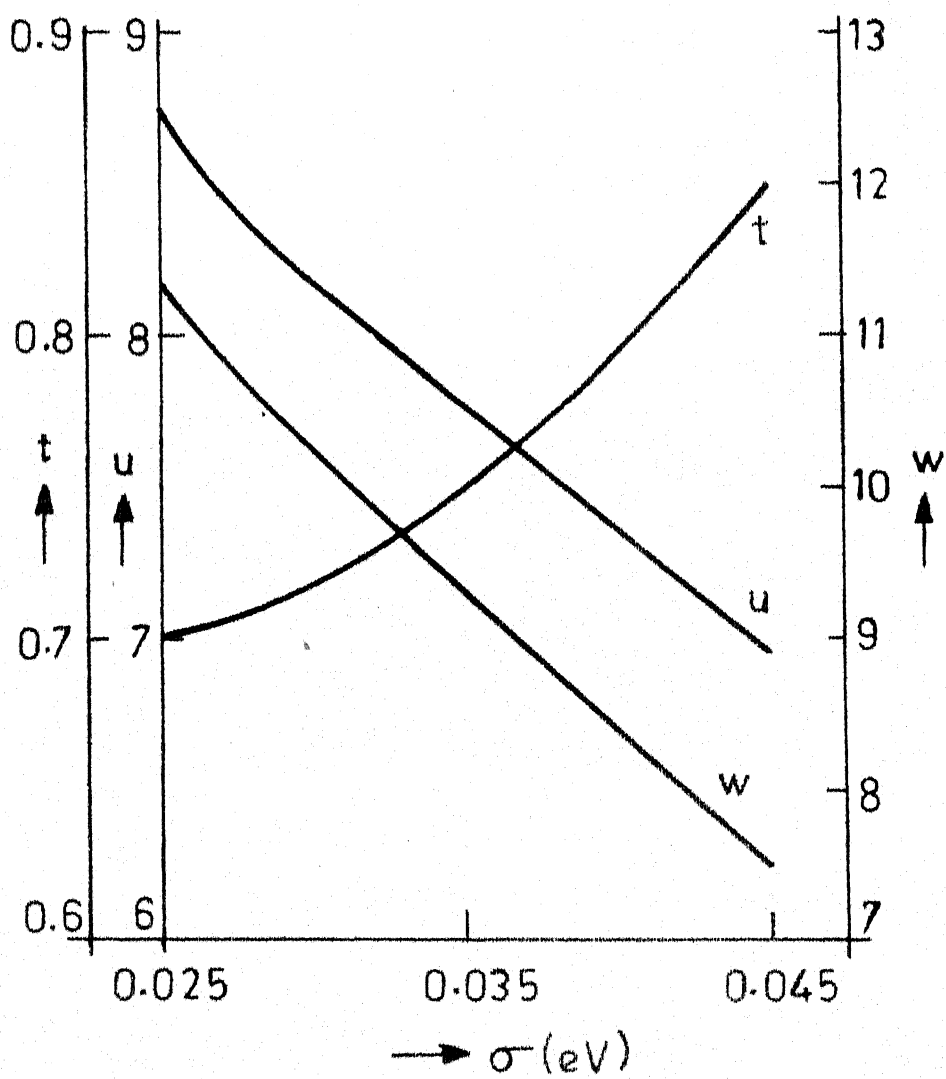


Fig.2.4 (a) A plot of  $u, w$  and  $t$  versus  $\sigma$  for  $\bar{E}_0 = 0.075 \text{ eV}$ .

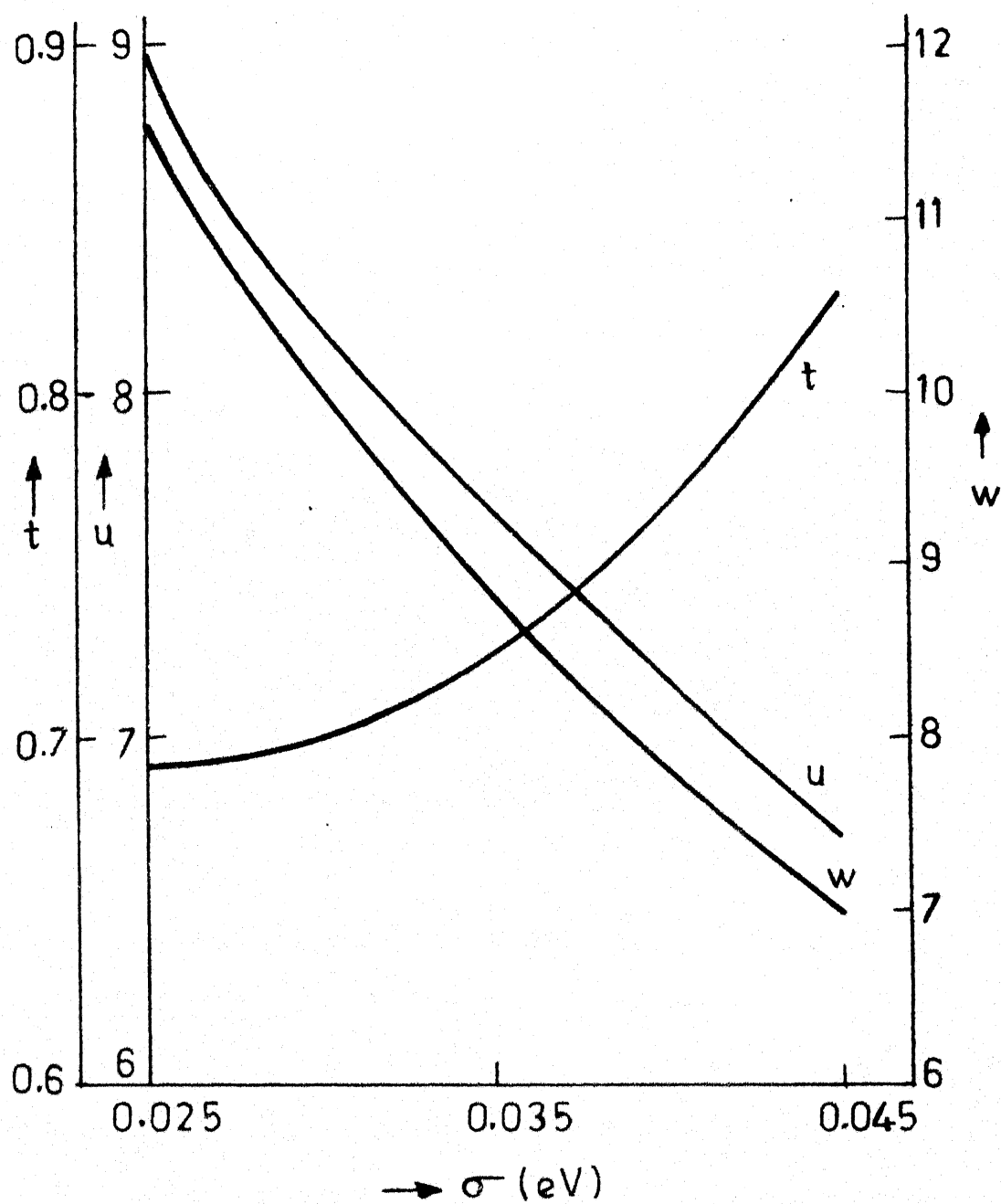


Fig.2.4 (b) Plot of  $u, w$  and  $t$  versus  $\sigma$  with  $\bar{E}_0 = 0.070 \text{ eV}$ .

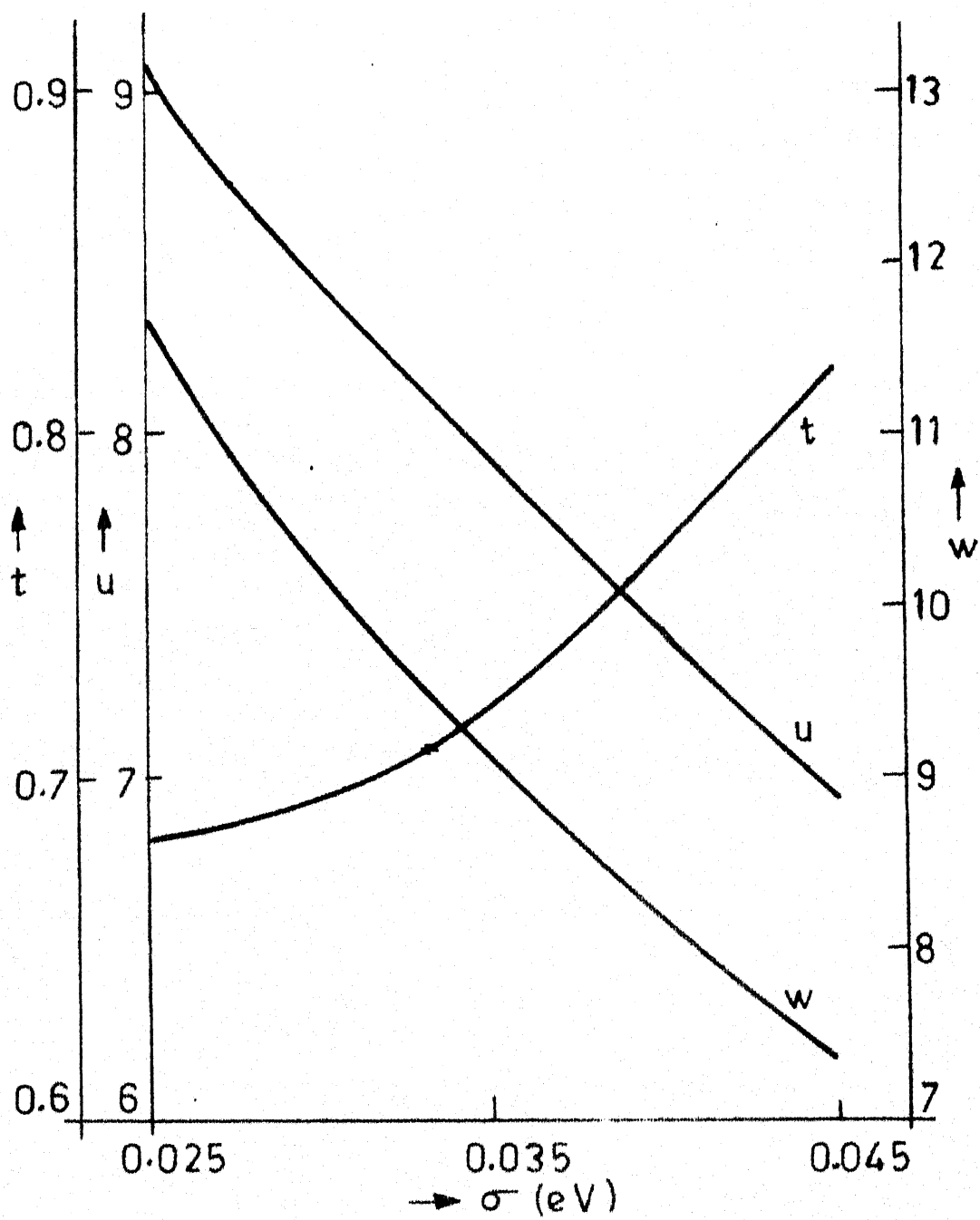


Fig.2.4(c) Plot of  $u, w$  and  $t$  versus  $\sigma$  with  $\bar{E}_0 = 0.065$  eV.

It is important to note that in the temperature range  $T_l \leq T \leq T_u$  the expression in eqn. (2.27) becomes negative, which indicates (from eqn. (2.19a)) that  $\partial (1/V_T)/\partial T$  is positive. This means that in this temperature range the value of  $(1/V_T)$  would increase with temperature, i.e.  $V_T$  would decrease with temperature. It is seen, however, that the rate of decrease in  $V_T$  is so small in this region that  $V_T$  can be regarded to be a constant. In the temperature range  $T < T_l$  and  $T > T_u$ , the value of  $V_T$  increases monotonically with temperature.

From the calculations presented in this section we see that there is no closed form relationship for the evaluation of  $V_T$ ,  $T_l$  and  $T_u$  in terms of  $\bar{E}_0$  and  $\sigma$ . This means that the value of  $\bar{E}_0$  and  $\sigma$  for a nonhomogeneous diode can be obtained only by template matching of the  $V_T$  versus  $\frac{kT}{q}$  plot. The steps to be followed for template matching are as follows.

(i) Compare the experimentally obtained  $V_T$  versus  $\frac{kT}{q}$  plot with the theoretically obtained plots for different  $\bar{E}_0$  with  $\sigma$  as a parameter. If the experimental plot matches with one of the theoretical plots, then the values of  $\bar{E}_0$  and  $\sigma$  are directly obtained as that of the theoretical plot which matches with the experimental one. In case the experimental plot does not match with any of the theoretical plots, it would then fall between the plots for two different

values of  $\sigma$  for a certain value of  $\bar{E}_0$ . This would give us the value of  $\bar{E}_0$  and the value of  $\sigma$  can be obtained by the method given in the next step.

(ii) Having obtained the value of  $\bar{E}_0$  using the relation  $T_l + T_u = (u-t) \times 100$ , the value of  $\sigma$  can be obtained from the corresponding plots of  $u$  and  $t$  as a function of  $\sigma$ .

As an illustration let us consider the plot of  $V_T$  versus  $\frac{kT}{q}$  given in Fig. (2.5) for a Au-nSi diode made in our laboratory. Comparing this plot with the various theoretical plots, we observe that it falls between the plots for  $\sigma = 0.035$  eV and  $\sigma = 0.025$  eV with  $\bar{E}_0 = 0.075$  eV. This gives us the value of  $\bar{E}_0$  to be 0.075 eV. From the experimental plot of  $V_T$  versus  $kT/q$  we obtain the value of  $T_l + T_u$  to be  $728^\circ\text{K}$ . Using the relationship  $T_l + T_u = 100 \times (u-t)$ , we get  $(u-t) = 7.28$ . From Fig. (2.5b) wherein a plot of  $u$ ,  $w$  and  $t$  versus  $\sigma$  is presented for  $\bar{E}_0 = 0.075$  eV, we obtain  $\sigma = 0.032$  eV for  $u-t = 7.28$ . Thus, we see that for the nonhomogeneous diode whose  $V_T$  versus  $kT/q$  plot is given in Fig. (2.5) the values of  $\bar{E}_0$  and  $\sigma$  are 0.075 eV and 0.032 eV respectively.

### 2.3 Summary

In this chapter, a study of the effect of fluctuations on the  $V_T$  versus  $T$  plot for a nonhomogeneous Schottky barrier diode has been carried out to identify the cause of ambiguity in the determination of the mechanism of current transport.



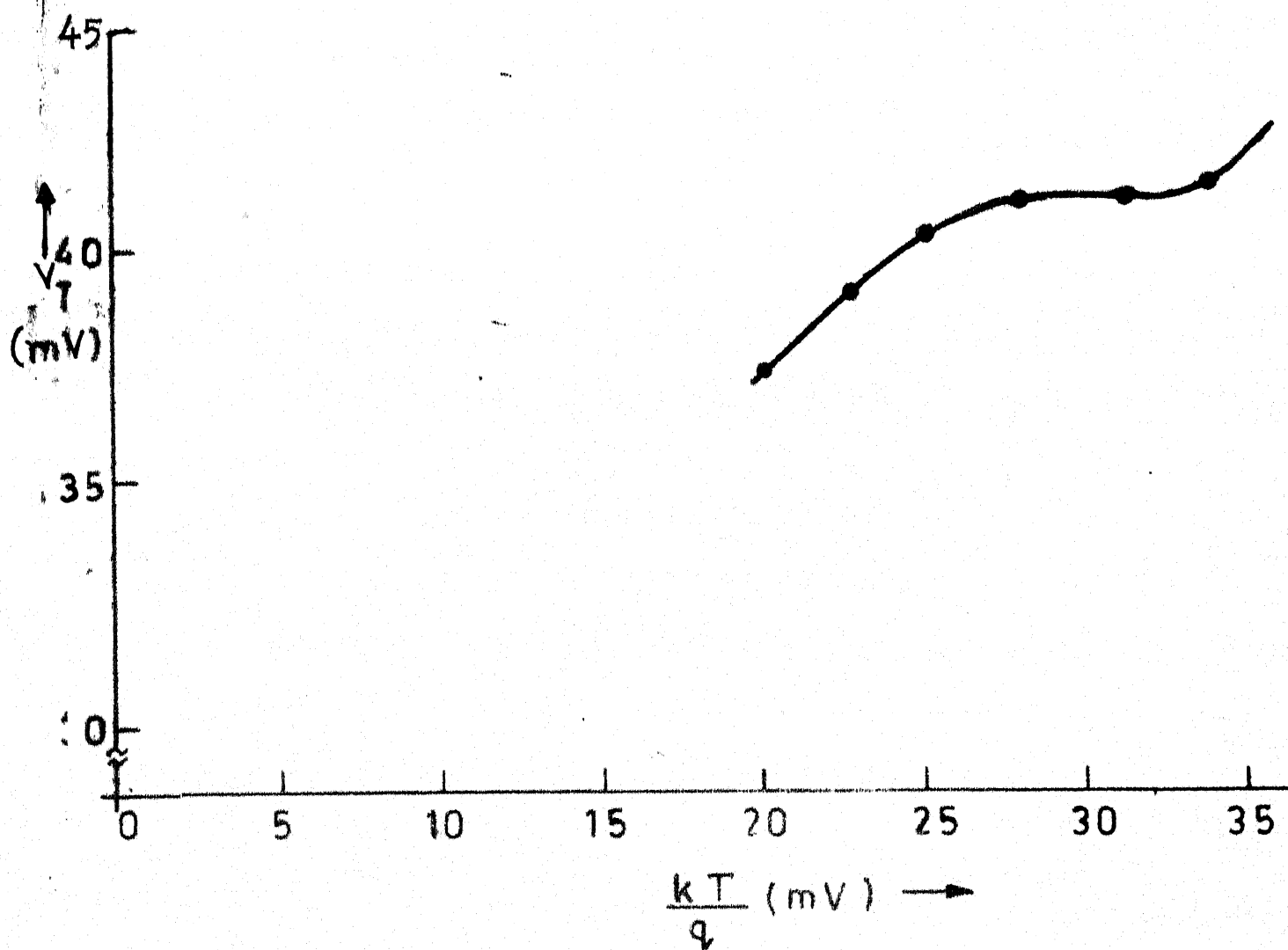


Fig.2.5 A Plot of  $V_T$  versus  $kT/q$  for a large area diode with  $N_D = 2.5 \times 10^{15} / \text{cm}^3$

I.I.T. KANPUR  
CENTRAL LIBRARY

Acc. No. A 62242

To do this the approach taken here is to look at the situation as one-dimensional with the fluctuation of parameter in the other dimension. This basically means that the non-homogeneous diode is considered to be composed of small homogeneous diodes, each identified by a particular value of the fluctuating parameter.

To identify the fluctuating parameters two kinds of diodes are considered viz. (i) diodes with a thin intervening oxide layer of thickness ' $\delta$ ' between the metal and the semiconductor (Tunnel MIS diodes [18]), and (ii) diodes showing  $T_0$  effect. The fluctuating parameter in the MIS diode is identified to be the oxide thickness ' $\delta$ '. In the diodes showing  $T_0$  effect, the fluctuating parameter has been identified to be  $E_0$ , the characteristic energy defining the exponential distribution of the surface states.

It is seen that the ambiguity that arises in the determination of the current transport from the  $V_T$  versus  $\frac{kT}{q}$  plot can be explained through the fluctuations in  $E_0$ . It has also been shown that the ambiguity has arisen due to the measurements having been carried out in a restricted range of temperature. One way to resolve this ambiguity is to check the  $V_T$  versus  $\frac{kT}{q}$  behaviour over a larger range of temperatures, extended preferably in the lower temperature range. The importance of the extension of the temperature

range of measurement in the lower temperatures will be clear from the following discussions.

Extension of the temperature range of measurements only to the higher temperatures would not resolve the ambiguity, as a monotonic increase after a flat region in the  $V_T$  versus  $\frac{kT}{q}$  plot also represents the case of thermionic field emission being the mechanism of current transport [7]. On the other hand, a monotonic increase in  $V_T$  with temperature at lower temperatures followed by a plateau, possibly occurs only in the presence of fluctuation of parameters in a nonhomogeneous diode.

Having presented the theoretical calculations in the effect of fluctuations in  $T_0$ , we shall go over to the experimental verification of the same in the next chapter.

## CHAPTER 3

### EXPERIMENTAL STUDY OF THE EFFECT OF FLUCTUATIONS IN $E_0$

In the previous two chapters, we have postulated and theoretically demonstrated that in the case of Schottky barrier diodes the temperature dependence of the ideality factor is affected by the fluctuation in some parameters. In this chapter an experimental verification of this fact is given. This has been done on metal (Au)-n Silicon Schottky barrier diodes which have been fabricated in our laboratory for this purpose.

The basic aims of this investigation are the following:

(i) It has been observed by Padovani [1] that several small area Au-nGaAs diodes made on the same wafer exhibited different values of  $T_0$ . It should be recalled that this observation had provided the starting point for the theoretical model given in the previous chapters. Thus, before this theoretical model could be applied to any system, it must be experimentally checked that  $T_0$  was different on several small area diodes made on the same wafer. The first aim in this chapter is to experimentally investigate whether

such fluctuations take place in case of metal-n silicon diodes. If the answer is in the affirmative then one proceeds to the step given below.

(ii) It is obvious that the theoretical analysis of a device in which the parameters are different at different points of area would require a two-dimensional analysis because transverse currents can flow. Only in the case that the role of the transverse current is not dominant that a simpler theoretical analysis using one-dimensional equations but with fluctuations superimposed can be done. It should be recalled that we have used the latter approach in the theoretical model developed in Chapters I and II. Thus, we have inherently assumed that the role of the transverse current is not important in explaining the temperature variation of the ideality factor. Our interest now is in checking whether this assumption holds true in the case of metal-n Silicon diodes. We have designed a simple experimental procedure to check this point. The basic idea is as follows. Prepare a large number of isolated small area diodes and measure the  $T_0$  in each. If the  $T_0$ 's are different then connect a few of the diodes in parallel and measure the temperature variation of ideality factor. If this plot shows features similar to the temperature variation in an identical system but with a large area then obviously the role of the transverse current is not dominant and the assumption made

earlier would hold good. Otherwise a two dimensional theoretical model should be developed.

The details of the experiment and the results are given later (sec. 3.3 and 3.4) after describing the fabrication of the diode (sec. 3.1 and 3.2). Since the leakage current of a Schottky barrier diode hinders the interpretation of the experimental results, we start the discussion with a study of the guard rings which suppress the leakage current.

### 3.1 Guard-ring Structures

A major problem in the case of Schottky barrier diodes made on low-doped semiconductors arises due to the presence of large surface leakage currents. The surface leakage currents are comparable to the normal diode currents, which would flow under reverse bias and small forward bias. Thus, it becomes obvious that for any meaningful interpretation of current voltage relation in these cases, the surface currents must be suppressed. The method commonly used to suppress or reduce the leakage current is to employ guard ring structures [1]. In published literature three kinds of guard ring structures are used, and are shown in Fig. 3.1.

The first type shown in Fig. 3.1a uses an extension of the metal film over the passivating oxide layer. This is referred to as the MOS guard ring (MOSGR) structure. The

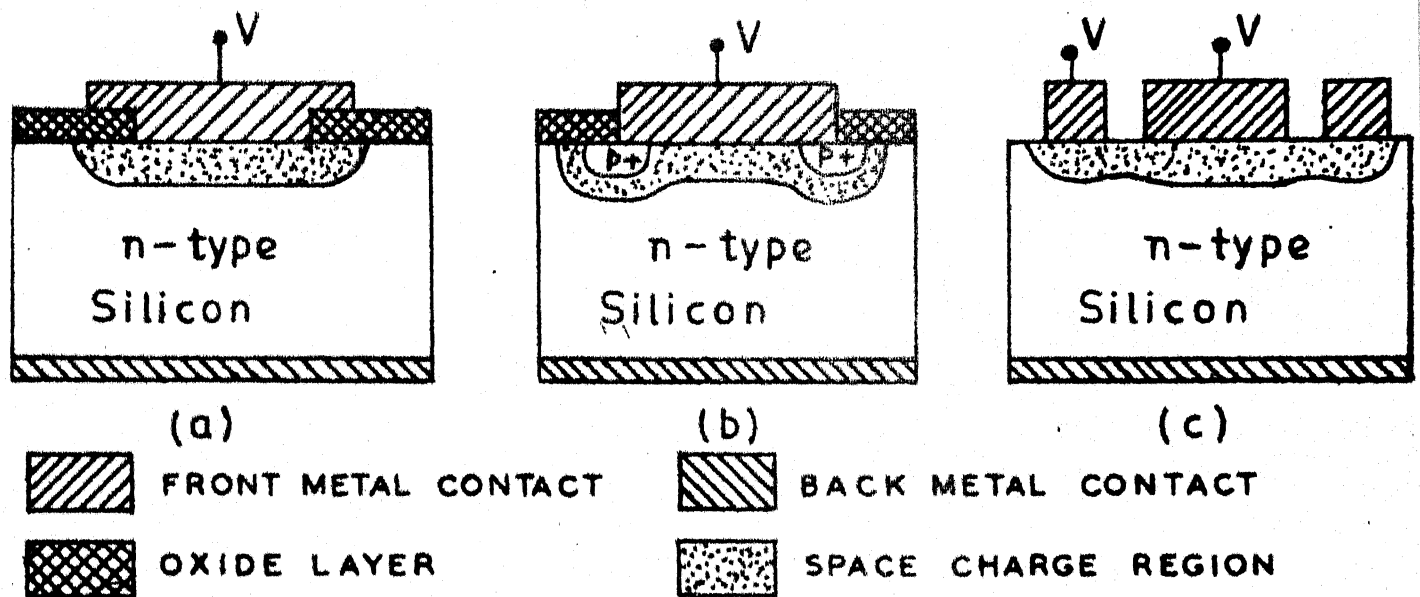


Fig.3.1 The three kinds of guard ring structures used in literature. (a) Mos guard ring (b) p-n junction guard ring (c) Auxiliary Schottky barrier guard ring.

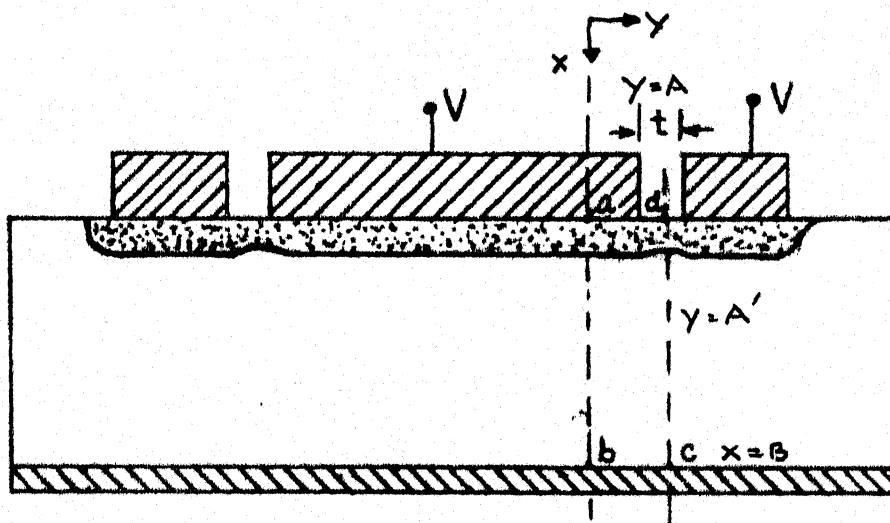


Fig.3.2 A cross-sectional elevation of a Schottky barrier diode with an auxiliary Schottky barrier guard ring structure. The rectangle  $abcd$  marks the boundary of the region over which the Poisson's equation is solved.

MOSGR acts as a field plate to keep the underlying surface in depletion when the diode is either reverse biased or slightly forward biased, thus reducing the excess currents at the corners [2]. The second type is shown in Fig. 3.1b and uses a diffused p-n junction guard-ring. Similar to the MOSGR here also the guard ring keeps the underlying structure in depletion, thus reducing the currents at the corners [3]. The third kind of guard ring structure is shown in Fig. 3.1c and uses an auxiliary Schottky barrier diode surrounding the main diode at a small distance, usually of the order of 1 mil [1]. In this structure the two dimensional nature of the potential distribution is exploited to obtain the guard ring action by biasing the auxiliary diode in such a manner as to form a space charge channel between the main diode and the auxiliary diode, thus reducing the field at the edges of the main diode [4].

Due to the ease of fabrication and the simplicity of the measurement set up for an unencapsulated device, we have used MOS guard ring structure. It is important to note that the yield using this type of a guard ring is poor. To overcome this, we have fabricated a number of devices and have chosen those devices which satisfied the following conditions:

- (i) The current density under a reverse bias of 10 V is less than  $5 \text{ mA/cm}^2$  at room temperature.



- (ii) The diode does not show time-dependent I-V characteristic i.e. the meter readings do not show any appreciable fluctuations.

This gave an yield of 25 percent for roughly one hundred diodes fabricated. In cases where the yield of the device assumes importance, one will have to go either for a diffused p-n junction guard ring structure or an auxiliary Schottky barrier guard ring structure.

Normally the thickness of the passivating oxide layer used in the MOSGR structure is of the order 2000-4000 Å. In the present case we have used an oxide thickness of about 200 Å - 300 Å and the reason for the reduced oxide thickness will be clear from the following discussion.

It has been shown by Yu and Snow [5] and Kano et al. [6] that when the underlying surface in the MOSGR is accumulated or inverted the guard ring action of the MOSGR fails and it contributes towards an increase in the surface leakage current, rather than suppressing it. In our case, we are thus interested in increasing the accumulation voltage and also see that in the range of forward bias used the underlying surface remains to be depleted. Based on the observation made by Kar [7], that the flatband voltage in metal-SiO<sub>2</sub>-n-Si system decreases with an increase in the oxide thickness, the MOSGR guard ring is used with an oxide thickness much less than the thickness normally used in literature [5,6]. Note that the accumulation voltage obtained in our

laboratory for an MOS diode (Au-nSi system) with an oxide thickness of 200-300 Å at room temperature is found to be in the range of 0.7V to 1.0V, which goes far enough into the forward bias region not to affect the forward I-V characteristics.

Before proceeding further, let us digress a little and briefly look into the design guidelines for an auxiliary Schottky barrier diode guard ring.

### 3.1.1 Design guidelines for an auxiliary Schottky barrier diode guard ring structure

A perusal of the literature on the auxiliary Schottky barrier diode guard ring structure shows that, though it has been extensively used by several authors [1,4,8], the spacing of the auxiliary diode and the main diode is chosen very arbitrarily. In this section we attempt to give a design guideline for the spacing between the main diode and the auxiliary diode.

The choice of the spacing between the main diode and the auxiliary diode is governed by the effectiveness of the auxiliary diode in modifying the field at the edges of the main diode. This means that to choose the proper spacing between the two diodes, a knowledge of the field profile for different spacing is necessary. The field profile is obtained by solving the two-dimensional Poisson's equation

with the proper boundary conditions.

The Poisson's equation, considering the mobile carriers (majority carriers) and the charge due to ionised donors ~~in the depletion region~~, can be written as [9],

$$\frac{\partial^2 V}{\partial X^2} + \frac{\partial^2 V}{\partial Y^2} = \frac{qN_D}{\epsilon_s} [1 - \exp(\frac{-qV}{kT})] \quad (3.1)$$

Normalising the potential with respect to the band bending given by  $(-V + \phi_B - \phi_f)$  where  $V$  is the applied potential, the distances with respect to the depletion width, and the charge density with respect to  $(qN_D)$ , we have,

$$\frac{\partial^2 \phi}{\partial x^2} + \frac{\partial^2 \phi}{\partial y^2} = 2[1 - \exp(-\phi_s \phi)] \quad (3.2)$$

where  $\phi_s = q(-V + \phi_B - \phi_f)/kT$ .

Note that Fig. 3.2 gives the cross-section of a Schottky barrier diode with an auxiliary Schottky barrier diode. The boundaries for the solution of the Poisson's equation marked by the rectangle abcd.

Considering the half width of the auxiliary diode to be greater than thrice the 'depletion width' under all bias of interest (see Appendix C), we can write the boundary conditions (refer Fig. 3.2)).

(i) Along ad

$$\phi(0, y) = 1.0 \quad 0 < y < A \quad (3.3a)$$

and from the continuity of potential and displacement vector we have,

$$\phi(O^+, y) = \phi(O^-, y) \quad A < y \leq A'$$

$$\eta \frac{\partial}{\partial x} \phi(O^+, y) - \frac{\partial}{\partial x} \phi(O^-, y) = 0 \quad A < y \leq A' \quad (3.3b)$$

$$\text{where } \eta = \epsilon_s / \epsilon_0.$$

(ii) Along dc

From symmetry conditions

$$\frac{\partial}{\partial y} \phi(x, A') = 0 \quad (3.4)$$

(iii) Along bc

$$\phi(B, y) = 0 \quad 0 \leq y \leq A' \quad (3.5)$$

(iv) Along ab

From symmetry conditions,

$$\frac{\partial}{\partial y} \phi(x, 0) = 0 \quad 0 \leq x \leq B \quad (3.6)$$

The details of the solution of eqn. (3.2) with the boundary conditions given in eqn. (3.3a) to eqn. (3.6) is given in Appendix D, and here we present only the results of the computations. It should be emphasized that these results are in normalized form, hence are of general value. The normalization factors of all the relevant parameters are given in Table 3.1.

Fig. 3.3 gives the constant electric field magnitude profile under reverse bias in the absence of a guard ring

Table 3.1. Normalisation factors used in the solution of two dimensional Poisson's equation.

S.No.	Parameter	Normalising Factor	Expression for the Normalising Factor
1	Distances (x and y)	Depletion width W	$W = \sqrt{\frac{2\epsilon_s}{qN_D} (\phi_B - V - \phi_f - \frac{kT}{q})}$
2	Charge ( $\rho$ )	Charge due to the ionized donors ( $\rho$ )	$\bar{\rho} = q_{ND} \text{ (complete ionization assumed)}$
3	Field ( $\mathcal{E}$ )	Half the field ( $\mathcal{E}_s$ ) at the surface for the one-dimensional case	$\mathcal{E}_s = \sqrt{2qN_D\epsilon_s (\phi_B - V - \phi_f - \frac{kT}{q})}$
4	Potential ( $v$ )	Band bending ( $v_b$ ) in the semiconductor.	$v_b = (-V + \phi_B - \phi_f)$

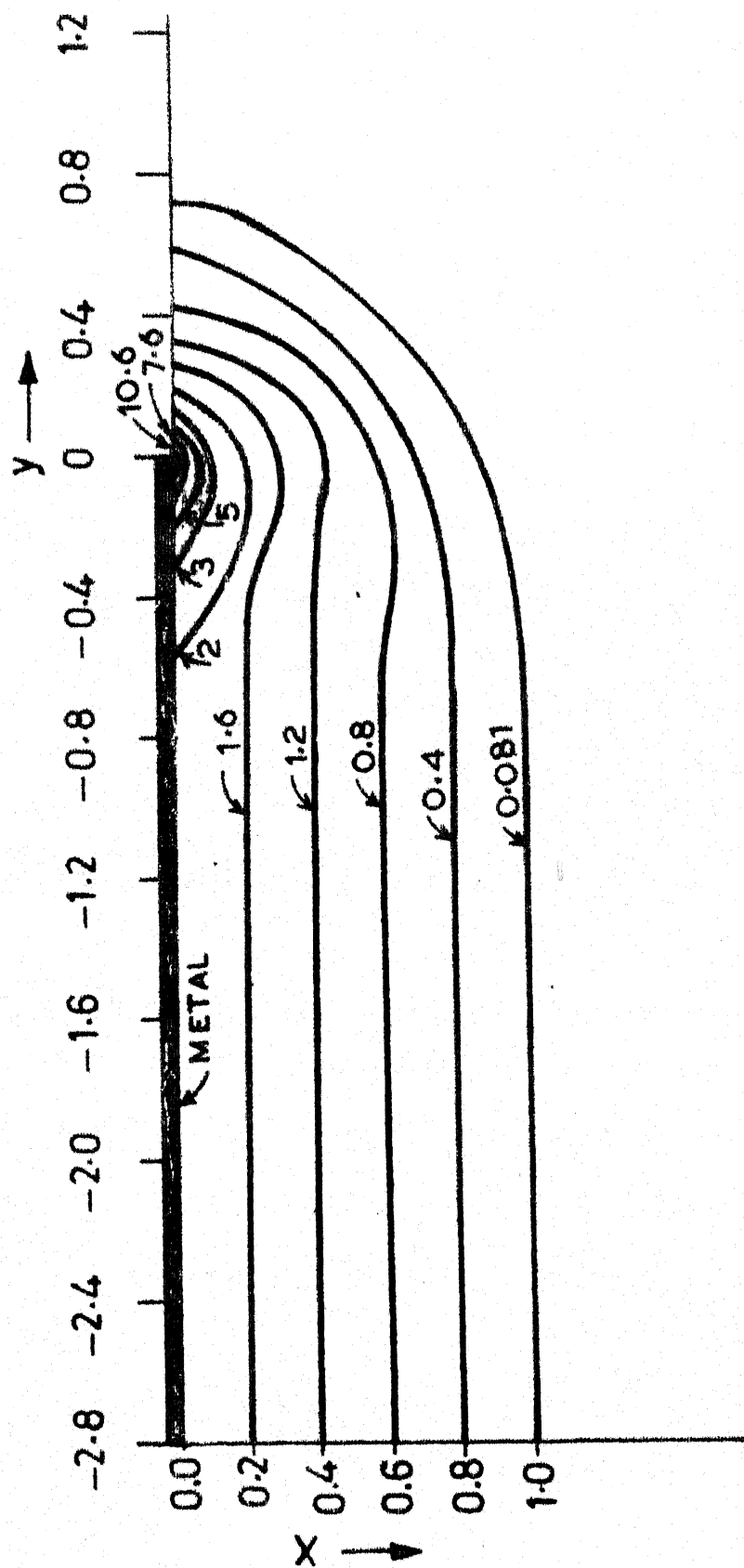


Fig.3.3 Constant field profile near the edge of a Schottky barrier diode without a guard ring.

structure, whereas Fig. 3.4 gives a plot of the constant electric field magnitude profile for three different spacings at a constant bias (zero bias with  $\phi_B = .8$  volts). The following features of the figures should be noted:

(1) In the absence of a guard ring structure (Fig. 3.3) the field at the edge of the metal gets to be as high as 8 to 10 times the field at the interior.

(2) In the presence of a guard ring (Fig. 3.4), we see that as the spacing is reduced the edge field decreases due to an enhanced interaction between the main diode and the auxiliary diode. This in turn reduces the edge current, thus improving the I-V characteristics of the main diode. Denormalising the distances we see that, for a base resistivity of 30 Kohm-cm, a spacing of 0.3 mm [4] would show a guard ring effect from zero bias onwards, whereas for a base resistivity of 10 Kohm-cm, it would require a spacing of about 0.15 mm. Based on the above observations we see that lower the resistivity of the semiconductor base, lower would be the spacing required to achieve the guard ring effect.

To summarise, one observes from the plots given in Figs. (3.3) and (3.4), that for an effective guard ring action, one requires the spacing at the maximum forward bias

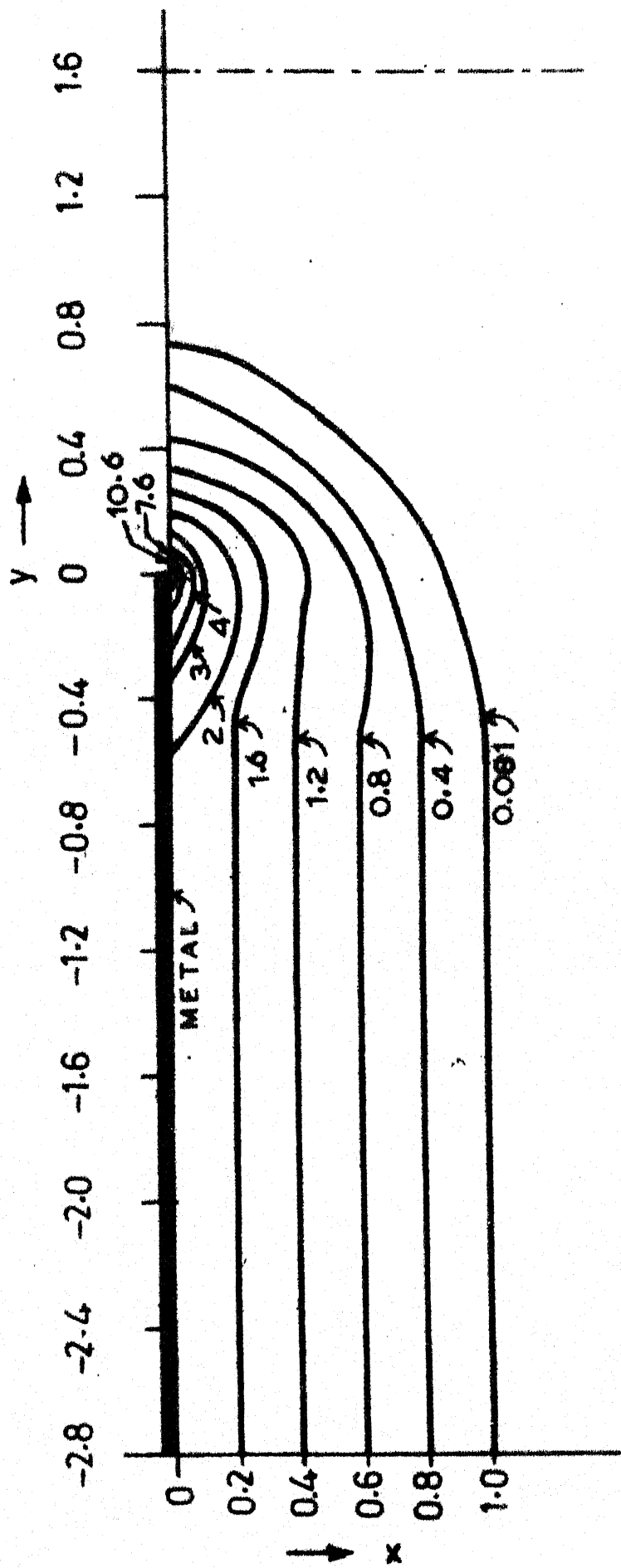


Fig.3.4(a) Constant field profile near the edge of a Schottky barrier diode with a guard ring at a distance of 3.2W .



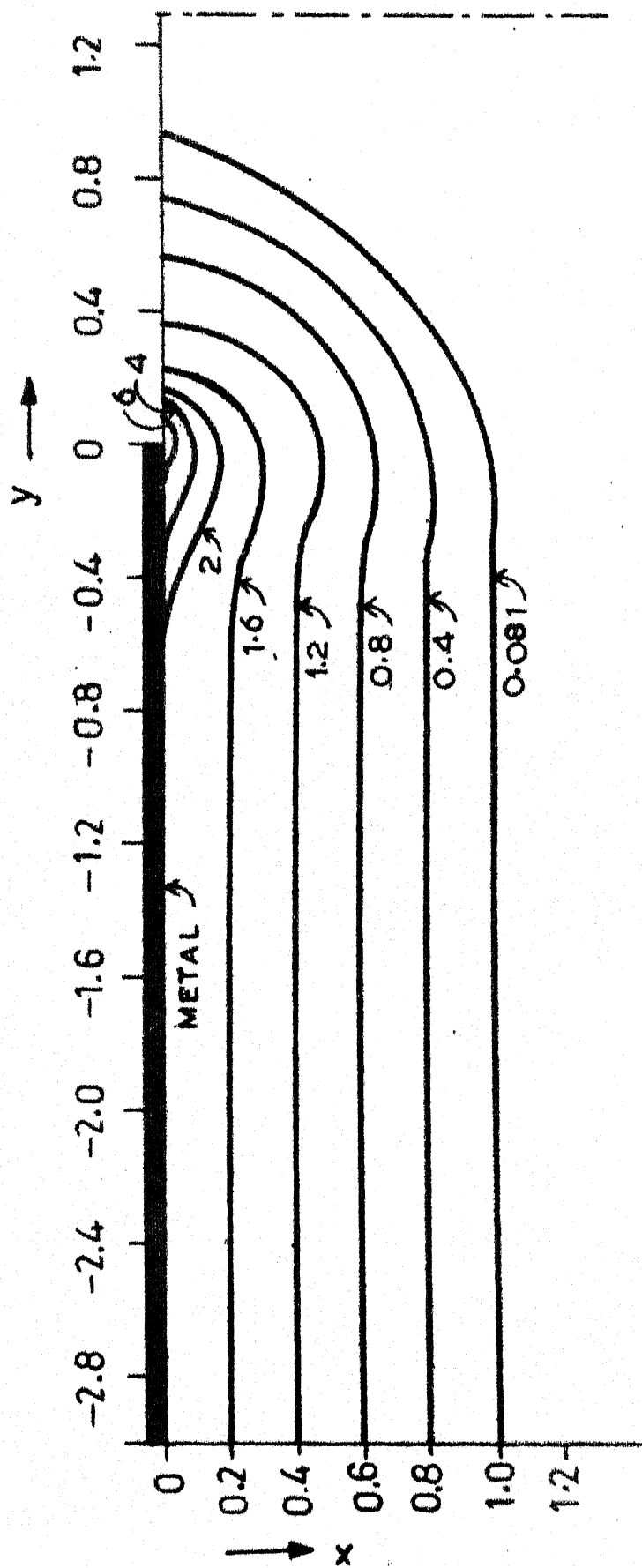


Fig. 3.4(b) Constant field profile as the edge of a Schottky barrier diode with a guard ring at a distance of 2.5 W .

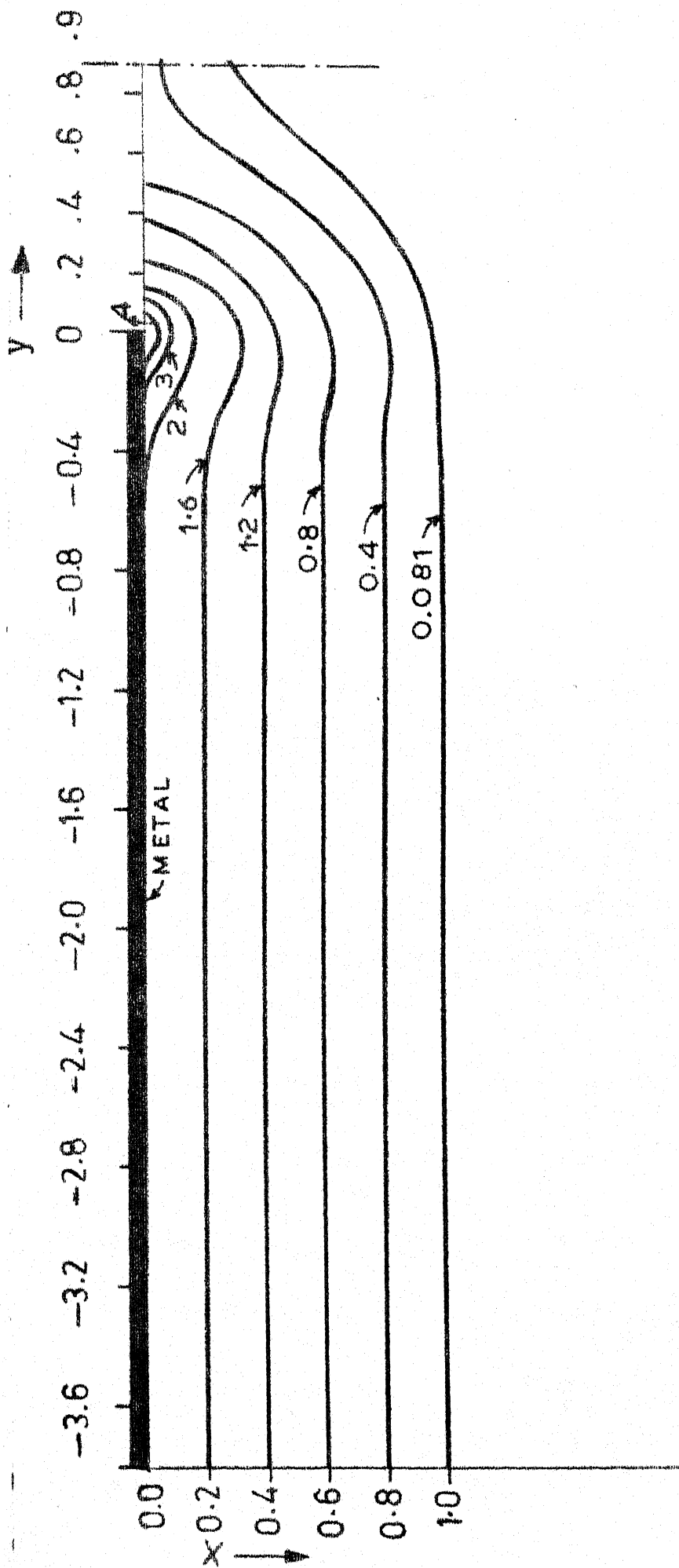


Fig.3.4(c) Constant field profile at the edge of a Schottky barrier diode with a guard ring at a distance of 1.8 W.

beyond which the leakage current is negligible, to be less than 2.5 times the depletion width at that bias.

Having looked into the choice of guard ring structure for the diodes under study, we now go over to the details of fabrication and the experimental setup in the next section.

### 3.2 Details of Fabrication and the Experimental Setup

In the first part of this section we present the details of diode fabrication in our laboratory and in the second part a description of the experimental setup is given.

#### 3.2.1 Details of fabrication

In Fig. 3.5 we present a flow diagram of the fabrication process for Au-n Silicon Schottky barrier diodes. The following points about the fabrication is to be noted:

(i) All the chemicals used in the cleaning of the silicon wafer are of electronic grade. (ii) Initially an oxide of 1500 Å thick is grown, which is later reduced to about 200-300 Å, after cutting windows in the oxide layer. This is necessary because better results are obtainable in photolithography with thicker oxides. After the completion of the fabrication process, the device is taken (without encapsulation) to the measurement table.

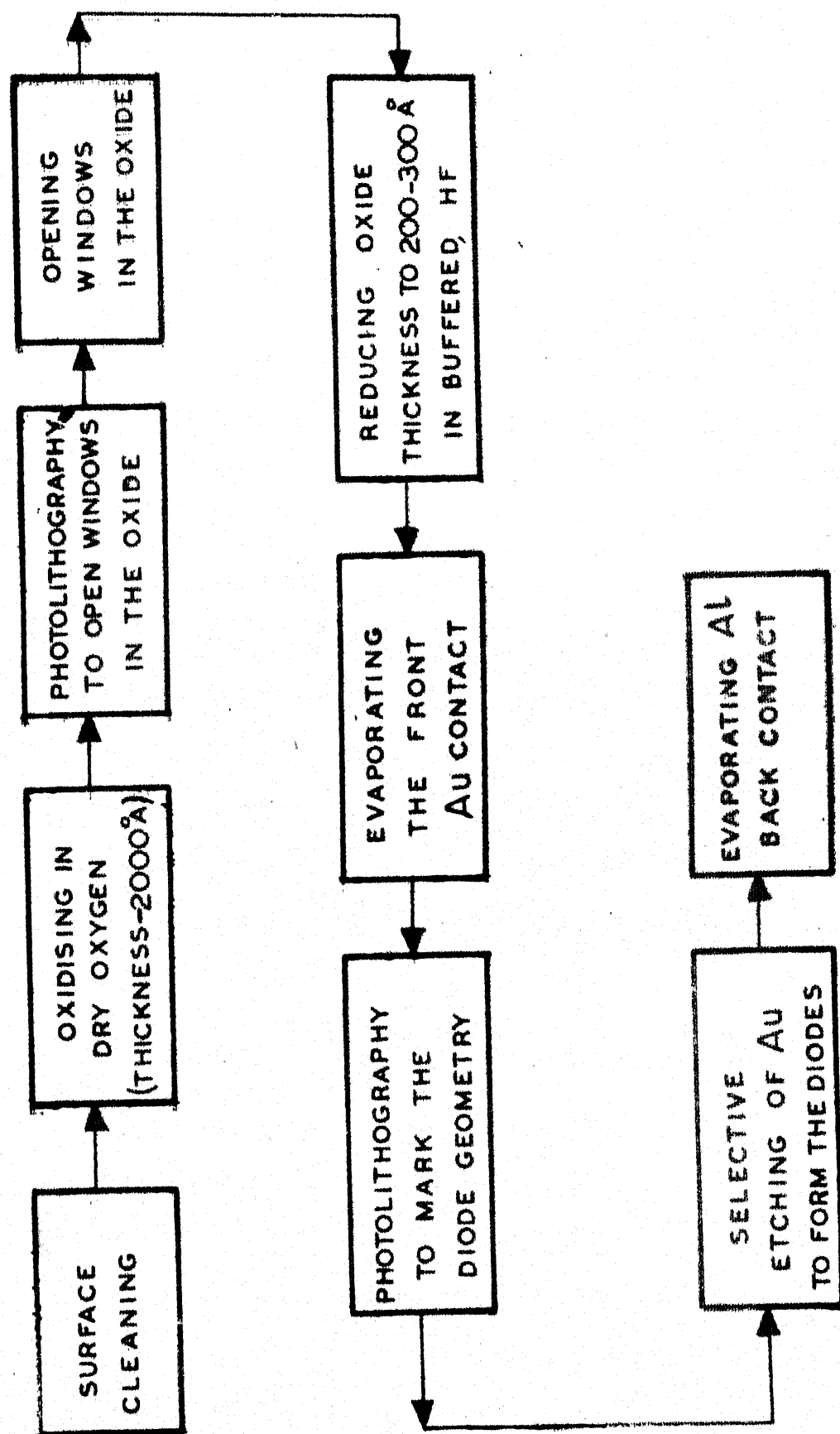


Fig.3.5 A Flow diagram showing the diode fabrication process.

### 3.2.2 Details of the Measurement setup

The details of the measurement setup are shown in Fig. 3.6; Fig. 3.6a shows the block diagram of the setup for the current-voltage (I-V) measurements and Fig. 3.6b shows the setup for the capacitance-voltage (C-V) measurements. The meters used for measuring voltage and current are standardized with respect to a standard source and the error bar is found to be about  $\pm 1\%$  over most of the range of interest in the I-V measurements. In the .1V range of the digital multimeter the error bar was about  $\pm 3\%$ .

The variation of the temperature of the sample from 80°K onward is obtained by using an arrangement shown in Fig. (3.7). Several choices were considered for obtaining a variation in the operating temperature of the device under test. The major constraint under which the choice had to be made was that the samples did not have bonded leads, hence a probe had to be used for making electrical contact to the front metal contact. The main difficulty in providing for the movement of a probe on cooled sample ensues from the fact that moisture quickly gets deposited on cooled exposed sample. To obviate this difficulty the system is designed in such a fashion that a positive pressure of dry nitrogen was always maintained near the sample.

The setup consists of a copper rod of 1 inch diameter held inside a copper tube of 1.5 inch diameter. The inner

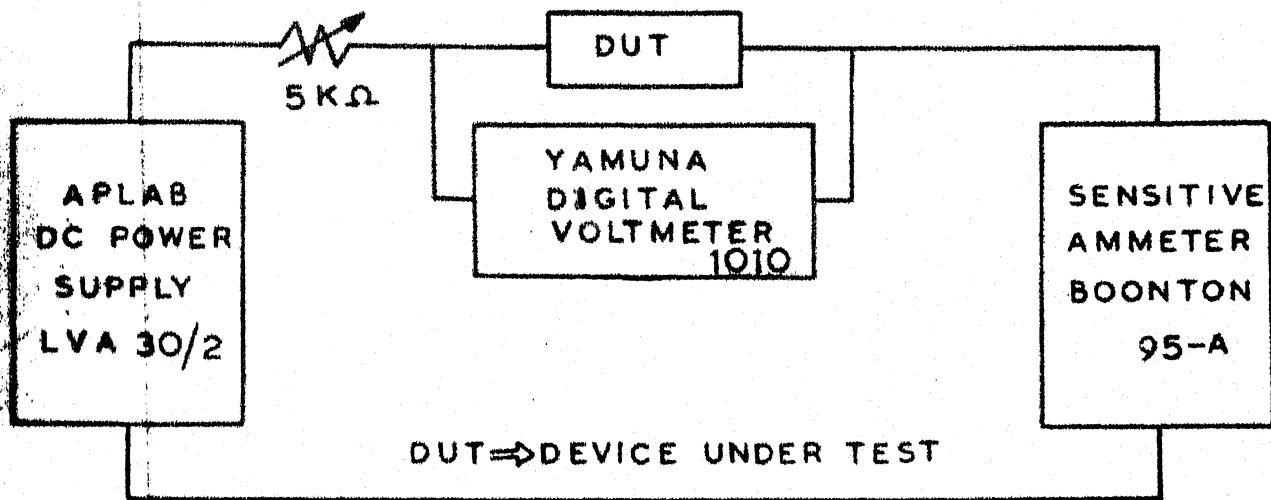


Fig.3.6(a) Block diagram of the I-V measurement setup.

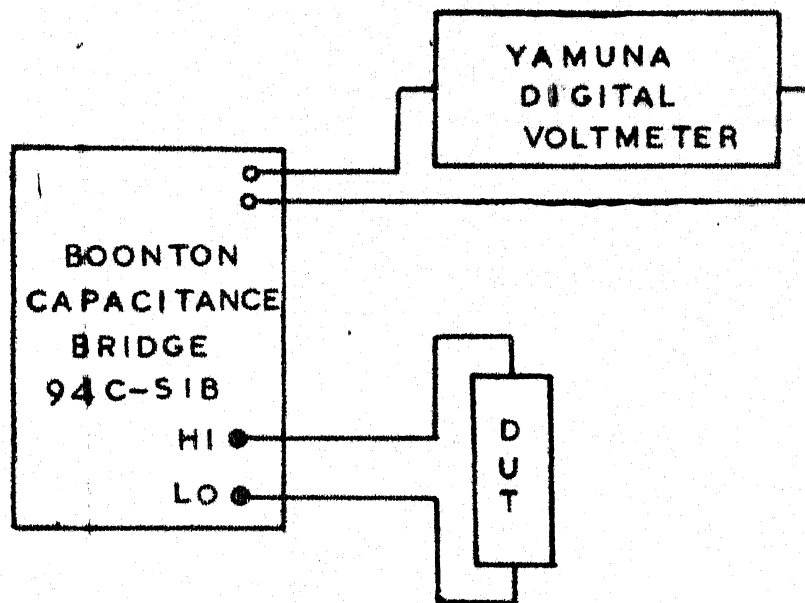


Fig.3.6(b) Block diagram for the C-V measurement setup.

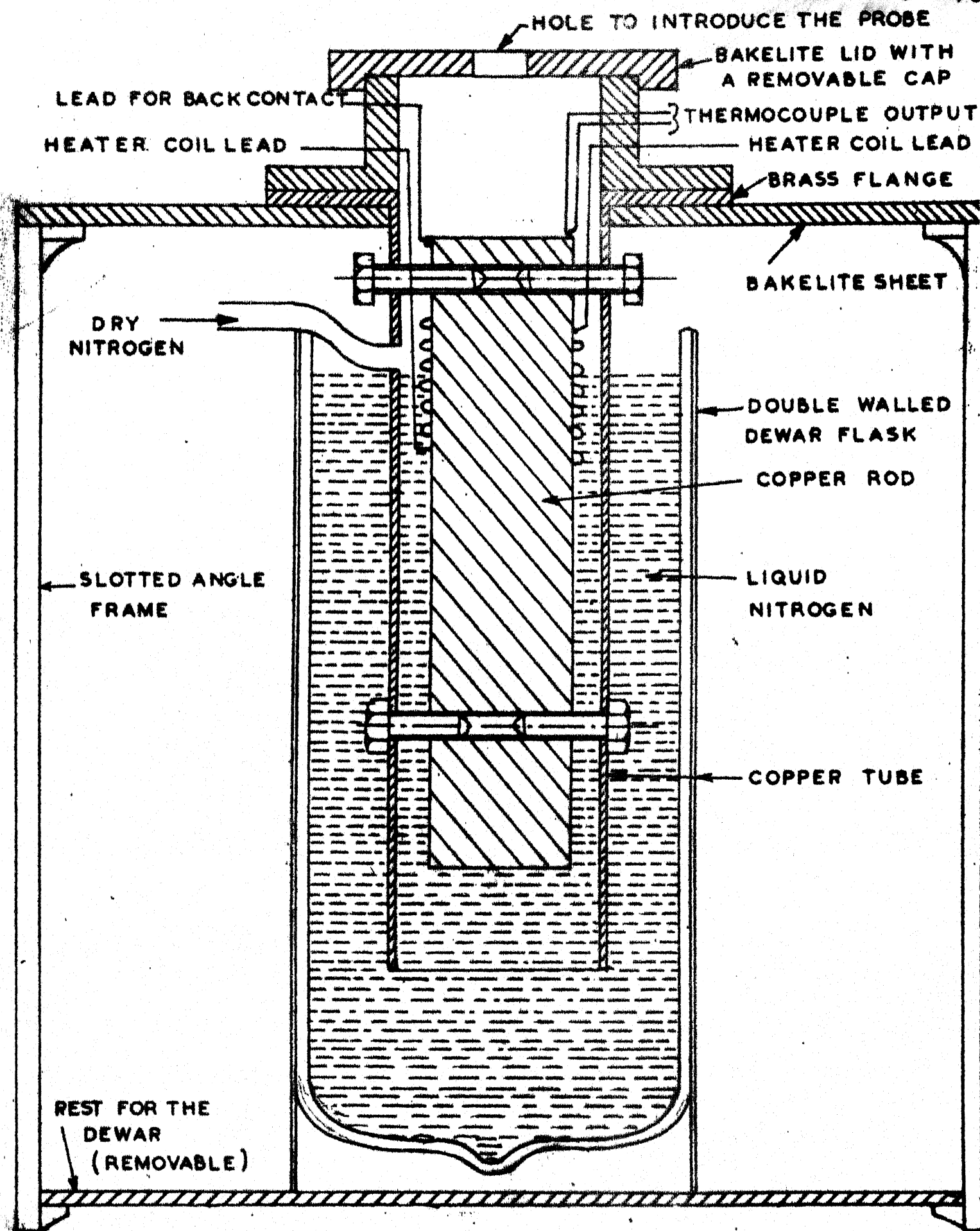


Fig.3.7 A cross-sectional elevation of the arrangement used to obtain controlled temperature from  $80^{\circ}\text{K}$  onwards.

copper rod is used for mounting the sample under test and carries a few windings of Nichrome heater coil at the top to vary the temperature. The copper tube with the copper rod is suspended from a bakelite sheet mounted on a slotted angle frame. The copper tube is fixed to the bakelite sheet at one end by means of a brass flange attached to the copper tube. Apart from supporting the copper rod, the tube also serves as a jacket around the copper rod, through which a continuous flow of dry nitrogen is maintained. The dry nitrogen is introduced into the copper tube through a small hole in the tube just below the bakelite sheet.

The portion of the copper tube carrying the copper rod which is below the bakelite sheet is introduced into a Dewar. The other end is closed with a bakelite lid, after loading the device under test. The bakelite lid has a central hole to introduce the contact probe. The central hole in the lid also functions as an outlet for the stream of dry nitrogen. Before filling up the Dewar with liquid nitrogen, the whole system is first completely flushed with dry nitrogen to remove any trace of air in the system.

The temperature variation is obtained by heating the copper tube to varying degree. This set up gives us a controlled temperature from  $80^{\circ}\text{K}$  onwards, correct to  $\pm 2^{\circ}\text{K}$ . The temperature of the system is measured at the top of the



rod using an Iron-Constantan thermocouple. The thermocouple was standardized at liquid nitrogen temperature, melting ice temperature, room temperature and at boiling water temperature, with the reference junction kept in a melting ice bath.

This brings us to the end of the description of the fabrication method and the measurement setup. In the next section we present a method for characterizing a Schottky barrier diode showing  $T_0$  effect.

### 3.3 Characterisation of a Schottky Barrier Diode Showing $T_0$ Effect

Before presenting the result of experimental investigation, let us consider the methods for the evaluation of some of the parameters of interest in a homogeneous diode exhibiting  $T_0$  effect. These parameters are  $E_0$ , the energy characterising the assumed exponential distribution of surface states of the equivalent Levine's model,  $\phi_{B0}$ , the barrier height at zero bias;  $\phi^*$ , the neutral level at the surface measured from the bottom of the conduction band, and  $D_{s0}$ , the surface state density at the neutral level. Methods for the determination of each of these parameters are given below.

#### 3.3.1 Determination of $E_0$

The value of  $E_0$  can be determined both from the forward and the reverse I-V data [10]. We present the method of

determining  $E_0$  from the reverse and the forward I-V data one by one.

(i) Evaluation of  $E_0$  from the reverse I-V data:

Under a reverse bias  $V > \frac{3kT}{q}$ , the reverse current  $I_R$  can be written as,

$$I_R = A^* T^2 \exp(-q \phi_B / kT) \quad (3.8)$$

From eqn. (1.14), for  $Q_{sc} \gg Q_f$ , we have

$$\phi_B = \phi^* - \frac{E_0}{q} \ln \left( \frac{Q_{sc}}{Q_f} \right) \quad (3.9)$$

hence we can rewrite eqn. (3.8) as,

$$I_R = A^* T^2 \exp \left( -\frac{q \phi^*}{kT} \right) (Q_{sc})^{E_0/kT} (Q_f)^{-E_0/kT} \quad (3.10a)$$

$$= I^* (\epsilon_s)^{E_0/kT} \quad (3.10b)$$

$$\text{where } I^* = A^* T^2 \exp \left( \frac{-q \phi^*}{kT} \right) (Q_f)^{-E_0/kT} (\epsilon_s)^{E_0/kT} \quad (3.11)$$

$$\epsilon_s = \frac{Q_{sc}}{\epsilon_s} = \sqrt{\frac{2qN_D}{\epsilon_s}} \left( \phi_B - V - \phi_f - \frac{kT}{q} \right) \quad (3.12a)$$

$$= \sqrt{\frac{2qN_D}{\epsilon_s}} (-V + \alpha) \quad (3.12b)$$

$$\text{where } \alpha = \left( \phi_B - \phi_f - \frac{kT}{q} \right)$$

From eqns. (3.10b) and (3.12a) we see that a plot of  $\ln I_R$  versus  $\ln (-V + \alpha)$  will be a straight line of slope  $m_2 = (E_0/2kT)$  and the value of  $E_0$  can be obtained from this slope using the relation,

$$E_0 = 2kT m_2 \quad (3.13)$$

It should be noted here that in our studies we have taken a mean value of  $\alpha = 0.4V$  at all temperatures.

(ii) Evaluation of  $E_0$  from the forward I-V data:

A method of evaluating  $E_0$  from the forward I-V data has been proposed by Levine [10] and is as follows:

From eqn. (1.21a) we obtain the voltage dependence of  $T_0$  of the form,

$$\frac{1}{T_0} = \frac{2q}{E_0 T} (\phi_B - V - \phi_f - \frac{kT}{q}) \quad (3.14)$$

This equation predicts that a plot of  $\frac{1}{T_0}$  versus  $V$  would be a straight line (taking  $\phi_B$  to be a slowly varying function of voltage) with a slope ( $m$ ) given by,

$$m = \frac{\partial \frac{1}{T_0}}{\partial V} = \frac{2q}{E_0 (T + T_0)} \quad (3.15)$$

Note that the slope 'm' has been obtained from eqn. (3.14), using the relation,

$$\frac{\partial \phi_B}{\partial V} = \frac{T_0}{T + T_0} \quad (3.16)$$

Let the value of  $T_0$  and  $m$  evaluated at a mean value of  $\bar{V}$  be called  $\bar{T}_0$  and  $\bar{m}$  respectively. Then we can obtain  $E_0$  by using  $\bar{m}$  and  $\bar{T}_0$  in eqn. (3.15).

We suggest that if a plot of  $1/T_0$  versus  $\ln I$  is used, rather than the  $1/T_0$  versus  $V$  plot, then it is easier to

determine  $E_0$ . The reasons for this can be seen from eqn. (1.21b), which is reproduced below:

$$\frac{1}{T_0} = -\frac{2k}{E_0} [\ln (I/A^*T^2S) + b + 1] \quad (3.17a)$$

$$= -\frac{2k}{E_0} [\ln I + b + 1 - \ln (A^*T^2S)] \quad (3.17b)$$

where  $I$  is the current flowing in the diode. From eqn. (3.17a) we see that the plot of  $\frac{1}{T_0}$  versus  $\ln I$  will be a straight line of slope  $m_1 = -2k/E_0$ . Therefore, one can obtain the value of  $E_0$  from the slope  $m_1$  using the relation,

$$E_0 = -\frac{2k}{m_1} \quad (3.18)$$

where  $k$  is the Boltzmann's constant.

The advantage of using the  $\frac{1}{T_0}$  versus  $\ln I$  plot compared to the  $\frac{1}{T_0}$  versus  $V$  plot lies in the fact that while  $\frac{1}{T_0}$  versus  $V$  is approximated to be a straight line, the  $\frac{1}{T_0}$  versus  $\ln I$  plot is an exact straight line.

### 3.3.2 Determination of $\phi_{B0}$

The barrier height at zero bias,  $\phi_{B0}$ , can be obtained from (i) a plot of  $\frac{1}{T_0}$  versus  $V$ , (ii)  $\frac{1}{C^2} - V$  plot and (iii) the extended saturation current from the forward I-V relationship. Let us briefly look into these methods one by one.

(a) From  $1/T_0$  versus  $V$  plot :

By requiring the plot of  $\frac{1}{T_0}$  versus  $V$  to be approximated by a straight line with an intercept  $V_i$ , it has been shown by Levine that the mean value of  $\phi_{BO}$  is less than  $\phi_i$  the barrier height at the voltage  $V_i$ , by an amount  $\frac{E_0}{2q}$  [10]. Thus,  $\phi_{BO}$  can be obtained from the intercept of the  $\frac{1}{T_0}$  versus  $V$  plot as,

$$\phi_{BO} = \phi_i - \frac{E_0}{2q} = V_i + \phi_f + \frac{kT}{q} - \frac{E_0}{2q} \quad (3.19)$$

(b) From the forward  $I$ - $V$  plot :

It has been shown by Levin [10] that the forward current  $I$ , at any voltage  $V$  can be written of the form,

$$I = I_{se} \exp(qV/k(T+T_0)) \quad (3.20)$$

where  $I_{se}$  = the intercept of the tangent at a current  $I$  on the current axis

$$= SA^* T^2 \exp(-q\phi_{BO}/k(T+T_0)) \quad (3.21)$$

From eqn. (3.21) we see that we can obtain the barrier height  $\phi_{BO}$  as,

$$\phi_{BO} = - \frac{k(T+T_0)}{q} [\ln(I_{se}/SA^* T^2)] \quad (3.22)$$

(c) From the  $1/C^2$ - $V$  plot :

For Schottky barrier diodes showing  $T_0$  anomaly, it has been shown by Levine [19] that the capacitance  $C$

can be written in the form

$$\frac{1}{C^2} = \frac{2S^{-2}}{\epsilon_s q N_D} \left( x + \frac{E_o}{q} + \frac{E_o^2}{q^2} / 4x \right) \quad (3.23)$$

where  $x = (\phi_B - V - \phi_f - \frac{kT}{q})$

For  $x$  large, i.e. small forward bias and reverse biases we have,

$$\frac{1}{C^2} = \frac{2S^{-2}}{\epsilon_s q N_D} \left( \phi_{BO} - V \cdot \frac{T}{T+\bar{T}_O} - \phi_f - \frac{kT}{q} + \frac{E_o}{q} \right) \quad (3.24)$$

where  $\phi_B = \phi_{BO} + \frac{\partial \phi_B}{\partial V} V = \phi_{BO} + V \cdot \frac{T_O}{T+\bar{T}_O}$  (3.25)

$$\frac{1}{C^2} = \frac{2}{\epsilon_s q N_D S^2} \frac{1}{(1+\bar{T}_O/T)} \left[ (1+\bar{T}_O/T) \left( \phi_{BO} - \phi_f - \frac{kT}{q} + \frac{E_o}{q} \right) - V \right] \quad (3.26)$$

where  $\bar{T}_O$  is the average value of  $T_O$  in the range of voltage over which the C-V measurement is made. From eqn. (3.26) we see that barrier height  $\phi_{BO}$  can be obtained from the intercept  $V_b$  of the  $\frac{1}{C^2} - V$  plot using the relation,

$$\phi_{BO} = V_b \cdot \frac{T}{(T+\bar{T}_O)} + \phi_f + \frac{kT}{q} - \frac{E_o}{q} \quad (3.27)$$

### 3.3.3 Determination of $\phi^*$ and $D_{so}$

A perusal of literature shows that there are various methods to determine  $\phi^*$ , the neutral level at the surface measured from the bottom of the conduction band and  $D_{ss}$  the

surface state density for Schottky barrier diodes with a thin interfacial layer [11,12] whereas for devices showing  $T_0$  effect, there is no method to determine  $\phi^*$  and  $D_{ss}$ . It should be noted that in the case of devices with an interfacial layer, the energy distribution of the surface state density ( $D_{ss}$ ) is considered a constant, on the other hand, for devices showing  $T_0$  effect Levine's model assumes an exponential energy distribution of surface states, given by the equation (ref. Fig. 1.3)

$$D_{ss}(E) = D_{so} \exp [(E - q\phi^*)/E_0] \quad (3.28)$$

From eqn. (3.28) we see that for the surface state density  $D_{ss}$ , we require, apart from  $\phi^*$  the values of  $D_{so}$  and  $E_0$ . A method to evaluate  $E_0$  has been given earlier and here we will be presenting a method to determine  $\phi^*$  and  $D_{so}$ .

We see from eqn. (1.14) that the zero bias barrier height  $\phi_{BO}$  at any temperature  $T$  can be written as

$$\phi_{BO}(T) = \phi^*(T) - E_0 \ln \left[ \frac{Q_{sco}(T)}{Q_f} + 1 \right] \quad (3.29)$$

where  $Q_f = q D_{so} E_0$

$Q_{sco}(T)$  = space charge in the semiconductor at zero bias.

Since this is the only equation available for the determination of  $\phi^*$  and  $D_{so}$ , we need to look for one more relation to obtain  $\phi^*$  and  $D_{so}$ . This we obtain from the temperature

dependence of  $\phi_{BO}$ , under the following assumptions.

(i) We assume that  $\phi^*$  is given by the relation,

$$\phi^*(T) = r E_g(T) \quad (3.30)$$

where  $E_g(T)$  is the band gap of the semiconductor at a temperature  $T$  and  $r$  is a proportionality constant. The temperature dependence of the band gap for silicon is obtained from the relation [11],

$$E_g(T) = E_g(0) - \alpha T^2 / (\beta + T) \quad (3.31)$$

where

$$E_g(0) = 1.16 \text{ eV}$$

$$\alpha = 7.02 \times 10^{-4} \text{ eV}/^\circ\text{K}$$

$$\text{and } \beta = 1108^\circ\text{K}.$$

(ii) Normally,  $Q_{sco}$ , the zero bias space charge in the semiconductor, is a temperature dependent quantity, but by restricting ourselves to the temperature range where  $Q_{sco}$  is a constant, we see that the plot of  $\phi_{BO}(T)$  versus  $E_g(T)$  will be a straight line of slope  $r$ .

Under these assumptions we see that the intercept of the  $\phi_{BO}(T)$  versus  $E_g(T)$  plot gives  $\frac{E_0}{q} \ln \left( \frac{Q_{sco}}{Q_f} + 1 \right)$  and the slope gives  $r$ . Thus  $\phi^*$  at any temperature  $T$  can be obtained from eqn. (3.30). Knowing the barrier height  $\phi_{BO}(T)$  at a fixed temperature, we can calculate  $Q_{sco}$  and hence  $Q_f$  from the intercept  $\phi_{BO}$  using the relation,



$$Q_f = Q_{sco} [\exp(q\phi'_{BO}/E_o) - 1]^{-1} \quad (3.32a)$$

From eqn. (3.18) and the relation  $Q_f = q D_{so} E_o$  we obtain  $D_{so}$  from the equation,

$$D_{so} = \frac{Q_f}{qE_o} = \frac{Q_{sco}}{qE_o} [\exp(\frac{q\phi'_{BO}}{E_o}) - 1]^{-1} \quad (3.32b)$$

Thus  $D_{so}$  can be obtained once the value of  $\phi_{BO}$  is obtained experimentally as a function of temperature. This concludes our discussion of the methods for determining  $E_o$ ,  $\phi_{BO}$ ,  $\phi^*$  and  $D_{so}$  for a diode showing  $T_o$  effect.

### 3.4 Results and Discussions

In this section we present the  $\ln I$ - $V$  and  $\frac{1}{C^2} - V$  plot at different temperatures, and other relevant plots required for the characterisation of (Au-nSi) Schottky barrier diodes, as derived from the  $\ln I$ - $V$  plots.

The basic trend of the results obtained is best described through the characteristics of four diodes made on the same wafer. Three of these diodes (EAu 110, EAU 120 and EAU 130) are of 1 mm diameter, and the fourth diode (EAu 410) is of 4.2 mm diameter. Figs. (3.8 to 3.12) give the  $\ln I$ - $V$  plot of EAU 110, EAU 120, EAU 130, EAU 410 and CD 123, the 'diode' obtained by the parallel combination of EAU 110, EAU 120 and EAU 130. Fig. (3.13) gives the  $V_T$  versus  $\frac{kT}{q}$  plot for EAU 110, EAU 120 and EAU 130 and Fig. (3.14) gives

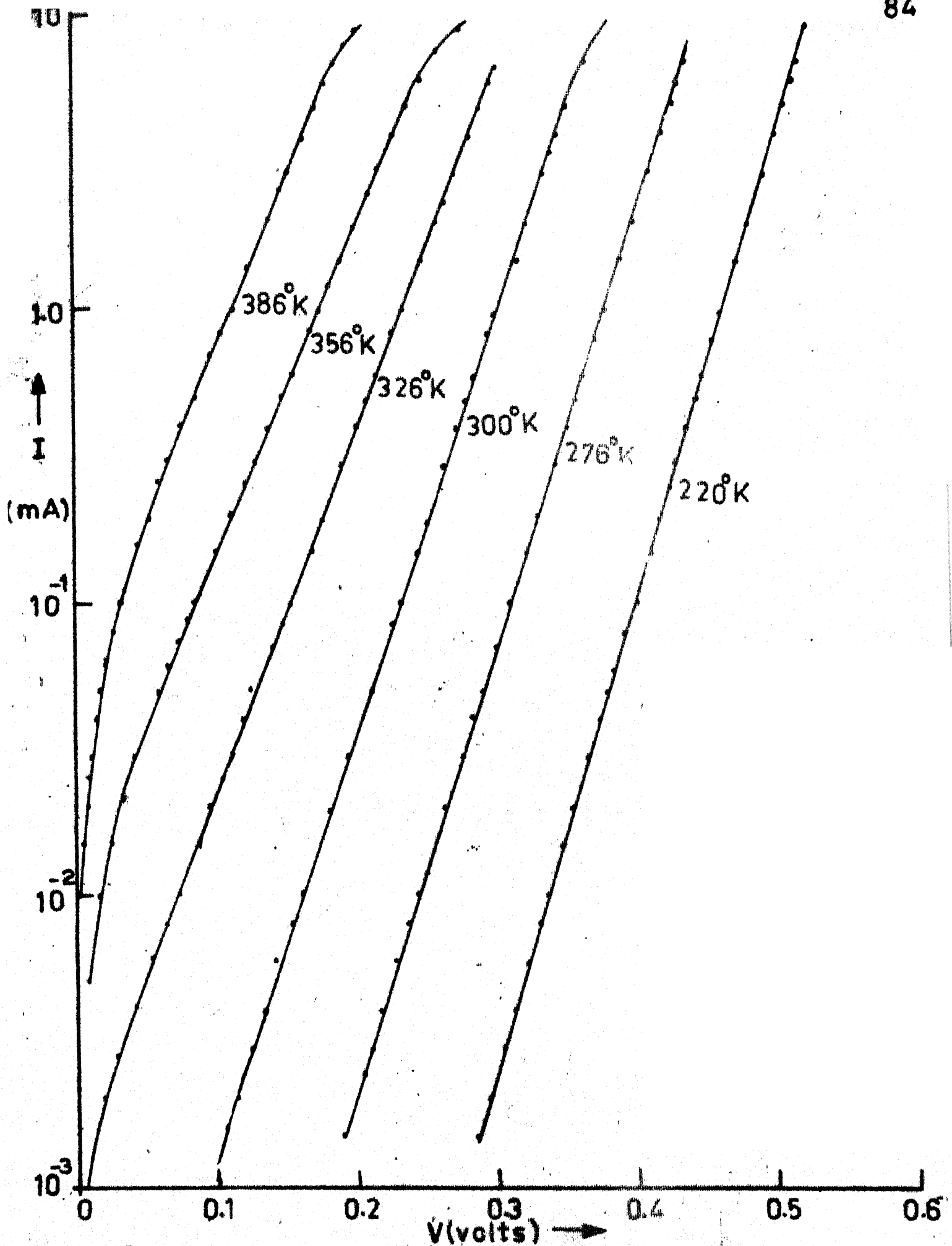


Fig.3.8  $\ln$   $I$ - $V$  plot at different temperature for the diode EAU 110.

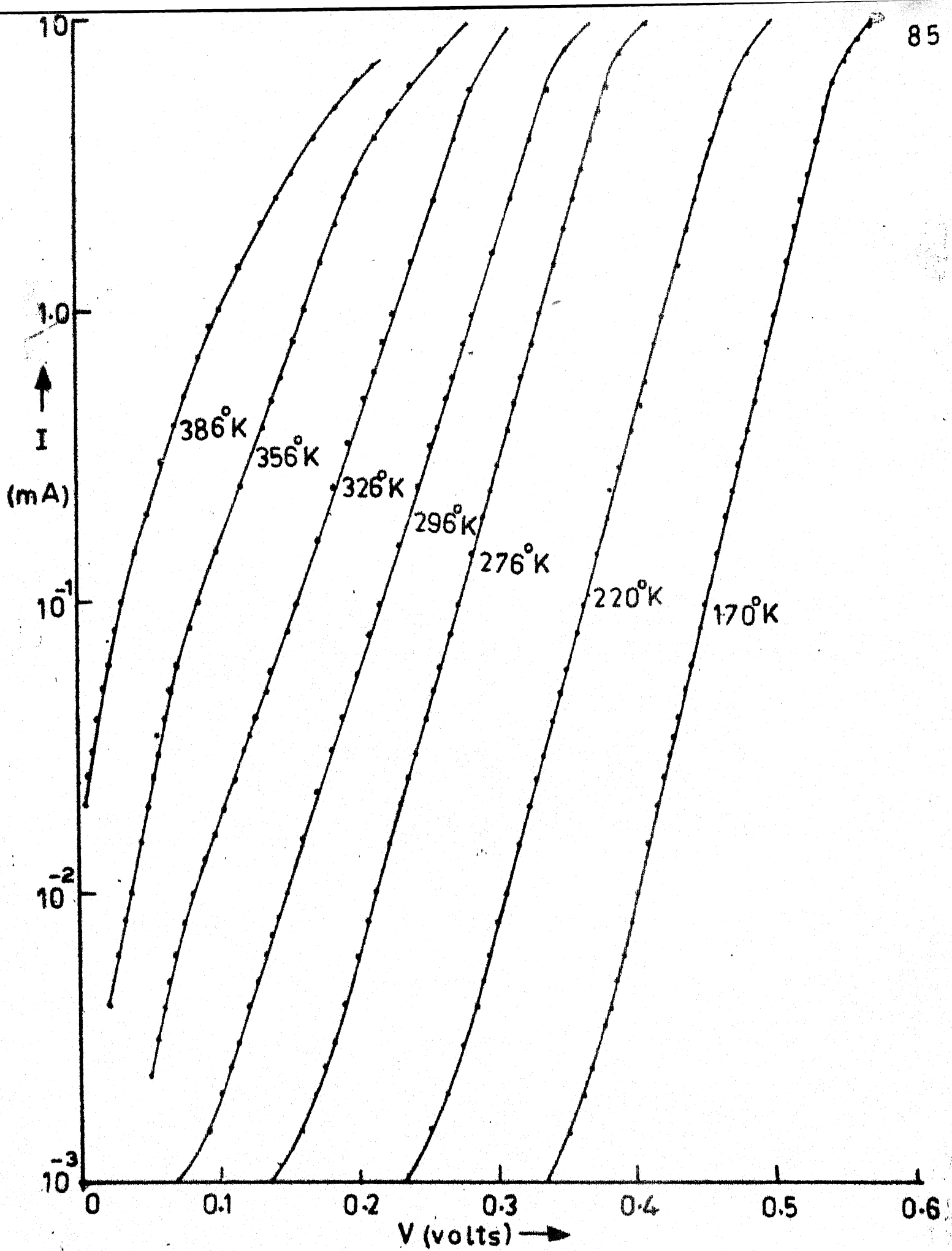


Fig.3.9 In I-V plot at different temperatures for the diode E Au 12n.

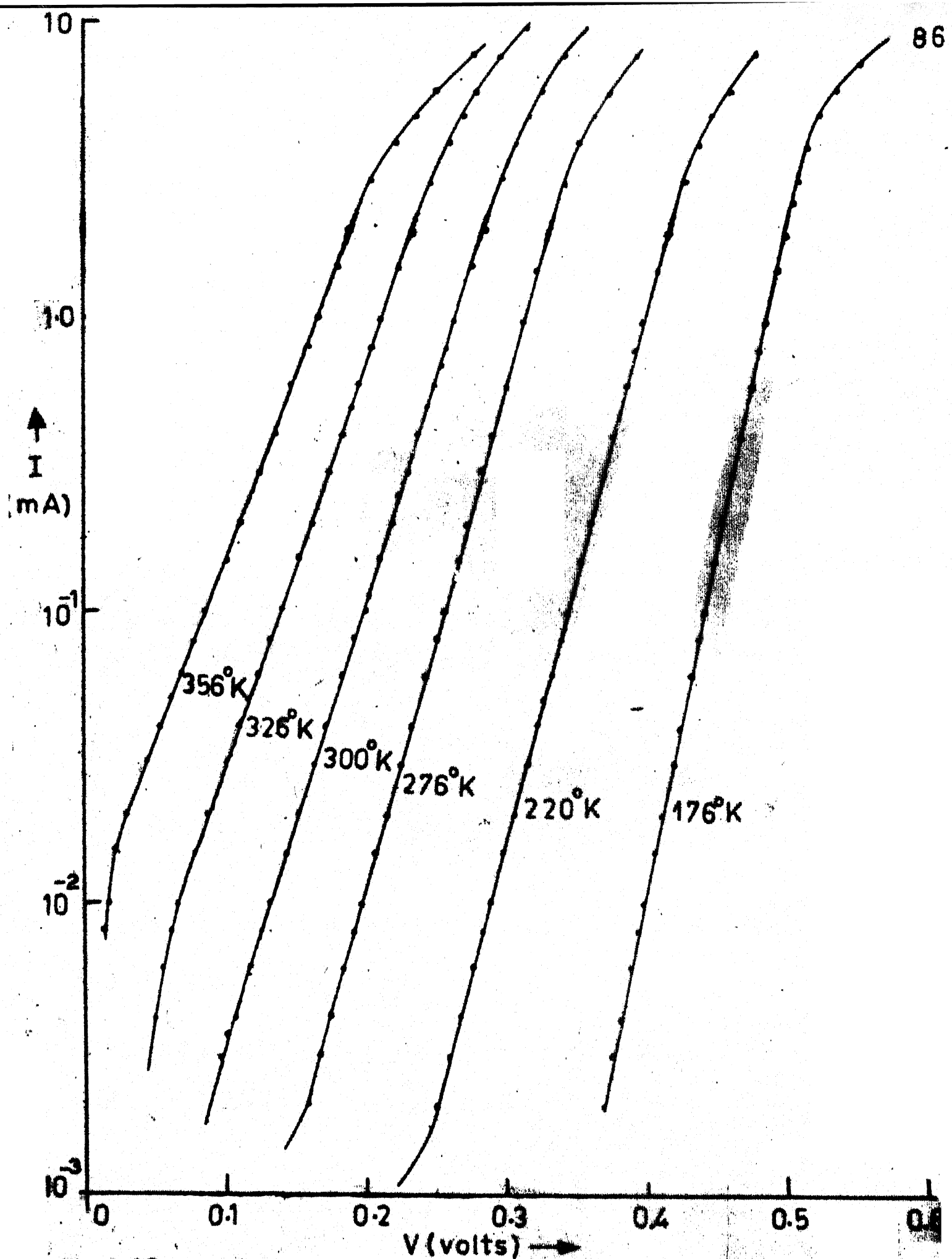


Fig.3.10 In I-V plot at different temperatures for the diode EAu130

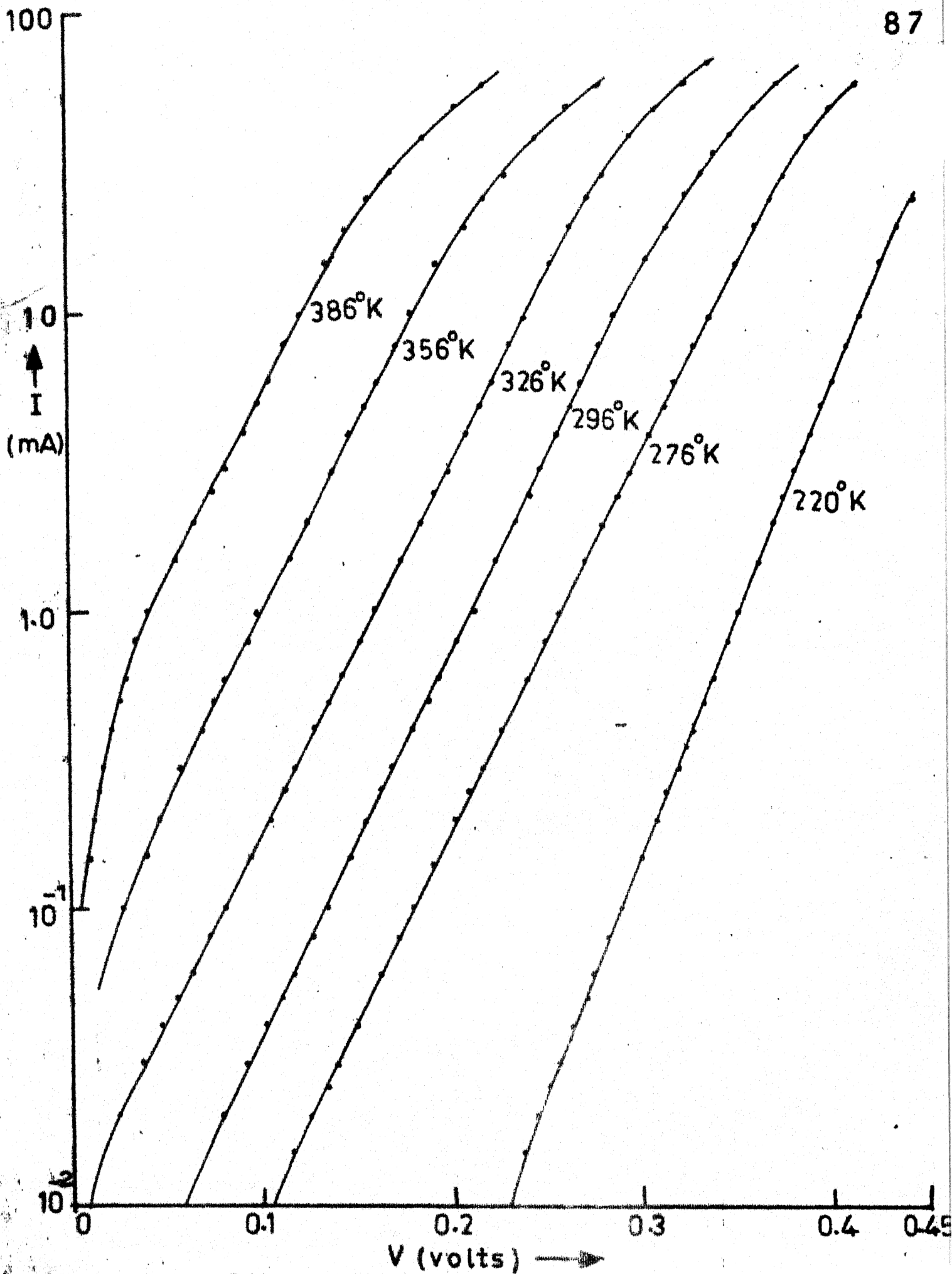


Fig.3.11 In I-V plot for the large area diode EAU410

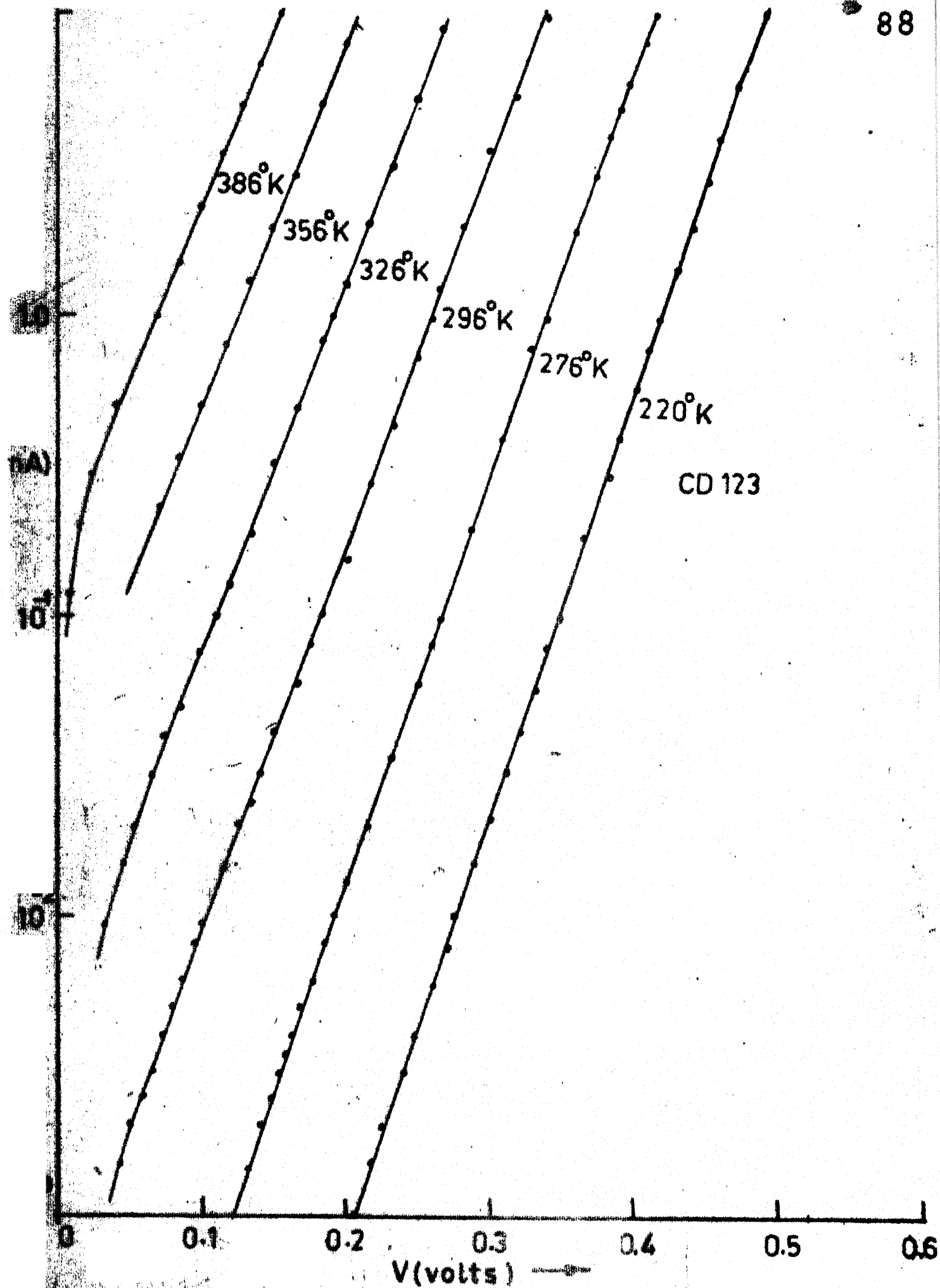


Fig. 3.12  $\ln I$ - $V$  plot for the combined CD 123.

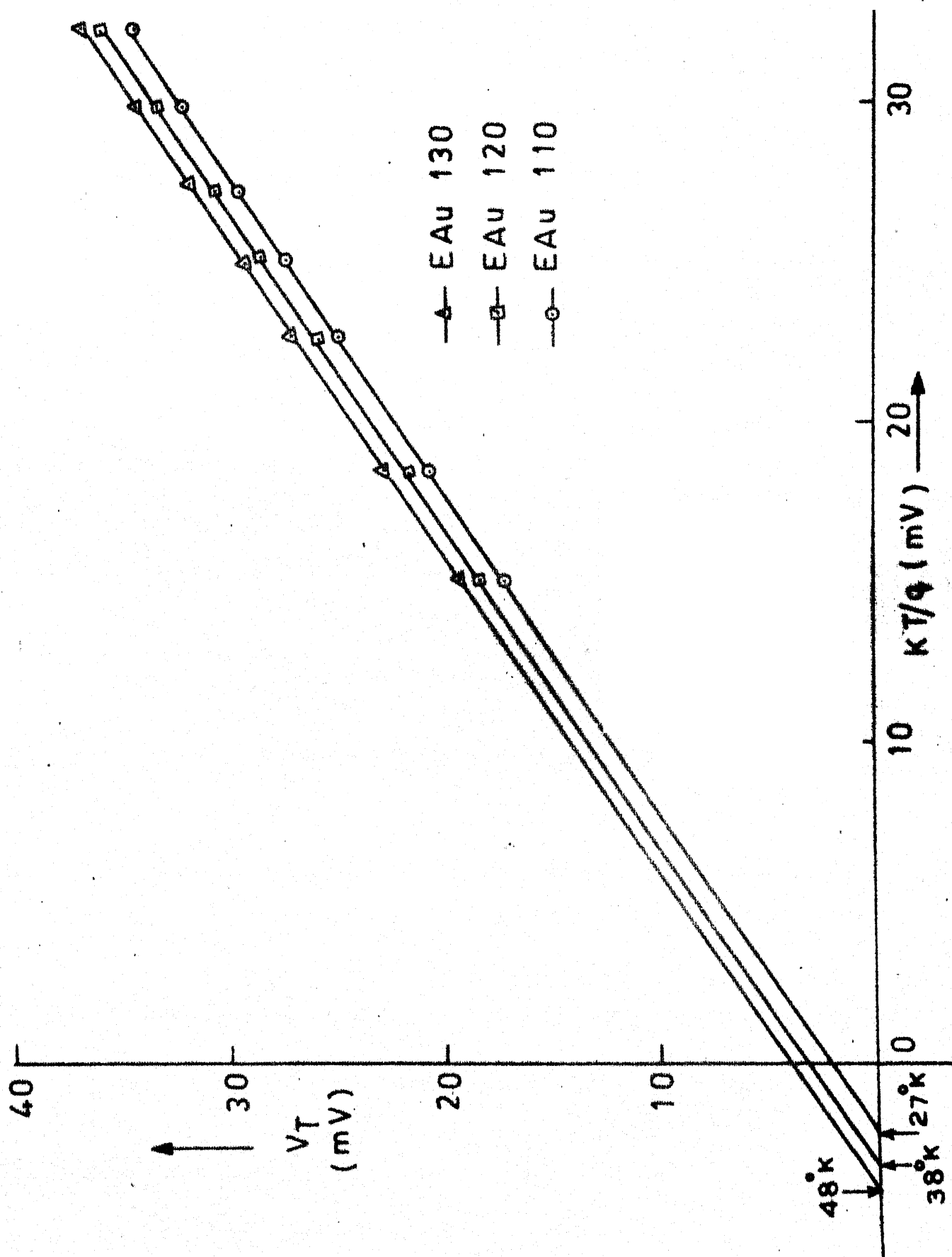


Fig. 3.13 A plot of  $V_T$  versus  $kT/q$  for different small area Au-n-Si Schottky barrier diodes.

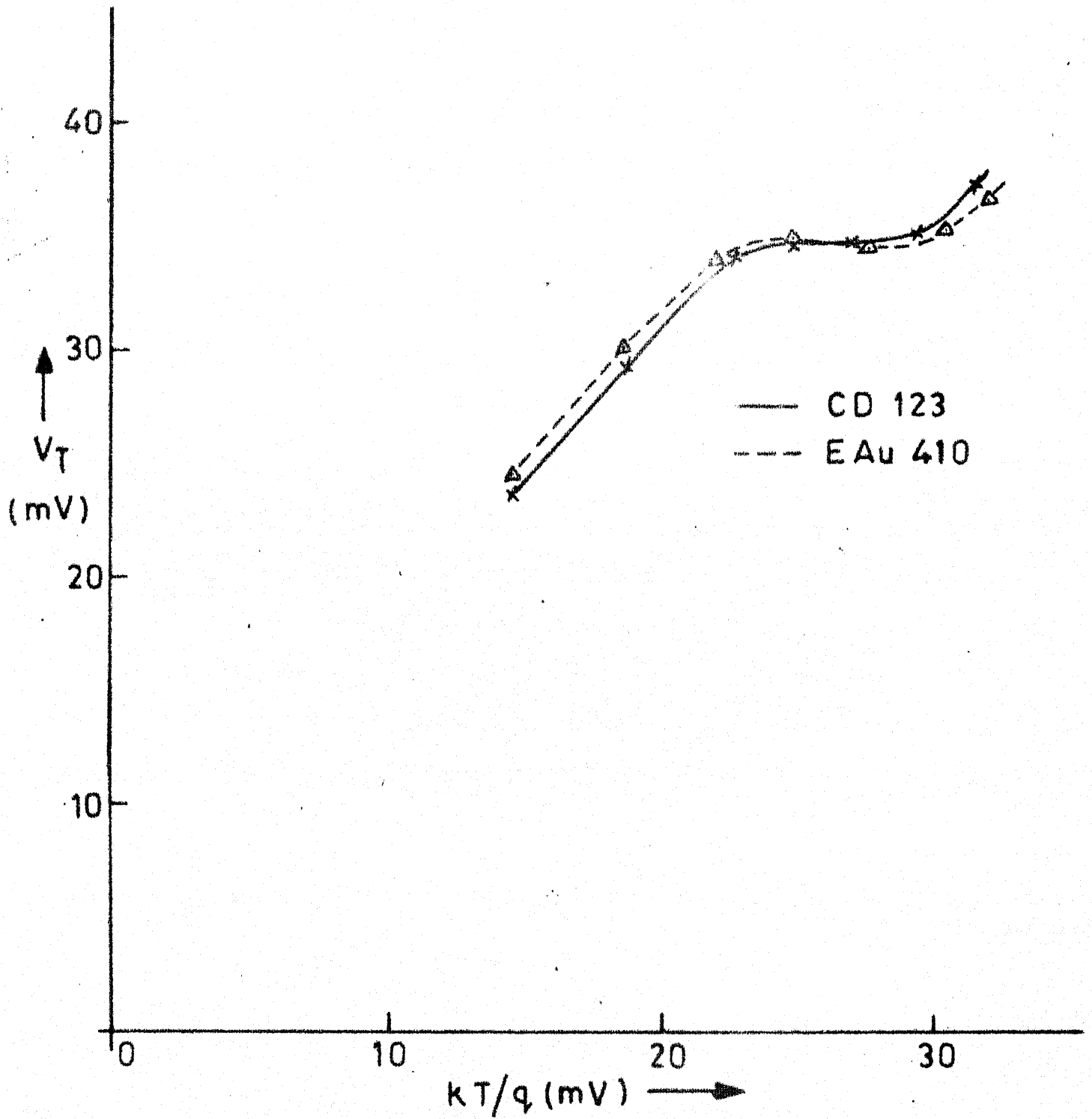


Fig.3.14 A plot of  $V_T$  versus  $kT/q$  for the large area diode EAu410 and combined diode CD 123.



the  $V_T$  versus  $\frac{kT}{q}$  plot for EAU 410 and CD 123. The following features of the plots in Fig. (3.13) and (3.14) are worth noting.

(1) From a plot of  $V_T$  versus  $\frac{kT}{q}$  given in Fig. (3.13) for the three diodes of 1 mm diameter, we see that in all the three diodes the current transport is by thermionic emission with  $T_0$  effect. The values of  $T_0$  for EAU 110, EAU 120, and EAU 130 are respectively  $27^\circ\text{K}$ ,  $38^\circ\text{K}$  and  $48^\circ\text{K}$ . Note that  $T_0$  was measured at a constant current of 1.0 mA.

(2) The plot of  $V_T$  versus  $\frac{kT}{q}$  for EAU 410 given in Fig. 3.14, shows a constant value for  $V_T$  for a temperature range  $270^\circ\text{K} \leq T \leq 356^\circ\text{K}$  and for temperatures  $T < 270^\circ\text{K}$  and  $T > 356^\circ\text{K}$   $V_T$  increases monotonically with temperature. Hence we see that though the small area diodes surrounding a large area diodes exhibited thermionic emission as current transport, a measurement of the large area diode restricted to the temperature range  $250^\circ\text{K} \leq T \leq 380^\circ\text{K}$ , would lead one to an erroneous conclusion that the mechanism of current transport in this case is field emission.

and (3) From the  $V_T$  versus  $\frac{kT}{q}$  plot of the combined diode CD123, we see that though the individual diodes showed thermionic emission as the current transport with  $T_0$  effect, the  $V_T$  versus  $\frac{kT}{q}$  plot of the composite diode goes through a temperature range ( $275^\circ\text{K} \leq T \leq 325^\circ\text{K}$ ) wherein  $V_T$  versus

$\frac{kT}{q}$  flattens out. The value of  $V_T$  for  $T < 275^\circ\text{K}$  and  $T > 325^\circ\text{K}$  is seen to increase monotonically with temperature.

Thus we see that the  $V_T$  versus  $\frac{kT}{q}$  plot of the parallel combination of three isolated small area diodes with different  $T_0$ 's shows features similar to that of an identical system but with a larger area. This means that the transverse current does not play a dominant role in explaining the temperature variation of the ideality factor in a large area diode and hence the assumption made earlier while developing the theoretical model holds good.

Having verified the basic assumptions and the results of our theoretical model, we now look into the characterisation of a diode showing  $T_0$  effect and identify the parameter whose fluctuation results in the fluctuation in  $T_0$ . The following plots which are necessary for the characterisation of the three small area diodes are given in Figs. (3.15) to (3.20):

- (i) Plots of  $1/T_0$  versus  $V$  are given in Figs. (3.15) to (3.17).
- (ii) Plots of  $\phi_{B0}(T)$  versus  $E_g(T)$  for all the three diodes are given in Fig. (3.18).
- (iii) Plots of  $\ln I_R$  versus  $\ln (-V + 0.4)$  at room temperature for all the three diodes are given in Fig. (3.19).
- (iv) A plot of  $1/T_0$  versus  $\ln I$  for all the three diodes is given in Fig. (3.20).

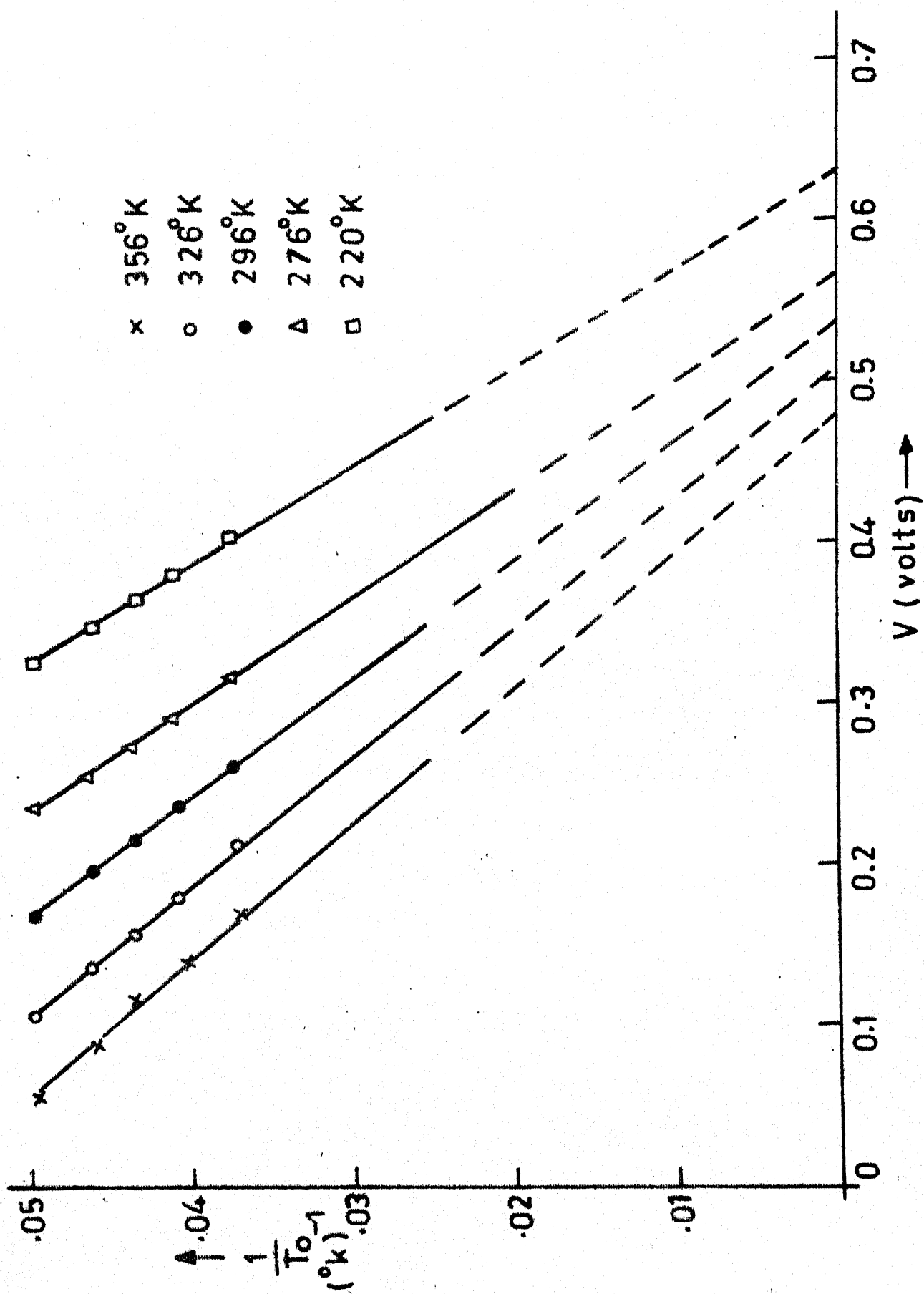


Fig.3.15 Plot of  $\frac{1}{T_0}$  versus  $V$  at different temperatures for EAU 110.

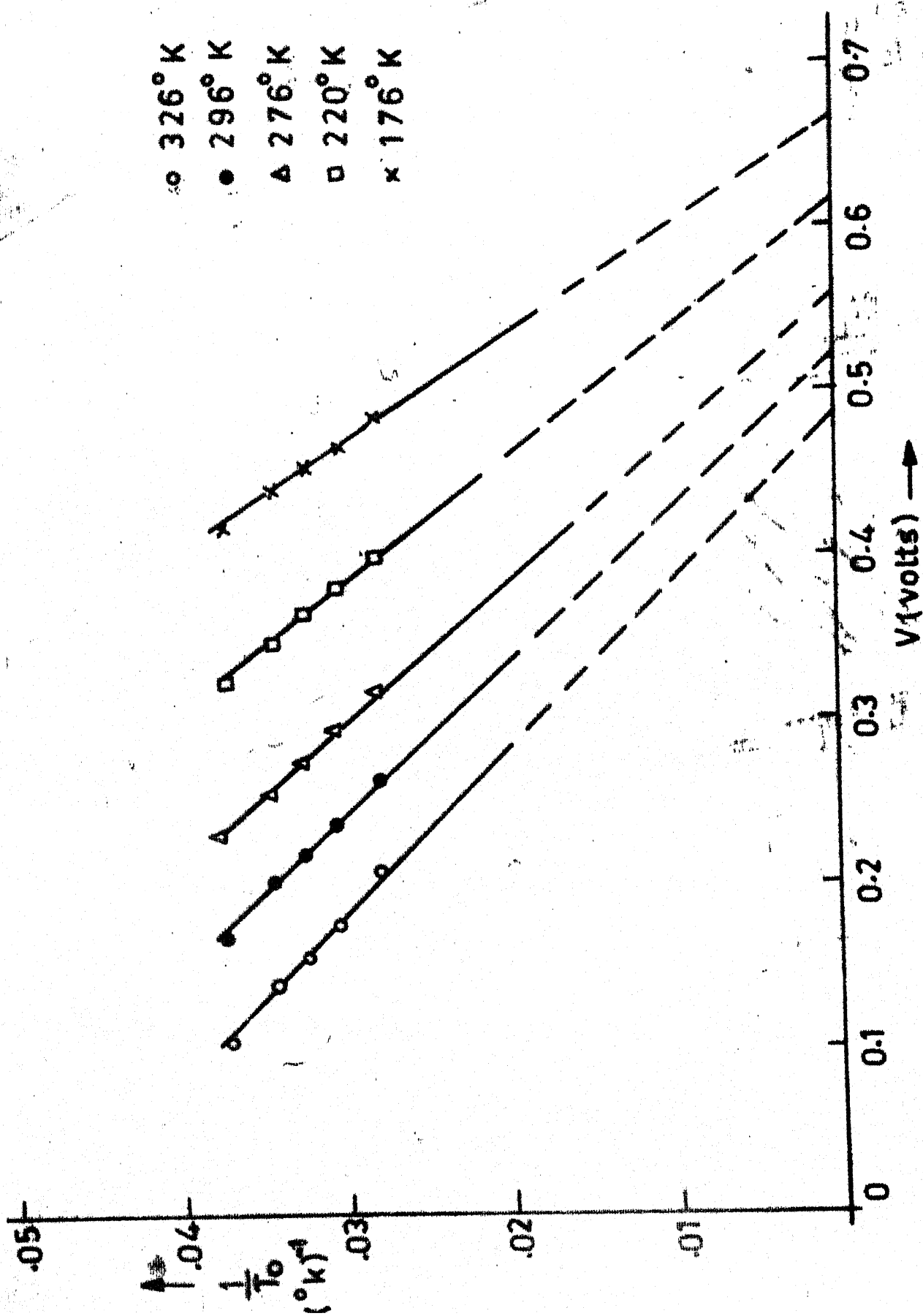


Fig.3.16 Plot of  $\frac{1}{T_0}$  versus  $V$  at different temperatures for EAU120

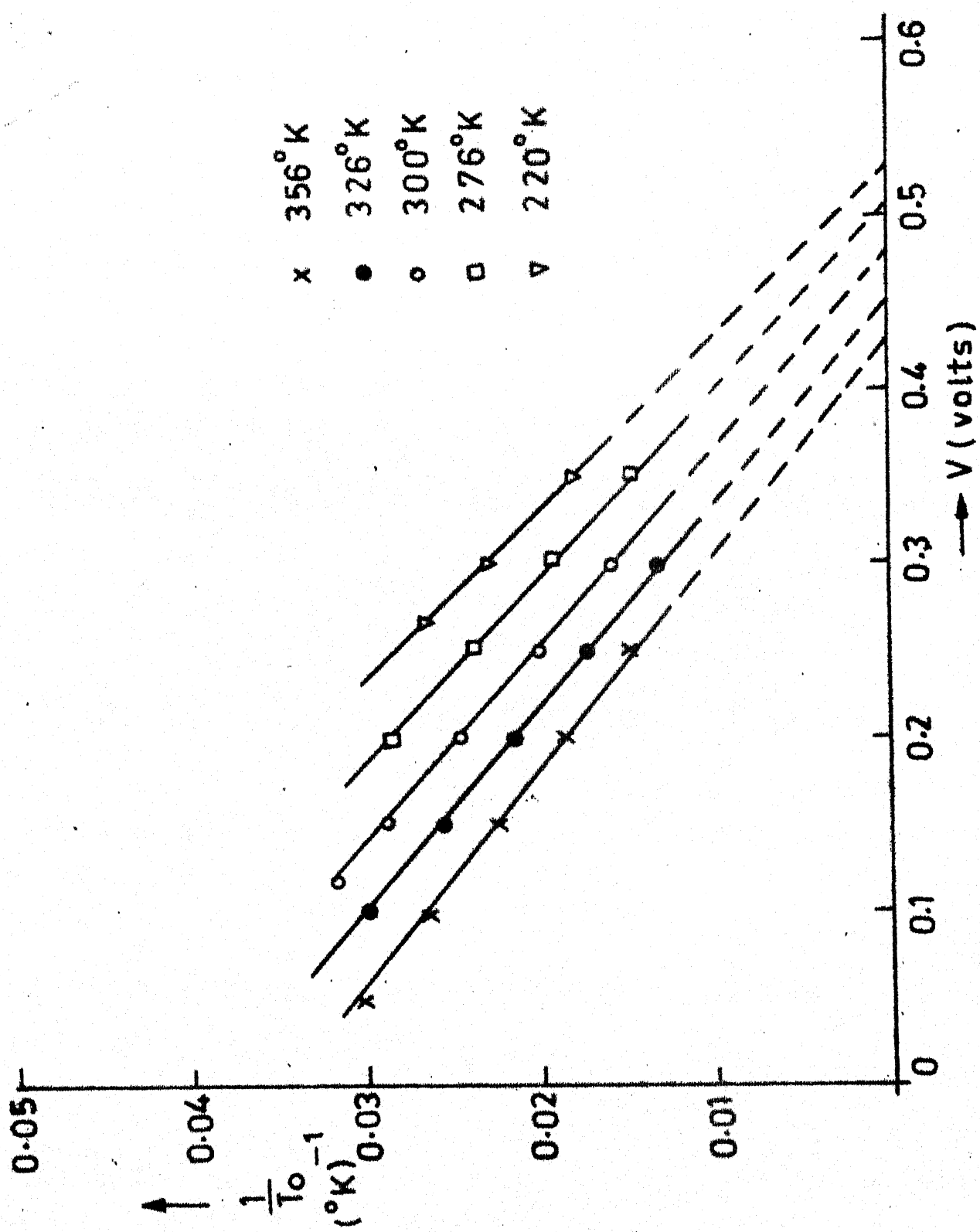


Fig 3.17 Plot of  $\frac{1}{I_0}$  versus  $V$  at different temperatures for EAU130 .

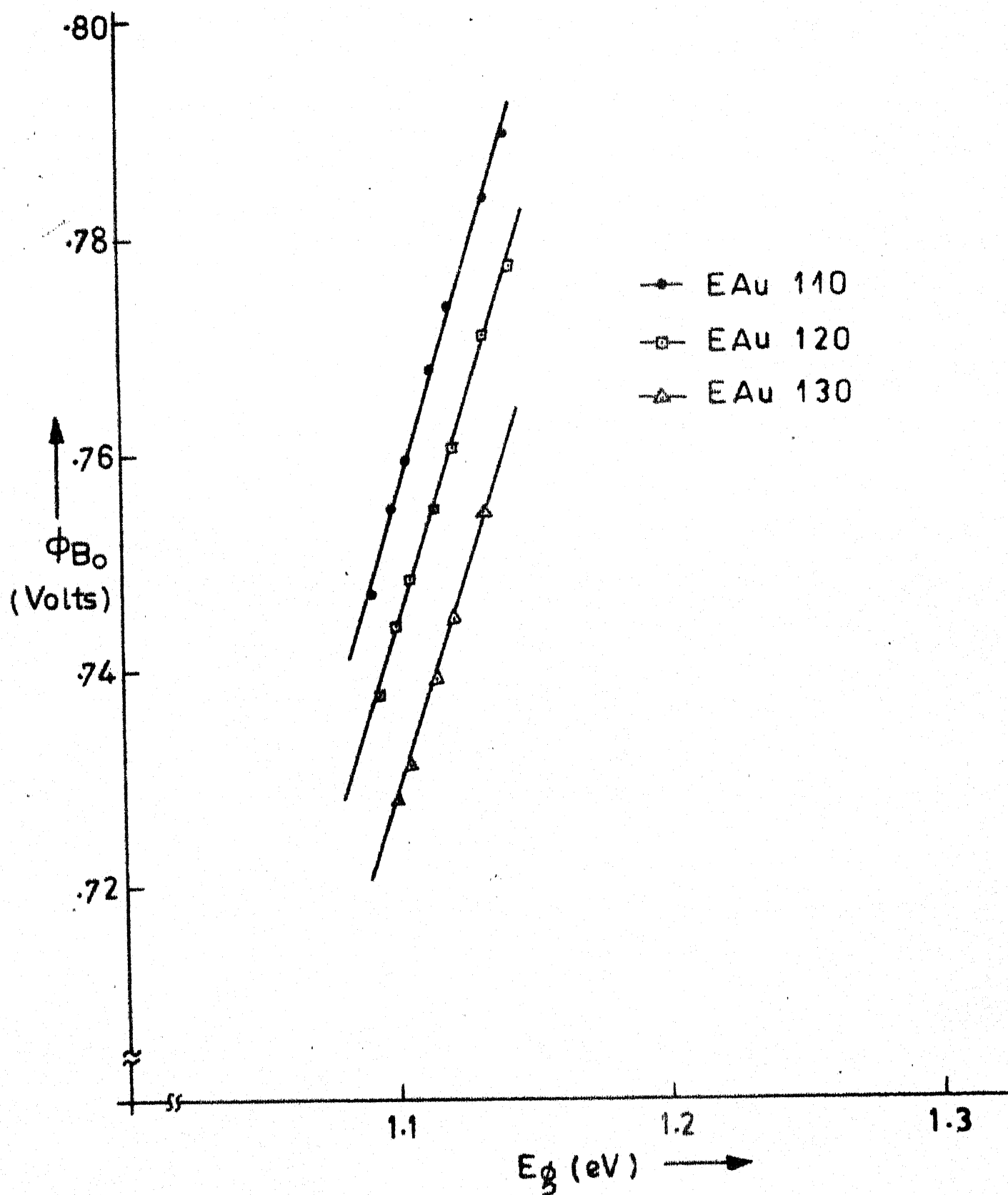


Fig.3.18 A plot of  $\Phi_{B0}(T)$  versus  $E_g(T)$  for the three small area diodes E Au 110, E Au 120, E Au 130.

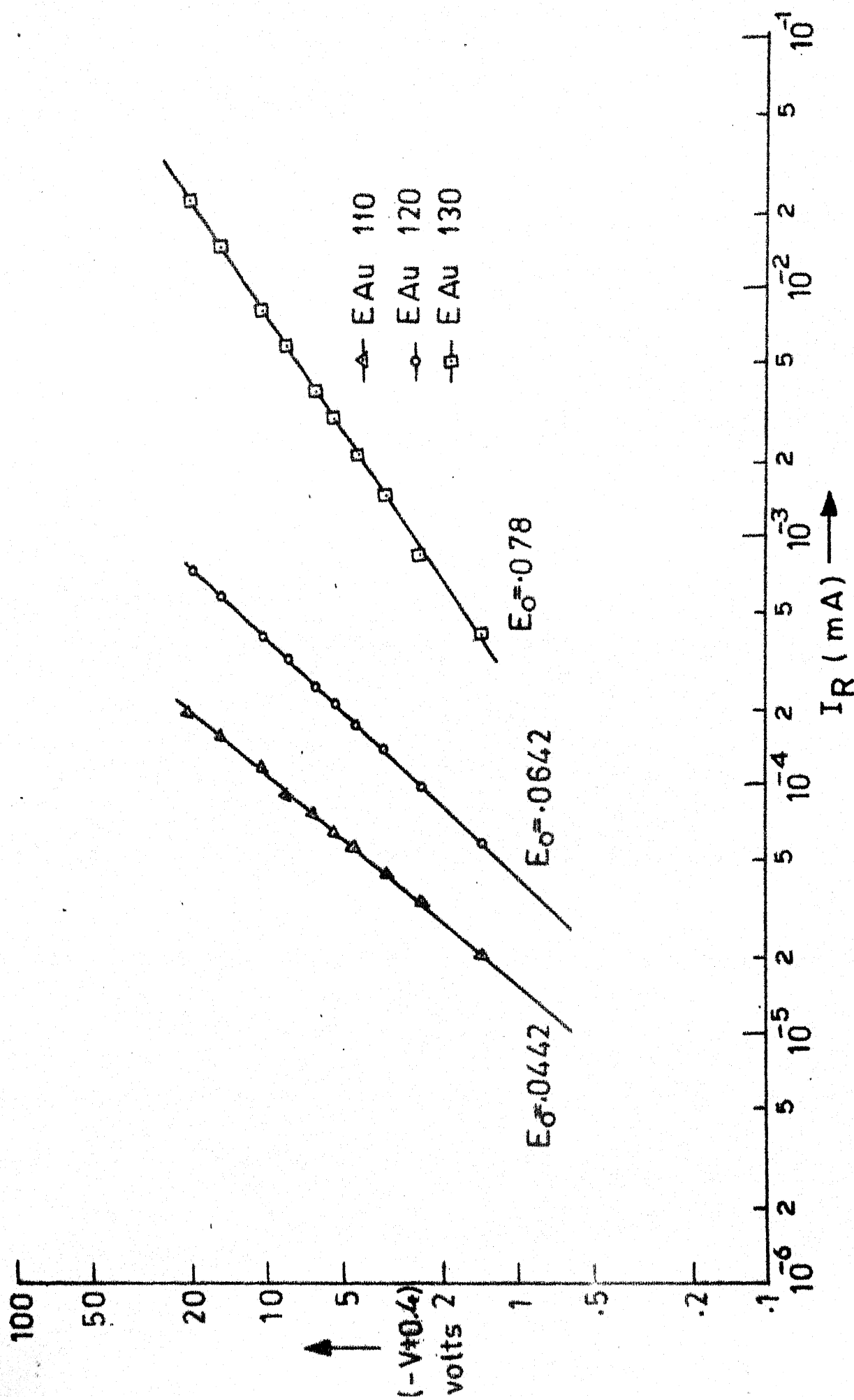


Fig. 3.19 A plot of  $\ln I_R$  versus  $\ln(-V+0.4)$  at room temperature for the three small area diodes EAu 110, EAu 120, EAu 130.

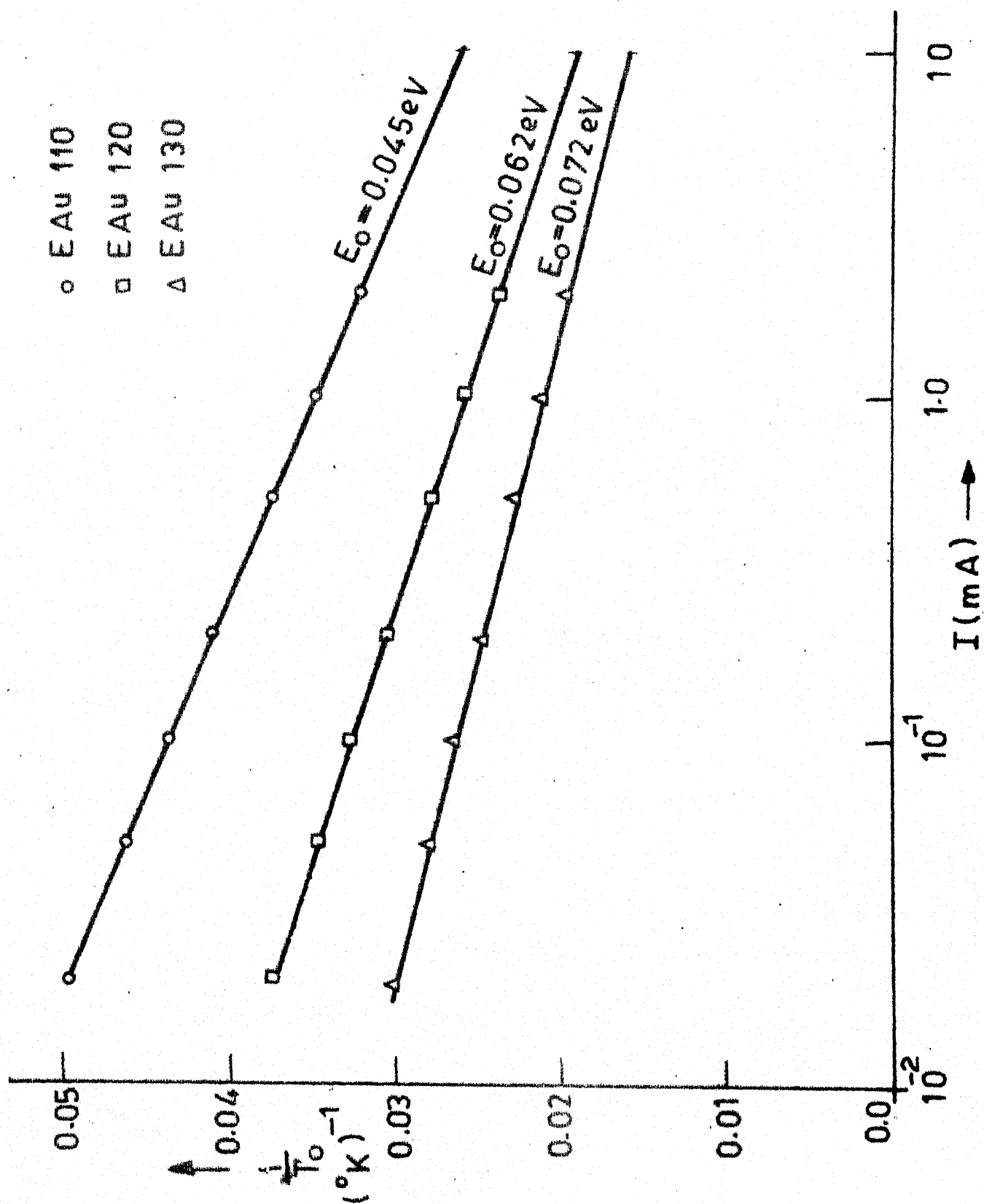


Fig.3.20 Plot of  $\frac{1}{T_0}$  versus  $\ln I$  for three small area diodes.



In table 3.2 we present the values of  $E_0$ ,  $\phi_{B0}$  (at different temperatures),  $\phi^*$  and  $D_{s0}$  for each of these diodes. There we have also included the results of two other sets of diodes made on different wafers.

The following points are worth noting from our results.

- (1) The barrier height determined using all the methods mentioned in sec. 3.3, match well with each other.
- (2) The value of  $E_0$ , obtained from the forward I-V data and the reverse I-V data are very nearly equal, and
- (3) For a given wafer, different diodes with different  $T_0$ , show a variation only in  $E_0$ , while  $\phi^*$  and  $D_{s0}$  remain constant. This means that most probably  $E_0$  is the parameter, whose fluctuation causes the fluctuation in  $T_0$ .

So far we have been considering the nature of the I-V characteristics and the various characteristics derived from them. We now move over to study the effect of  $T_0$  effect, and  $E_0$  fluctuations on the C-V characteristics.

Before we present the experimental plot of  $\frac{1}{C^2} - V$  for the diodes made by us, let us look into the basic difference between the  $\frac{1}{C^2} - V$  plot for a tunnel MIS diode [18] and for a diode showing  $T_0$  anomaly. It should be noted that the basic motivation behind this comparative study is to look for an effect of  $T_0$  anomaly on the  $\frac{1}{C^2} - V$  plot as opposed to

Table 3.2 Values of  $E_0$ ,  $\phi$ ,  $\frac{q\phi}{E_g}$ ,  $D_{so}$  and  $\phi_{B0}$  (at different temperatures) for three sets of diodes showing  $T_0$  effect.

Device	$E_0$ (eV)	$\frac{q\phi}{E_g}$	$D_{so}$ $10^{11}/\text{cm}^2\text{eV}$	$\phi_{B0}$ (eV)											
				$1/T_0$ -V Plot				$1/c^2$ -V Plot				$\ln I$ -V Plot			
				220 $^{\circ}\text{K}$	276 $^{\circ}\text{K}$	296 $^{\circ}\text{K}$	326 $^{\circ}\text{K}$	220 $^{\circ}\text{K}$	276 $^{\circ}\text{K}$	296 $^{\circ}\text{K}$	326 $^{\circ}\text{K}$	220 $^{\circ}\text{K}$	276 $^{\circ}\text{K}$	296 $^{\circ}\text{K}$	326 $^{\circ}\text{K}$
EAu 110	.045	.79	2.06	.804	.786	.781	.777	.801	.781	.775	.768	.806	.789	.783	.780
EAu 120	.065	.79	2.07	.794	.771	.766	.762	.798	.780	.755	.760	.802	.776	.770	.765
EAu 130	.072	.79	2.05	.759	.751	.726	.722	.759	.742	.730	.732	.762	.732	.728	.725
EAu 210	.038	.80	1.96	.783	.773	.768	.764	.731	.774	.766	.762	.784	.770	.766	.782
EAu 220	.045	.80	1.98	.767	.757	.753	.746	.767	.756	.753	.746	.767	.758	.754	.748
EAu 230	.045	.79	1.95	.768	.756	.752	.745	.768	.754	.751	.744	.768	.755	.754	.746
EAu 240	.052	.80	1.96	.761	.751	.746	.740	.761	.751	.748	.741	.761	.753	.748	.742
EAu 250	.060	.795	1.96	.753	.744	.740	.733	.753	.742	.740	.734	.753	.746	.748	.735
DAu 111	.045	.78	1.48	.761	.750	.746	.740	.762	.750	.744	.740	.763	.752	.748	.741
DAu 121	.055	.78	1.48	.742	.731	.728	.721	.742	.729	.728	.719	.744	.733	.730	.725
DAu 131	.048	.78	1.46	.755	.744	.740	.734	.754	.746	.741	.733	.754	.745	.740	.736
DAu 141	.065	.78	1.42	.733	.721	.718	.712	.733	.723	.719	.714	.735	.724	.720	.714

a thin interfacial layer between the metal and the semiconductor and to use the difference, if any, to identify diodes showing  $T_o$  anomaly from the  $\frac{1}{C^2} - V$  plot.

(i) Diode showing  $T_o$  effect :

We see from eqn. (3.19) that  $\frac{1}{C^2}$  is given by

$$\frac{S^2}{C^2} = \frac{2}{q\epsilon_s N_D} \cdot \frac{1}{(1 + \bar{T}_o/T)} \left[ (1 + \bar{T}_o/T) (\phi_{BO} - \phi_f - \frac{kT}{q} + \frac{E_o}{q} - V) \right] \quad (3.26)$$

We see from eqn. (1.21a) that for measurements made under constant voltage conditions ( $T_o/T$ ) is a constant [10] and hence the average value ( $\bar{T}_o/T$ ) will also be a constant, evaluated over the same voltage range at all temperatures. Thus, we can rewrite equation (3.13) of the form,

$$\frac{S^2}{C^2} = \frac{2}{q\epsilon_s N_D} \cdot \frac{1}{n_1} \cdot \left[ n_1 (\phi_{BO} - \phi_f - \frac{kT}{q} + \frac{E_o}{q}) - V \right] \quad (3.33)$$

From eqn. (3.21) we see that the effect of  $T_o$  effect on the  $\frac{1}{C^2} - V$  plot is two fold and are:

- (1) The slope of the  $\frac{1}{C^2} - V$  plot is scaled down by a factor  $n_1 = (1 + \bar{T}_o/T)$  and
- (2) The intercept  $V_b$  is given by,  $V_b = n_1 (V_{bi} + \frac{E_o}{q})$ , where  $V_{bi}$  is the intercept in the ideal case.

(ii) Diodes with a thin interfacial layer (Tunnel MIS diodes):

We see from the basic definition that,

$$\frac{C}{S} = - \frac{dQ_{sc}}{dV} = \frac{d}{dV} \left[ \sqrt{2q\epsilon_s N_D} (\phi_B - V - \phi_f - (kT/q)) \right] \quad (3.34)$$

where  $Q_{sc}$  = total space charge in the semiconductor

$C$  = depletion capacitance

and  $V$  is negative for reverse bias.

Carrying out the differentiation eqn. (3.34) reduces to,

$$\frac{C}{S} = - \sqrt{\frac{q \epsilon_s N_D}{2(\phi_B - V - \phi_f - \frac{kT}{q})}} \left( \frac{\partial \phi_B}{\partial V} - 1 \right) \quad (3.35)$$

Using the relationship  $n = (1 - \frac{\partial \phi_B}{\partial V})^{-1}$ , eqn. (3.35) is rewritten as,

$$\frac{C}{S} = \frac{1}{n} \sqrt{\frac{q \epsilon_s N_D}{2(\phi_B - V - \phi_f - \frac{kT}{q})}} \quad (3.36)$$

$$\text{i.e., } \frac{1}{C^2} = \frac{1}{n^2} \cdot \frac{2S^{-2}}{q \epsilon_s N_D} (\phi_B - V - \phi_f - \frac{kT}{q}) \quad (3.37)$$

Using the relation,  $\phi_B = \phi_{B0} + \frac{\partial \phi_B}{\partial V} \cdot V$ , eqn. (3.34) reduces to

$$\frac{1}{C^2} = \frac{2S^{-2}}{q \epsilon_s N_D} \cdot n \cdot [n(\phi_{B0} - \phi_f - \frac{kT}{q}) - V] \quad (3.38)$$

From eqn. (3.38) one observes that the effect of an interfacial layer is to scale up both the slope and the intercept of a  $\frac{1}{C^2} - V$  plot, as compared to an ideal diode.

Comparing eqn. (3.26) and eqn. (3.28) we see that the only difference between the  $\frac{1}{C^2} - V$  plot of diodes with an interfacial layer and diode showing  $T_0$  effect is that in the former case the slope of the  $\frac{1}{C^2} - V$  plot underestimates

the doping density, while in the latter it is overestimated. The basic nature of the  $\frac{1}{C^2} - V$  plot in both the cases is the same and the differentiation between the two models from the  $\frac{1}{C^2} - V$  plot is not possible. In Figs. 3.21 to Fig. 3.23 we present a plot of  $\frac{1}{C^2}$  versus  $V$  at different temperatures for EAU 110, EAU 120 and EAU 130. In Fig. 3.24 and 3.25 we present a plot of  $\frac{1}{C^2}$  versus  $V$  at different temperature for EAU 410 and CD 123. The following features of these plots are of interest.

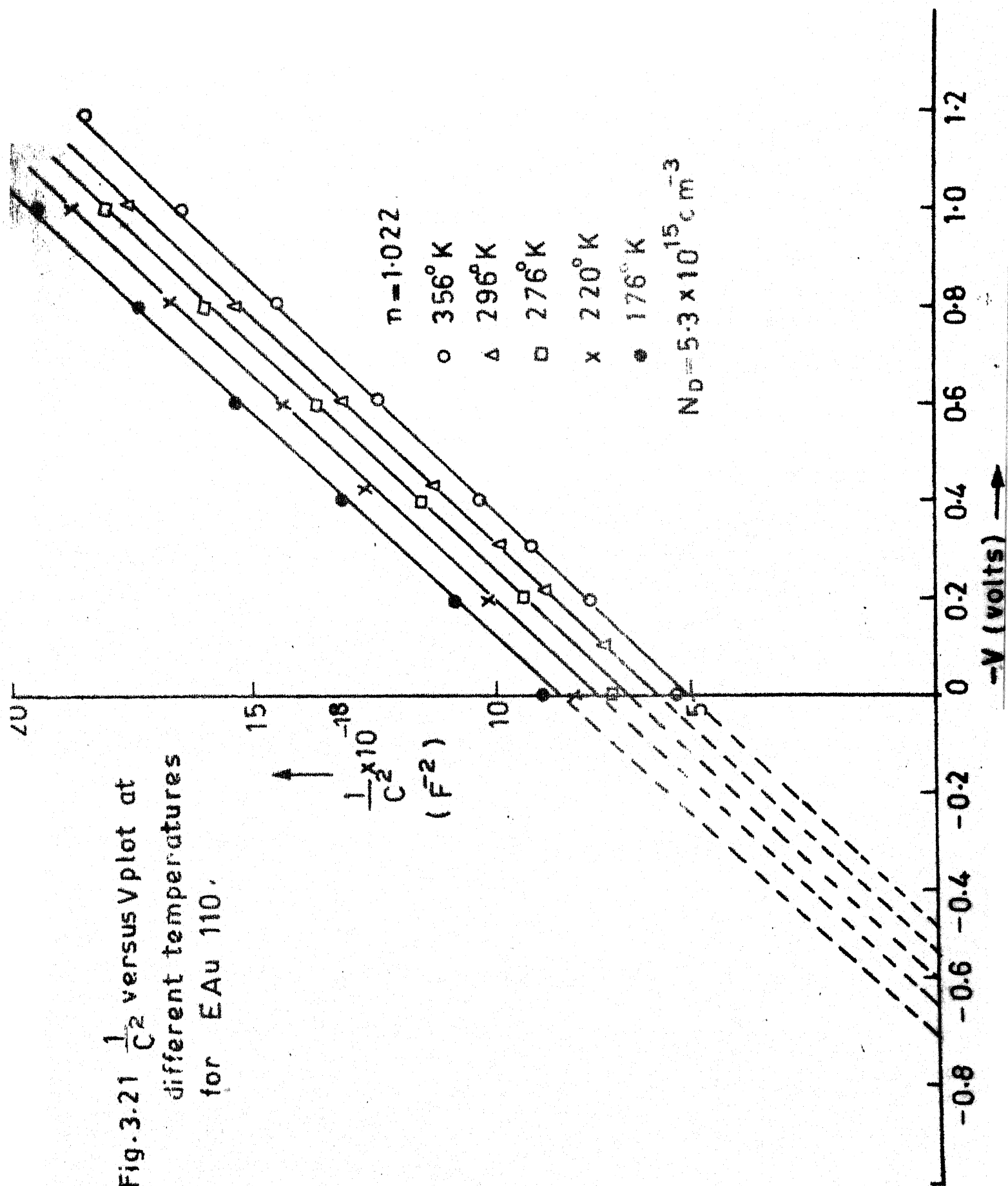
- (1) The plot of  $\frac{1}{C^2}$  versus  $V$  is a straight line for small area diodes with a constant slope at different temperature as predicted by eqn. (3.26), and
- (2) The nature of the  $\frac{1}{C^2}$  versus  $V$  plot for a large area diode and the diode formed by the combination of the three small area diodes do not show any considerable variation from that of a small area diode.

### 3.5 Summary

In the previous two chapters we have developed a theoretical model to show that in the case of Schottky barrier diodes the temperature dependence of ideality factor is affected by the fluctuation of some parameters. The theoretical model is derived based on the following assumptions.

- (1) There is a scatter in the values of  $T_0$  for the different homogeneous diodes made on the same wafer.

Fig. 3.21  $\frac{1}{C^2}$  versus  $V$  plot at different temperatures for EAu 110.



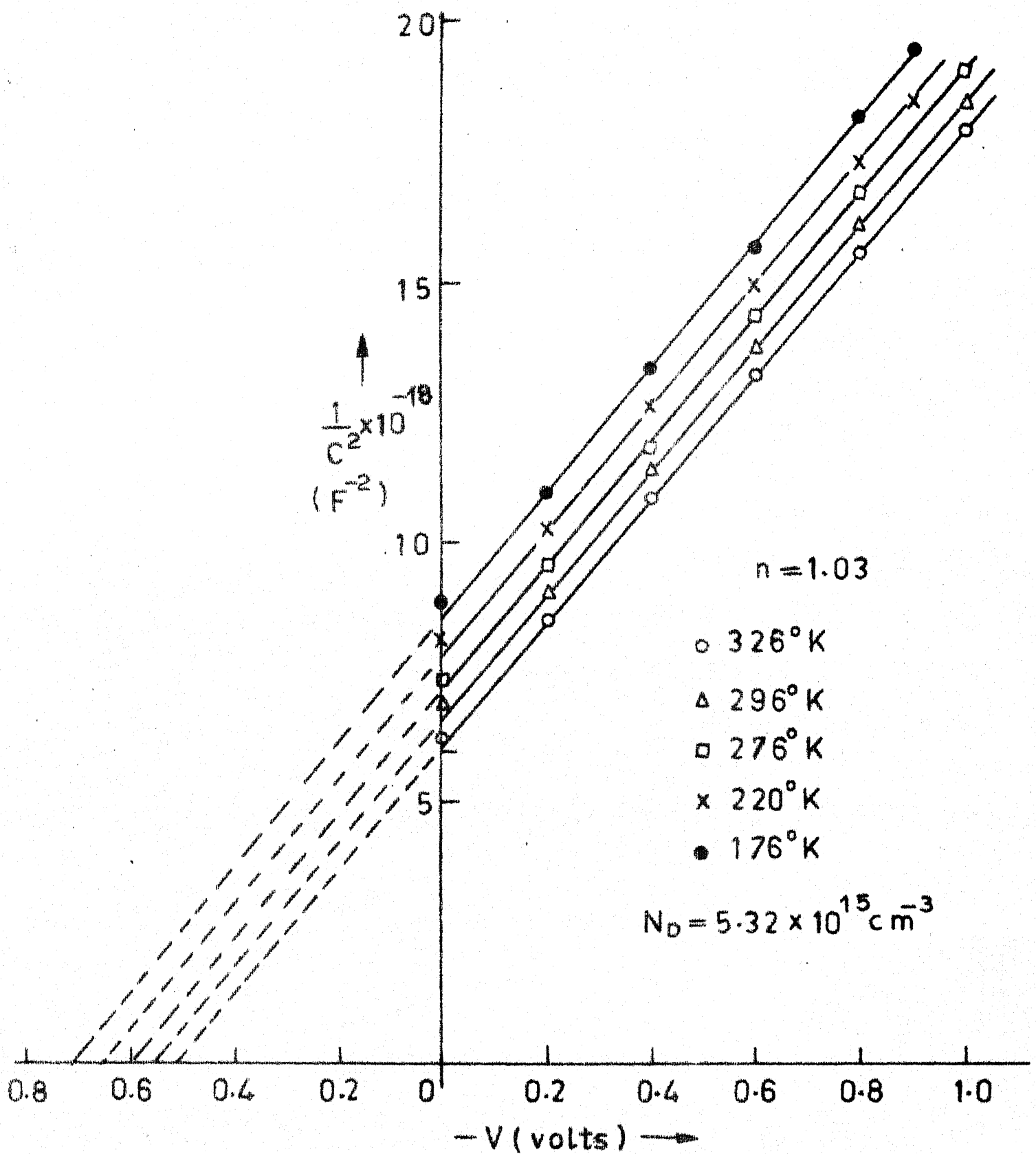


Fig. 3.22  $1/C^2$  versus  $V$  plot at different temperatures for the diode E Au 120 .

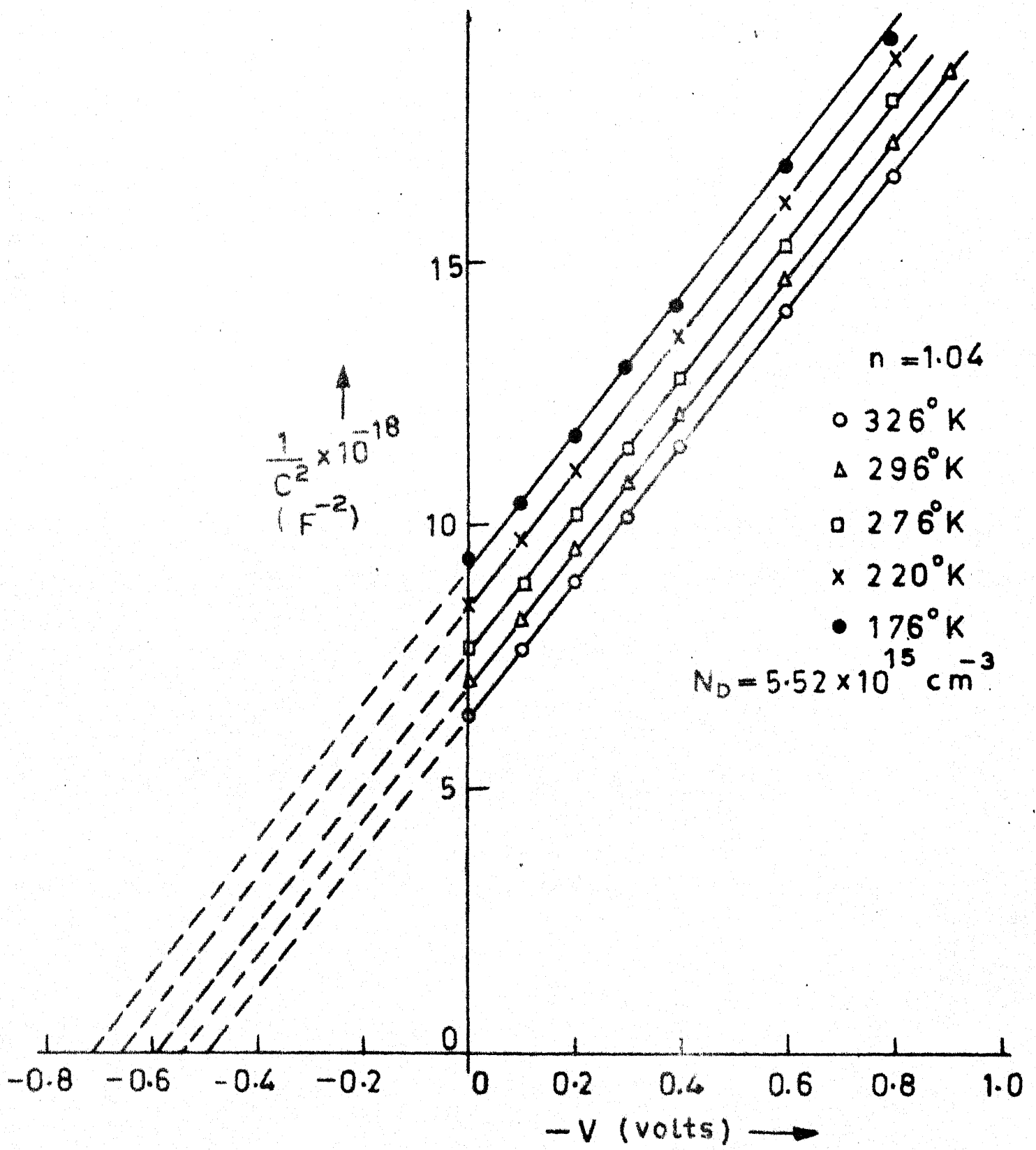


Fig.3.23  $\frac{1}{C^2}$  versus  $V$  plot at different temperatures for the diode EAu 130.



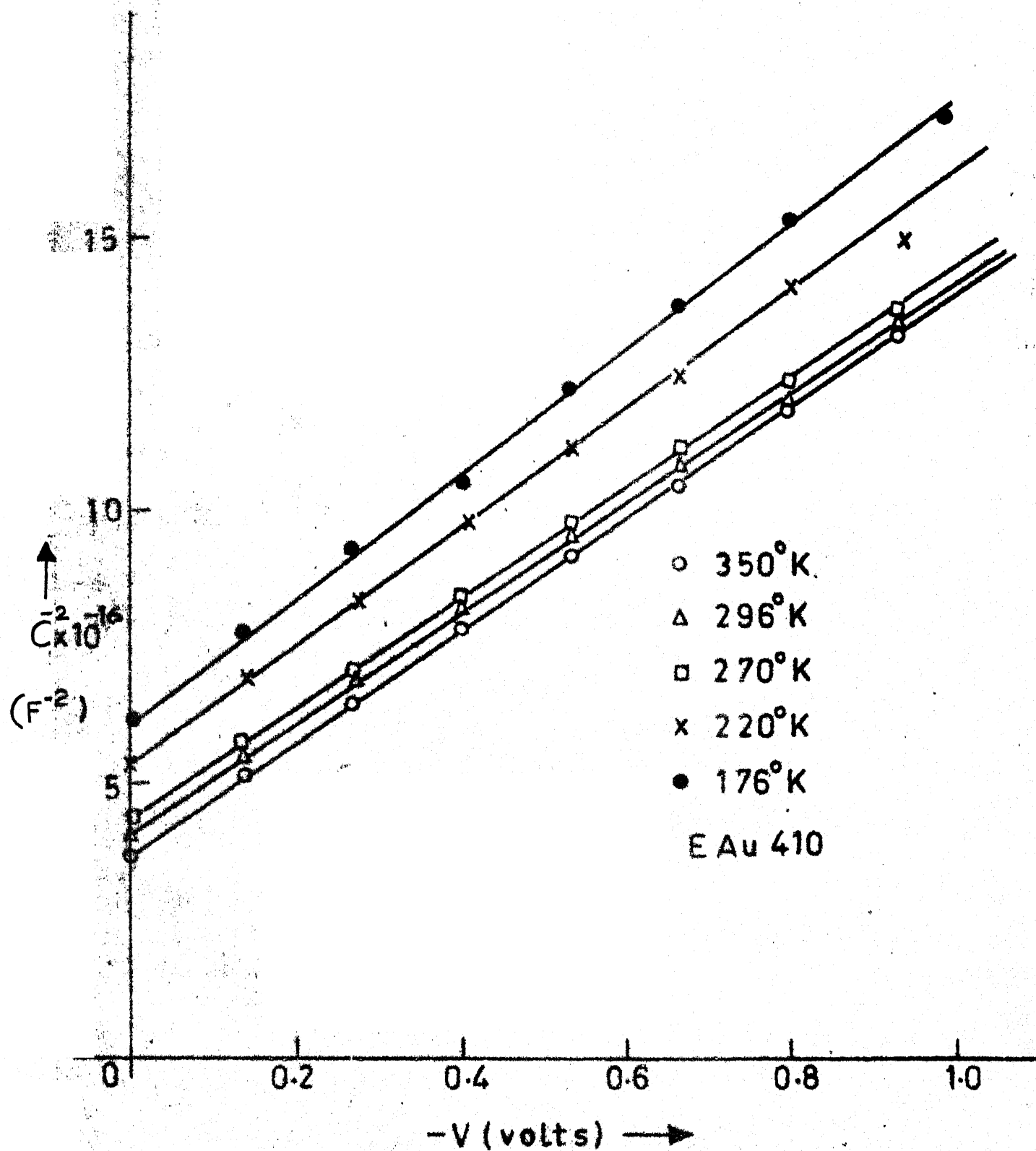


Fig. 3.24  $\frac{1}{C^2}$  versus  $V$  plot at different temperatures for the large area diode E Au 410.

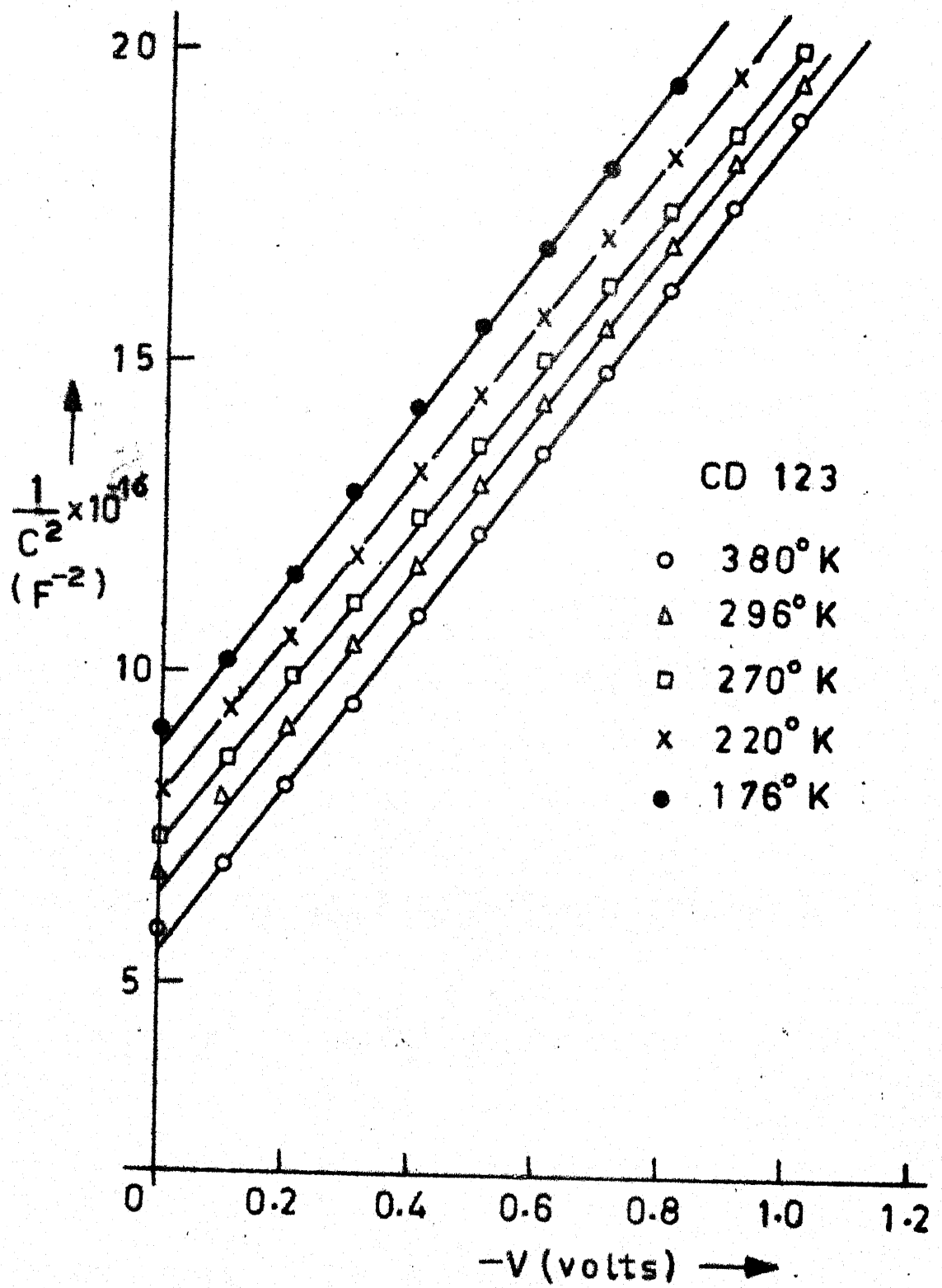


Fig.3.25  $\frac{1}{C^2}$  versus  $V$  plot at different temperatures for the combined diode CD 123.

(2) The theoretical analysis of a device in which the parameters are different at different points of area would require a two-dimensional analysis, as transverse current could flow. We have reduced the two-dimensional analysis to a one-dimensional analysis superimposed with the fluctuation in the other dimension, with the assumption that the transverse current does not play a dominant role in the nature of temperature dependence of the ideality factor.

In this chapter we have set about to experimentally verify the above mentioned assumptions. To do this following simple experiment has been carried out. A large number of isolated small area Au-nSi diodes are fabricated and the  $T_0$  in each of these diode is measured. It is found that different diodes made on the same wafer have different values of  $T_0$ . A few of these diodes are connected in parallel and the temperature variation of the ideality factor in the combined diode is measured. This plot is found to show features similar to the temperature variation in an identical system but with a large area, thus verifying the assumption that the transverse current does not play a dominant role in the temperature dependence of the ideality factor in a large area diode.

The next step in our experimental study was to establish a parameter, the fluctuation of which results in the fluctuation of  $T_0$ . To do this, we require the values of  $E_0$

$\phi^*$  and  $D_{SO}$ , the three parameters which characterise the exponential surface states responsible for the  $T_0$  anomaly. A perusal of literature shows that there is no method proposed for the determination of the values of  $\phi^*$  and  $D_{SO}$  in a diode showing  $T_0$  effect. Here we have developed a method to determine the values of  $\phi^*$  and  $D_{SO}$  from the temperature dependence of the zero bias barrier height  $\phi_{BO}$ . The method outlined to determine  $\phi^*$  and  $D_{SO}$  is formulated under the following assumptions.

(1) The neutral level  $\phi^*$ , measured from the bottom of the conduction band bears a constant ratio  $\Gamma$  to the band gap  $E_g(T)$  at all temperatures.

(2) The total depletion charge  $Q_{SCO}$  of the semiconductor at zero bias is nearly a constant over the temperature range of interest.

From the values of  $E_0$ ,  $\phi^*$  and  $D_{SO}$  determined for different sets of diodes made on the same wafer, we observed that for diodes with different  $T_0$ 's, the values of  $E_0$ 's are different while  $\phi^*$  and  $D_{SO}$  remain constant. This vindicates the choice of  $E_0$  as the fluctuating parameter in the theoretical model.

To conclude, we see that our experimental investigations justify the assumptions under which the theoretical model

has been developed to study the effect of fluctuations in geometrical and material parameters in the temperature dependence of the ideality factor in a Schottky barrier diode.

## CHAPTER 4

### T<sub>0</sub> AS AN EFFECT OF TUNNELING OF METAL ELECTRONS INTO THE FORBIDDEN BANDGAP OF THE SEMICONDUCTOR

Depending upon the physical configuration of the Schottky barrier diodes several theoretical models for explaining the T<sub>0</sub> effect have been developed [1-3]. Some of these models, along with the one that we have developed using Heine's model of a Schottky barrier, are the subject matter of this chapter. We start by briefly mentioning the main features of each of these models.

#### (i) M-N contact with localised surface states :

A model to explain the T<sub>0</sub> effect from the temperature dependence of the ideality factor in the forward I-V characteristics was first proposed by Levine [1]. Levine showed that for T<sub>0</sub> effect to take place, the surface states at the metal-semiconductor interface should be exponentially distributed in energy with a characteristic energy E<sub>0</sub>, centered at an energy level  $\phi^*$ . Thus the expression for the surface state charge Q<sub>ss</sub> that must hold (as shown by Crowell [2]) is:

$$Q_{ss} = Q_f [\exp(-(\phi^* - \phi_B)/E_0) - 1] \quad (4.1)$$

Here  $\phi_B$  is the barrier height and Q<sub>f</sub> is a constant charge

Starting from (4.1) a relation between  $E_0$  and  $T_0$  can be obtained. It is important to note that according to Levine, there is a unique relationship between  $T_0$  and  $E_0$ . An important conceptual advancement in this area came with the work of Crowell, who clearly showed that the relationship between  $T_0$  and  $E_0$  was not unique, as a matter of fact, it is possible that some other distributions in energy (of surface states) may also show  $T_0$  anomaly provided eqn. (4.2) is satisfied

$$\frac{\partial \ln Q_{sc}}{\partial \phi_B} = \text{constant} \quad (4.2)$$

at all temperatures and bias [2]. In eqn. (4.2)  $Q_{sc}$  represents the depletion charge in the Schottky barrier diode at a given bias. Based on eqn. (4.2) Crowell showed that  $T_0$  anomaly can be obtained in the case of parabolic surface states also [2].

(ii) MIN Contact :

Based on Levine's exponential surface state model [1], Rhoderick [3] has proposed a model for  $T_0$  anomaly in MIN contacts. He has modified eqn. (4.1) as follows,

$$Q_{ss} + Q_m = Q_f [\exp q(\phi^* - \phi_B)/E_0 - 1] \quad (4.3)$$

where  $Q_m$  is the charge on the metal.

(iii) M-P-N contact :

A model to describe  $T_0$  anomaly in M-P-N contacts was proposed by Crowell [2], who showed  $T_0$  anomaly to be a result of the modification in the potential profile of a metal-semiconductor diode, due to an inversion of semiconductor type at the surface. Fig. (4.1) shows a schematic charge profile and energy band diagram for a Schottky barrier diode with conversion of semiconductor type at the surface [2].

(iv) M-N contacts with distributed surface states :

A perusal of literature on M-N contacts with distributed surface states [4-6] shows that (to the best of our knowledge) no theoretical model for  $T_0$  effect has been developed for this kind of contacts. In this chapter, an attempt has been made in this direction. For this purpose one needs a model of a Schottky barrier diode with distributed surface states. A model for such diodes has already been developed by Heine [4] and detailed calculations using this model have been done by Pellegrini [6]. We have heavily drawn on the works of Heine and Pellegrini while developing our model which is presented in sec. 4.3.2.

Before proceeding further we would like to bring out the basic difference between Heine's model [4] and other surface state models [1,7,8]. This is done in the following section.



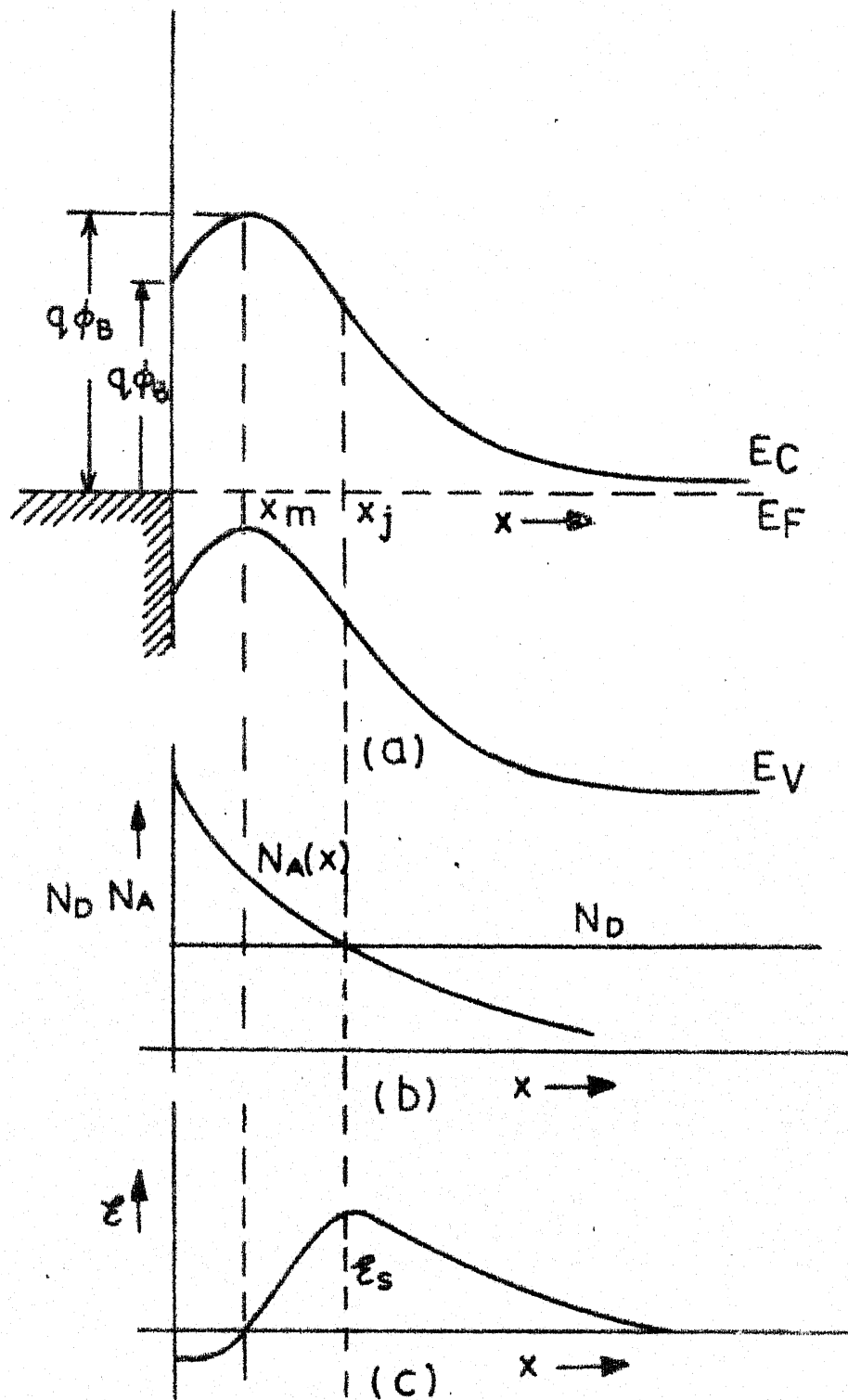


Fig.4.1(a) Energy band diagram for a Schottky barrier with conversion of semiconductor near the surface (b) Schematic doping profile for the energy band diagram in (a). (c) Electrical field distribution.

#### 4.1 Generalised Approach to the Surface State Models

The initial studies on surface state models were carried out by Bardeen [7] and Heine [4]. Their attempt was to explain the experimentally observed weak dependence of barrier height on the metal work function in some metal-semiconductor diodes. This weak dependence on work function could not be reconciled with the direct dependence of barrier height on work function as predicted by Mott [9]. The basic methodology followed in all the surface state models is to solve the Poisson's equation in the semiconductor with the condition of charge neutrality providing one of the boundary conditions. It should be noted that the various surface state models have arisen due to the different approaches adopted to evaluate the surface state charge. Let us now consider the charge neutrality equation and identify each of the surface state models.

For a metal semiconductor contact in the presence of an interfacial layer, the charge neutrality condition can be written as,

$$Q_m + Q_{sc} + Q_{ss} + Q_{ox} = 0 \quad (4.4a)$$

where  $Q_m$  = charge on the metal

$Q_{sc}$  = space charge in the semiconductor

$Q_{ss}$  = surface state charge

and  $Q_{ox}$  = charge in the interfacial layer.

In this chapter we deal only with the cases where  $Q_{ox} = 0$ , where the charge neutrality equation simplifies to the relation

$$Q_m + Q_{ss} + Q_{sc} = 0 \quad (4.4b)$$

The starting point for Cowley and Sze's [8], Levine's [1] and Heine's [4] model is equation (4.4) (because they all have  $Q_{ox} = 0$ ). In the models developed by Cowley and Sze [8] and Levine [1], both of which are <sup>based</sup> on Bardeen's surface state model [7], the surface state charge ( $Q_{ss}$ ) is taken to be localised at the semiconductor surface. In Heine's model [4]  $Q_{ss}$  is distributed in the semiconductor bulk close to the semiconductor surface. For the evaluation of  $Q_m$ , Cowley and Sze's model [8] considers a charge free interfacial layer of thickness ' $\delta$ ', across which there is a potential drop  $\Delta$ . Choosing a 'Gaussian-pill' at the metal-interfacial layer interface, assuming that there are no localised charges at this interface, one can write the charge in the metal as equal to the flux flowing out from the interfacial layer,

$$D_{out} = Q_m = \epsilon_{ox} \mathcal{E}_{ox} \quad (4.5)$$

where  $\epsilon_{ox}$  = di-electric constant of the interfacial (oxide) layer

and  $\mathcal{E}_{ox}$  = the field in the interface layer.

As opposed to Cowley and Sze's model [8], both Levine's [1] and Heine's [4] model assume a direct contact between the

metal and semiconductor resulting in a situation where one would have to solve Poisson's equation in the metal with the proper boundary conditions to obtain the charge in the metal. In the case of Levine's model [1] the calculation of  $Q_m$  is got over with by assuming that  $Q_m = 0$ ; while Pellegrini [5] in his calculations based on Heine's model, obtains the charge on the metal by assuming that the potential in the metal ( $v_m$ ) can be described by the relation,

$$v_m(x) = v_0 \exp(-x/\lambda_{TF}) \quad (4.6)$$

where  $v_0$  is the potential at the metal-semiconductor interface, and  $\lambda_{TF}$  is the Thomas Fermi screening length in the metal.

From Fig. (4.2) wherein we have presented the energy band diagram for the various barrier height along with the respective potential profile for the Poisson's equation, we note the following:

- (1) In the case of localised surface state models, the presence of the surface states govern only the boundary conditions. While the charge profile and hence the nature of the potential profile remain to be the same as in the work function model, and
- (2) In the case of distributed surface state model, the surface state charge not only modifies the boundary condition, but also the space charge term in the Poisson's equation.

# Barrier Height Models

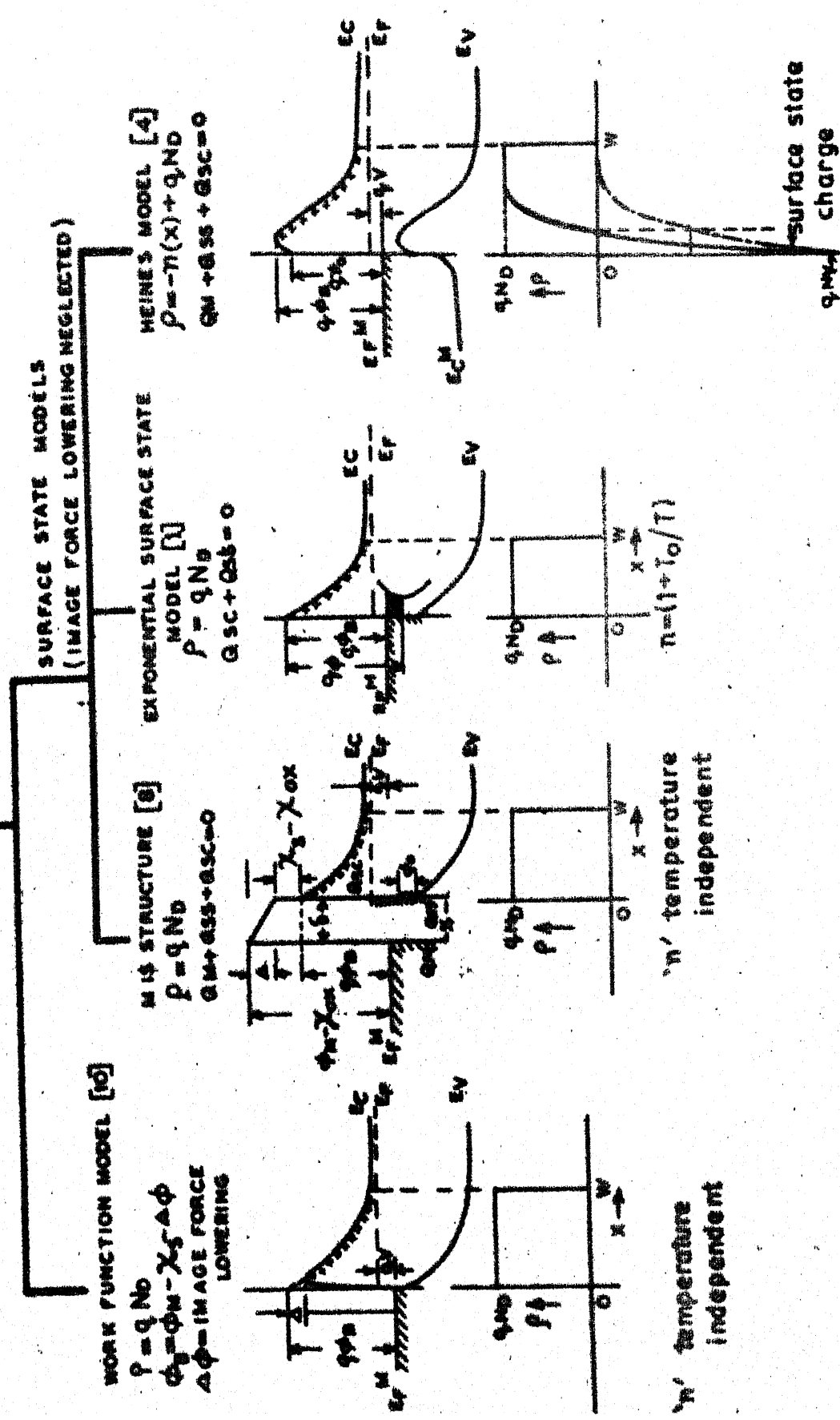


Fig. 4.2 A schematic of the various barrier height models with the corresponding energy band diagram and charge profile.

Having considered the various surface state models and their essential differences, let us next consider the models to explain the  $T_0$  effect.

#### 4.2 Existing Models for $T_0$ effect

The various models advanced to explain  $T_0$  effect can broadly be divided into three categories, (i) Work function model, (ii) Surface state model, (iii) Doped interface model. Let us now look into them one by one.

##### 4.2.1 Work function model [10] (M-N contact free of surface state)

This model was advanced based on the following observations [10],

(i) In the case of diodes showing  $T_0$  effect, the reverse saturation current follows the relation,

$$I_s = SA^*T^2 \exp(-\phi_{mso}/k(T+T_0)) \quad (4.7)$$

where  $S$  = area of the diode, and

$\phi_{mso}$  = effective barrier height (independent of temperature).

and (ii) The temperature dependence of the barrier height follows the temperature dependence of the work function ( $\phi_m$ ) of the metal, the electron affinity ( $\chi_s$ ) being assumed temperature independent.

From eqn. (4.8) the barrier height  $\phi_B(T)$  at temperature  $T$  is given by,

$$\phi_B(T) = \phi_{ms0} / (1 + T_0/T) \quad (4.8)$$

Considering the temperature dependence of the metal work function of the form,

$$\phi_m(T) = \phi_{ms0} - \alpha T \quad (4.9)$$

and using the relation  $\phi_B = \phi_m - \chi_s$  we have,

$$T_0 = T [(\phi_{ms0}/\alpha T) - 1]^{-1} \quad (4.10)$$

The work function model fails because of the following reasons:

(i) It does not explain the bias dependence of the barrier height observed in most diodes [10].

(ii) It does not explain that the value of  $T_0$ , when evaluated under constant current conditions, becomes independent of temperature.

#### 4.2.2 Surface state models

The barrier formed between the metal and semiconductor in the presence of surface states can be classified into strongly pinned barrier or weakly pinned barrier. Strongly pinned barriers are a limiting case of the surface state model, where there is a large surface state present on the semiconductor surface [11]. The weakly pinned barriers are

the barriers which fall between the two extreme cases of strongly pinned barrier, where the barrier height is independent of the metal workfunction and the workfunction model where the barrier height is directly proportional to the workfunction of the metal. We shall be looking into the  $T_0$  anomaly in the case of weakly pinned barriers and the strongly pinned barriers separately.

Before proceeding further, let us consider the necessary condition for a temperature independent  $T_0$  [2]. Assuming that the image force lowering is negligible and that the potential energy maximum is defined right at the junction we can express the space charge  $Q_{sc}$  as

$$Q_{sc} = \left( \frac{2N_D}{\epsilon_s} (\eta - 1) \frac{kT}{q} \right)^{\frac{1}{2}} \quad (4.11)$$

where  $\eta = \frac{q(\phi_B - V)}{kT} - \ln(N_c/N_D)$

$N_c$  = effective density of states in the semiconductor conduction band.

For an applied forward bias  $V > \frac{3kT}{q}$ , we have

$$\frac{\partial \ln I}{\partial V} = \frac{q}{k(T + T_0)} = \frac{q}{nkT} \quad (4.12a)$$

and  $\eta = \ln(A^{\frac{1}{2}} T^2 / J) - \ln(N_c/N_D) \quad (4.12b)$

From eqn. (4.11), (4.12a) and (4.12b) we obtain,



$$\frac{kT_o}{q} = - \frac{\partial \phi_B}{\partial \eta} = -(\partial \phi_B / \partial Q_{sc}) \cdot (\partial Q_{sc} / \partial \eta) = \frac{1}{2} \cdot \frac{1}{(\eta-1)} \cdot \frac{\partial \phi_B}{\partial \ln Q_{sc}} \quad (4.13)$$

Thus if  $T_o$  is measured at constant  $\eta$  it will be temperature independent only when  $(\partial \phi_B / \partial \ln Q_{sc})$  is a constant over the bias range associated with the operation at constant  $\eta$ . It should be noted that operating at constant  $\eta$ , if the logarithmic variation of temperature in eqn. (4.12b) is neglected, is equivalent to operating at constant current.

Having considered the necessary condition for a temperature independent  $T_o$ , let us look into the models for  $T_o$  effect in weakly pinned barriers and strongly pinned barriers one by one.

(i)  $T_o$  effect in weakly pinned barriers :

There are three models to describe  $T_o$  effect in weakly pinned barriers and are (a) Levine's exponential surface state model [1], (b) Crowell's parabolic surface state model [2], and (c) MIS model with exponential surface states [3].

Let us now consider them one by one.

(a) Levine's exponential surface state model.

The first model for  $T_o$  anomaly in Schottky barrier diodes proposed by Levine [1] has already been dealt with in sec. 1.4 of Chapter I. Here we bring out only the salient features of this model starting from surface state charge of the form,

$$Q_{ss} = Q_f [\exp (q(\phi^* - \phi_B)/E_o) - 1] \quad (4.14)$$

We have from eqn. (4.14) with  $Q_{ss} = Q_{sc}$  (considering  $Q_m=0$ ) we obtain,

$$\phi_B = \phi^* - \frac{E_o}{q} \ln \left( \frac{E_f + \mathcal{E}}{E_f} \right) \quad (4.15)$$

where  $\mathcal{E} = Q_{sc}/\epsilon_i$  and  $E_f = Q_f/\epsilon_s$ .

Using eqn. (4.13) and eqn. (4.15) we obtain

$$T_o = \frac{q}{k} \cdot \frac{1}{2(\eta-1)} \cdot \frac{E_o}{(\mathcal{E} + E_f)} \quad (4.16)$$

$$\text{where } \partial \phi_B / \partial \ln \mathcal{E} = \mathcal{E} \cdot E_o / (\mathcal{E} + E_f) \quad (4.16a)$$

Under the condition that for a weakly pinned barrier  $\mathcal{E}/E_f \gg 1$ , we can obtain,

$$\begin{aligned} T_o^{-1} &= \frac{2k}{qE_o} \cdot (\eta - 1) \\ &= \frac{2q}{E_o T} (\phi_B - V - \phi_f - \frac{kT}{q})^{-1} \end{aligned} \quad (4.17)$$

Using the expression  $J = A^* T^2 \exp (q(V - \phi_B)/kT)$ , where  $\phi_B$  is the barrier height at the voltage 'V',  $\frac{1}{T_o}$  is re-written in terms of the current density J as,

$$\frac{1}{T_o} = \frac{2k}{E_o} \cdot [\ln (J/A^* T^2) - (b+1)]^{-1} \quad (4.18)$$

where  $b = q \phi_f / kT = \ln (N_C/N_D)$ .

From (4.18) we observe that under constant current conditions,

due to the very slow variation on  $\ln T$ ,  $T_0$  can be considered temperature independent.

(b) Crowell's parabolic surface state model [2]

From eqn. (4.15) the variation in  $\phi_B$  is given by,

$$q(\phi_B - \phi_{B0}) = E_0 \ln \left( \frac{\xi + \xi_f}{\xi_0 + \xi_f} \right) = E_0 \ln \left[ 1 + \frac{\xi - \xi_0}{\xi_0 + \xi_f} \right] \quad (4.19)$$

where  $\phi_{B0}$  is the barrier height at a field  $= \xi_0$ . Taylor expanding eqn. (4.19) up to the second term, and neglecting the higher order terms ( $\frac{\xi - \xi_0}{\xi_0 + \xi_f} \ll 1$ ) eqn. (4.19) reduces to

$$(\phi_B - \phi_{B0}) = \frac{E_0}{q} \left[ \frac{\xi - \xi_0}{\xi_0 + \xi_f} \right] - \frac{1}{2} \left[ \frac{\xi - \xi_0}{\xi_0 + \xi_f} \right]^2 \quad (4.20)$$

Equation (4.20) defines the barrier height-field relation in the parabolic surface state model. In Fig. (4.3) we have reproduced from Crowell [2] a plot of  $(\phi_{B0} - \phi_B)/E_0$  versus  $(\xi - \xi_0)/(\xi_0 + \xi_f)$  for a comparison of the exponential surface state model and parabolic surface state models. Fig. (4.3) shows a very good match between the plots representing the parabolic and the exponential surface state models.

(c) MIS model

$T_0$  effect in MIS model was identified by Rhoderick [3] by including the metal charge in Levine's formulation. The charge neutrality in the presence of a finite metal charge  $Q_m$  is given by,

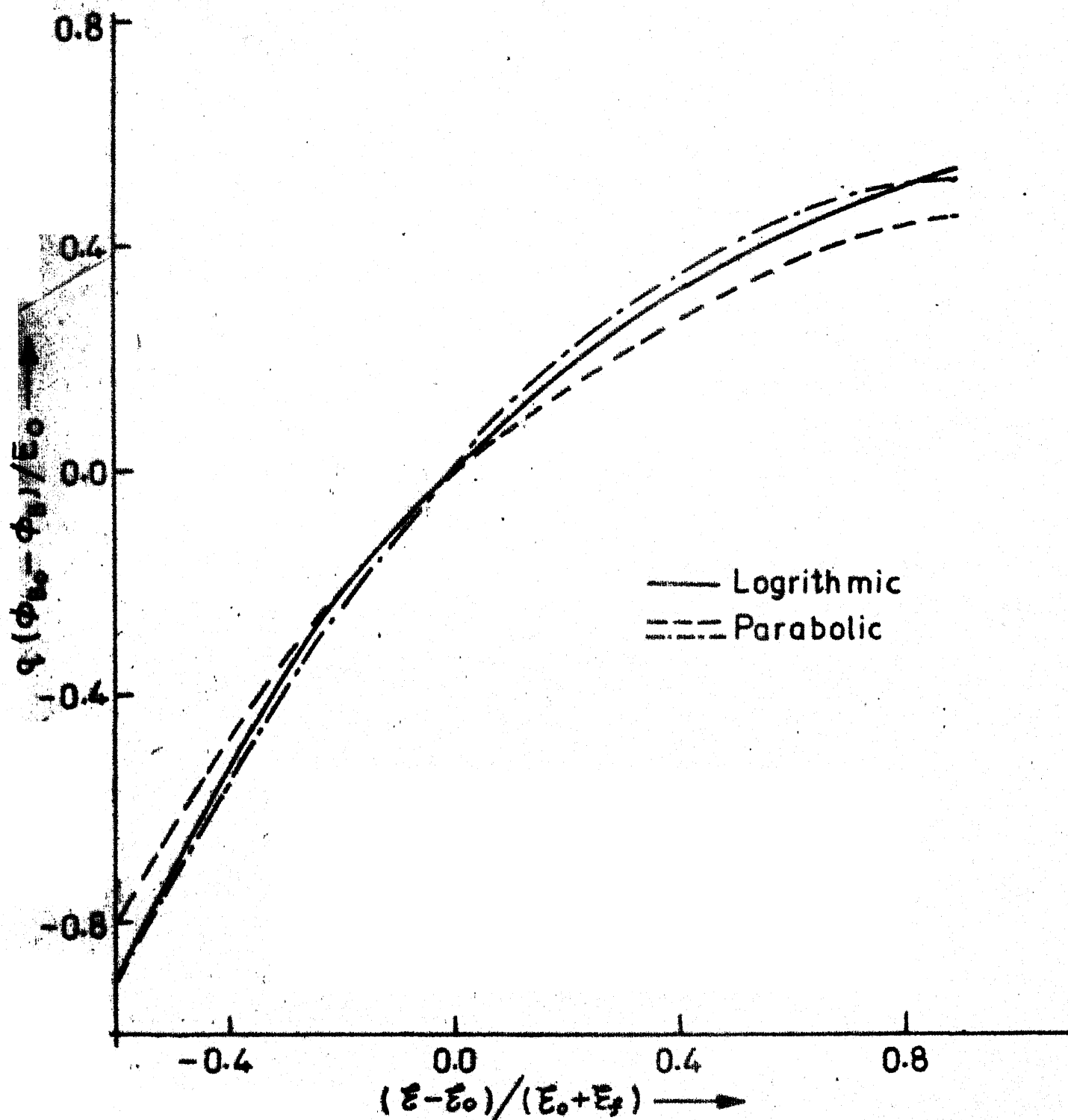


Fig.4.3 Comparison of electrical field dependence of the barrier height in units of  $E_0/q$  according to the exponential interface state model and two parabolic interface models, one of which matches value, slope and curvature at  $E = E_0$  and the other which features a three point match.

$$Q'_{ss} = Q_{ss} + Q_m = Q_{sc} \quad (4.21)$$

Following the methodology used by Levine [1], (see sec. 1.4, Chapter I), it can be shown that  $T_o$  anomaly can be seen in MIS diode under the condition,

$$Q'_{ss} = Q_m + Q_{ss} = Q_f [\exp(q(\phi^* - \phi_B)/E_o) - 1] \quad (4.22)$$

$$\text{with } T_o = T (\partial Q_{sc} / \partial \theta) / (\partial Q_{ss} / \partial \phi_B), \text{ where } \theta = (\phi_B - V) \quad (4.23)$$

In the case of an MIS diode  $Q_m$  is given by the equation,

$$Q_m = \epsilon_{ox} \mathcal{E}_{ox} = \epsilon_{ox} \cdot \frac{\Delta}{\delta} \quad (4.24)$$

where  $\mathcal{E}_{ox}$  is the field in the charge free interfacial oxide layer;  $\delta$  is the thickness of the interfacial layer; and  $\Delta$  is the drop across the interfacial layer. From potential profile given in Fig. (4.2), we obtain

$$Q_m = \frac{\epsilon_{ox} (\phi_m - \chi_s - \phi_B)}{\delta} \quad (4.25)$$

$$\text{hence } \frac{\partial Q_m}{\partial \phi_B} = - \frac{\epsilon_{ox}}{\delta} \quad (4.25a)$$

Using (4.24a) into equation (4.24b) we obtain,

$$T_o = T \cdot \frac{\partial Q_{sc}}{\partial \theta} / \left( \frac{\partial Q_{ss}}{\partial \phi_B} - \frac{\epsilon_i}{\delta} \right) \quad (4.26)$$

(ii)  $T_0$  effect in strongly pinned barriers :

As compared to a weakly pinned barrier, in the case of a strongly pinned barrier, the barrier height is very close to  $\phi^*$ , the barrier height at flatband, and hence  $\mathcal{E}_f \gg \mathcal{E}$ . Under this condition, eqn. (4.16a) reduces to

$$\frac{\partial \phi_B}{\partial \ln \mathcal{E}} = - \frac{E_0 \cdot \mathcal{E}}{\mathcal{E}_f} \quad (4.27)$$

We find that eqn. (4.27) does not satisfy the criterion for  $T_0$  effect, hence in a strongly pinned barriers  $T_0$  cannot be observed.

#### 4.2.3 Doped interface model [2]

Based on the necessary condition for the existence of  $T_0$  anomaly, Crowell [2] has proposed a model for  $T_0$  anomaly by considering a doped interface layer between the metal and semiconductor. Fig. (4.1) gives a schematic charge profile and energy band diagram for a Schottky barrier diode with conversion of semiconductor type at the surface.

The maximum field  $\mathcal{E}$  and the apparent barrier height  $\phi_B$  for an M-P-N contact are given by,

$$\mathcal{E} = \int_{x_m}^x j \frac{q(N_A - N_D)}{\epsilon_s} dx = \int_{x_j}^W \frac{q(N_A - N_D)}{\epsilon_s} dx \quad (4.28)$$

$$\text{and } \phi_B = \phi_0 + \int_0^{x_m} \frac{xq(N_A - N_D)}{\epsilon_s} dx \quad (4.29)$$

In equation (4.28)  $W$  represents the depletion width in the n-type semiconductor. From eqn. (4.28) we obtain for

$$N_A(x) = N_D \cdot (x_j/x)^2.$$

$$= \frac{qN_D x_j^2}{x_m} (1 - x_m/x_j)^2 = \frac{qN_D x_j^2}{\epsilon_s W} (1 - W/x_j)^2 \quad (4.30)$$

taking  $W/x_j \gg 1$ , we have

$$\epsilon_s = qN_D W = Q_{sc} \quad (4.31)$$

Using eqn. (4.28) to (4.31) we obtain,

$$\frac{\partial \phi_B}{\partial \ln Q_{sc}} = \frac{\partial \phi_B}{\partial \ln \epsilon} = \frac{qN_D x_j^2}{\epsilon_s} [1 - x_m/x_j]^2 \quad (4.32)$$

$$= \frac{qN_D x_j^2}{\epsilon_s} = E_0 \quad \text{for } x_m \ll x_j \quad (4.32a)$$

From eqn. (4.32a) we see that  $T_0$  anomaly can be obtained from an M-P(thin)-N contact with the doping in the p-layer  $N_A(x) = N_D(x_j/x)^2$ . It should be noted that, while the doped interface model gives a physical origin for  $E_0$ , the model is heavily process dependent, as well as the metal used for the formation of the Schottky barrier [2]. It should be noted that this model is restricted to a limited types of doping profile in the p-layer.

#### 4.3 $T_0$ as an Effect of Tunneling of Metal-Electron into the Forbidden bandgap of the Semiconductor

From the various models for  $T_0$  effect described in the previous section, the following important observations are made.

(i) The necessary condition for the existence of  $T_0$  effect in a Schottky barrier diode is that the slope of the  $\ln Q_{sc} - \phi_B$  plot should be a constant at all temperatures and biases.

(ii) Levine [1] showed that to obtain a constant slope of  $\ln Q_{sc} - \phi_B$  plot, the surface states should be exponentially distributed in energy. According to Crowell [3], however, this restriction of exponential energy distribution of surface states is not the only one that would lead to  $T_0$  effect. For example, Crowell has shown that the potential profile of a Metal-P(thin)-N diode is such that one can obtain linear  $\ln Q_{sc} - \phi_B$  relationship for certain doping profiles of the P-layer.

(iii) Heine [4] has considered metal-semiconductor contacts with the surface state charges due to the tunneling of metal electrons into the forbidden band gap of the semiconductor. It is interesting to note that the potential profile in this case has a very large correspondence with that of M-P(thin)-N diodes. Hence it seems worthwhile to investigate whether in these (Heine's) cases also a  $T_0$  effect can be obtained. Let us reiterate that  $T_0$  effect can be observed in M-P-N diodes for very limited types of profile in the P-layer. To search for a similar restriction, if any, in case of Heine's model [4] is the main purpose of the study presented in this chapter. The steps to be followed are summarised below,



(1) Pellegrini [6] has carried out the quantum mechanical calculations for Schottky barriers obeying Heine's model. His method can be used (as shown in sec. 4.3.1) to calculate the depletion charge  $Q_{sc}$  and the barrier height  $\phi_B$  at different bias for various temperatures.

(2) Then one can check for the linearity of the  $\ln Q_{sc} - \phi_B$  plot at room temperature. This study is repeated at various temperatures and the temperature range in which  $\ln Q_{sc} - \phi_B$  plot is linear is noted.

(3) The forward I-V characteristics is calculated and hence the value of  $V_T$  at various temperatures under constant current condition is obtained. Check is then made whether the  $V_T$  versus  $T$  plot exhibits a  $T_0$  effect, in the temperature range determined in (2), for the cases where slope of  $\ln Q_{sc} - \phi_B$  plot is a constant independent of temperature. The details of the calculations are given below.

#### 4.3.1 Pellegrini's Calculations for Heine's model [6] (Heine-Pellegrini model)

When a metal is brought into contact with an n-type semiconductor a region on the latter to the right of the interface (see Fig. 4.2) is depleted of the conduction band electron and at the same time its forbidden energy gap becomes occupied by electrons as a result of the quantum mechanical tunneling from the conduction band of the metal. In

an analogous way the electrons of the semiconductor valence band may penetrate below the conduction band of the metal, giving rise to Thomas-Fermi charge. It should be noted that when the Thomas-Fermi charge at the metal is considered we have a dipole at the surface, whose field is directed away from the metal. This is in addition to the dipole due to the charge due to the ionized donors, whose field is directed towards the metal. The presence of these two dipoles gives rise to the potential profile shown in Fig. (4.2). Let us now consider the salient features of the calculations carried out by Pellegrini for Heine's model.

(i) Calculation of the surface state charge

It has been shown earlier that in the case of Heine's distributed surface state model a knowledge of the space distribution of the surface state charge is necessary, since it contributes to the charge in the Poisson's equation. Parker et al. [5] have solved the Poisson's equation by assuming a surface charge distribution of the form

$$\rho_{ss} = \frac{qN}{d} \exp(-x/d) \quad (4.33)$$

and choosing an arbitrary value of  $N$  to fit their experimental data. Pellegrini in his calculations differs from others in that he treats the metal-semiconductor contact as a single system and solves (i) Schrödinger's equation and (ii) Poisson's equation self consistently for the

evaluation of the space charge due to the tunneling of metal electron into the forbidden bandgap of the semiconductor and the potential distribution respectively. For this the potential energy term in the Schrödinger equation is assumed to be a constant equal to the potential at the metal-semiconductor junction. Using the wavefunction ' $\Psi$ ' the space charge due to the surface state is found, which is used to solve the Poisson's equation. Thus an improved potential energy form is obtained. The process is continued till self-consistency is obtained and hence the final charge and the potential profiles are obtained. Since the investigations carried out here are of an exploratory nature, we will not go into the details of Pellegrini's calculations, but only present the results relevant to our study.

Before proceeding further we would like to point out the salient feature of the Heine-Pellegrini models. The most important aspect of Pellegrini's calculations is the introduction of a phenomenological parameter  $E_T'$ , the limit value of the transverse energy beyond which the electron quantum penetration into the forbidden energy gap is zero. The genesis of  $E_T'$  would be clear from the following discussion.

Fig. (4.4) shows a plot of  $E_{ks} - k_{xs}^2$  for different values of  $E_T'$ , where  $E_{ks}$  is the energy in the semiconductor

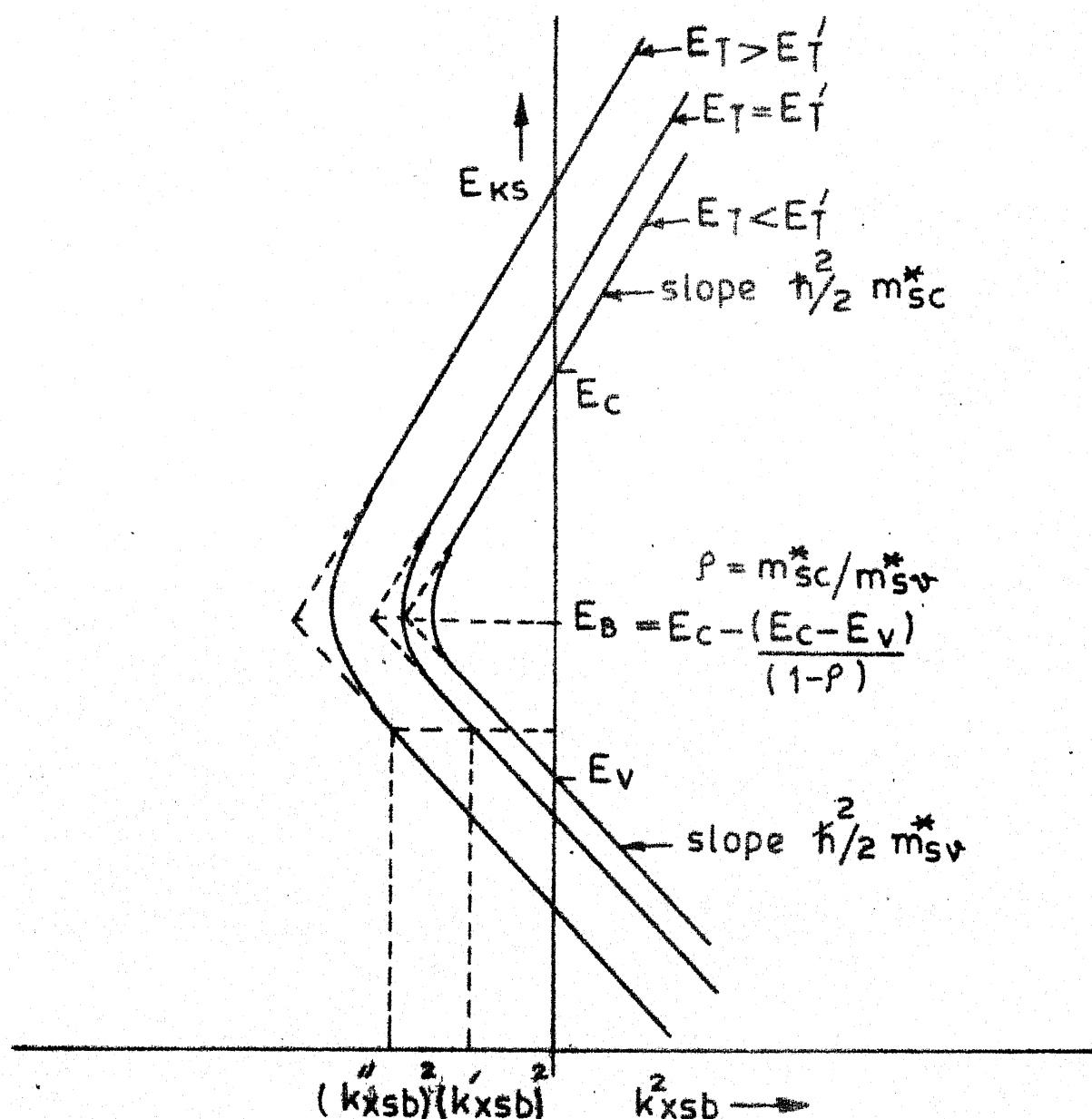


Fig.4.4 Electron energy diagram in the semiconductor as a function of  $k_{xsb}^2$  and  $E'_T$

and  $k_{xsb}$  is the propagation vector in the band  $b$  of the semiconductor in the direction of tunneling. From the figure, one can see that for a given value of  $E_{ks}$  (say  $E'_{ks}$ ) the corresponding value of  $|k''_{xsb}|$  for  $E_T > E'_T$  is much greater than the value of  $|k'_{xsb}|$  for  $E_T < E'_T$ , so that the associated value of the wave function becomes negligible compared with those depending on  $k'_{xsb}$ . Here  $E_T$  represents the energy in the direction transverse to the direction of tunneling. Note that in Fig. (4.4) is a plot of  $E_{ks}$  versus  $k_{xsb}^2$ , rather than the conventional  $E_{ks}-k_{xsb}$  plot. The reason for this is as follows.

Generally, near the bandedge ( $E_c$  or  $E_v$ ) the energy is quadratic in  $k$ , and usually written by analogy with the free electron theory as,

$$E_{ks} = \frac{1}{2} \hbar^2 \frac{k_{xsb}^2}{m_{xsb}^*} + \frac{1}{2} \hbar^2 \frac{k_{Tsb}^2}{m_{Tsb}^*} \quad (4.34)$$

$$\text{where } k_{Tsb}^2 = k_{ysb}^2 + k_{zsb}^2$$

and a plot of this is given in Fig. (4.4). For  $E \geq E_c$ ,  $k^2$  is positive, therefore,  $k$  is real and propagating  $g$  solution exists. For energies in the forbidden gap,  $E_c < E < E_v$ ,  $k^2$  is negative, and exponentially damped solutions result [12].

Having looked into the salient point in the Heine-Pellegrini model, let us now look into the results of Pellegrini's calculations.

(ii) Evaluation of potential profile:

The charge due to the penetration of metal electrons are considered to have two components  $n_{sc}(x)$  and  $n_{sv}(x)$  which occupy states in the bandgap near the conduction and the valence band respectively. These are given by the relation,

$$n_{sc}(x) = N_c \exp(-x/\lambda_c) \quad (4.35a)$$

$$n_{sv}(x) = N_v \exp(-x/\lambda_v) \quad (4.35b)$$

where  $N_c$ ,  $N_v$ ,  $\lambda_c$  and  $\lambda_v$  are obtained in terms of the known parameters of the metal and the semiconductor and the limit energy  $E_T'$ .  $N_c$  and  $N_v$  are the densities of the metal electron tunneling close to the conduction and the valence band and  $\lambda_c$  and  $\lambda_v$  are the respective mean penetration depths. Contribution of  $n_{sc}(x)$  and  $n_{sv}(x)$  to the built in potential is obtained as

$$V_q = \frac{q}{\epsilon_s} (N_c \lambda_c^2 + N_v \lambda_v^2) \quad (4.36)$$

Incorporating the charges  $n_{sc}(x)$  and  $n_{sv}(x)$  into the Poisson's equation along with the charge due to the ionised donors we obtain,

$$\frac{d^2 v(x)}{dx^2} = \frac{q}{\epsilon} (n_{sc}(x) + n_{sv}(x) - N_D) \quad (4.37)$$

A closed form solution for eqn. (4.37) is obtained by assuming that there exists a length  $w$  of a section of the depletion region characterised by the inequalities,

$$v_c - V - v_i(w) \gg kT/q \quad (4.38a)$$

$$W \gg w \gg \lambda_c, \lambda_v \quad (4.38b)$$

where  $v_c = (\phi_m - \chi_s - \phi_f)$  is the contact potential difference

$v$  = applied bias

$v(w)$  = the potential at the point  $w$ ,

and  $W$  = depletion width.

Under this assumption the field at any point within the semiconductor can be attained as,

$$\mathcal{E}(x) = -\frac{q}{\epsilon_s} [N_c \lambda_c \exp(-x/\lambda_c) + N_v \lambda_v \exp(-x/\lambda_v) - N_D(W-x)] \quad (4.39)$$

Integrating eqn. (4.39) with the boundary condition that  $v(0) = v_0$ , one obtains the potential profile,

$$\begin{aligned} v(x) = v_0 - \frac{qN_D x^2}{\epsilon_s} \left(W - \frac{x}{2}\right) + \frac{q}{\epsilon_s} [1 - \exp(-x/\lambda_v)] N_v \lambda_v^2 \\ + \frac{q}{\epsilon_s} [1 - \exp(-x/\lambda_c)] N_c \lambda_c^2 \end{aligned} \quad (4.40)$$

$$W = \sqrt{\frac{2\epsilon_s}{qN_D} (v_b - V)}$$

$$v_b = (v_0 + v_q - \frac{kT}{q})$$

The quantities  $v_q$ ,  $\mathcal{E}(x)$ , and  $v(x)$  are all dependent on the voltage ( $V$ ) through the voltage dependence of  $\mathcal{E}_0$  and  $v_0$ , the field and the potential at the surface. These equations

along with the condition of charge balance give a transcendental equation for  $v_0$ . The solution of this transcendental equation leads to the knowledge of  $v_0$ ,  $W$ ,  $\mathcal{E}(x)$  and  $v(x)$  (for details see Appendix D).

(iii) Evaluation of Current:

For the potential profile obtained as above, a general expression for the current is obtained as [5,13],

$$i = SA^* T^2 \tau \exp(-q\phi_B/kT) [\exp(qV/kT) - 1] \quad (4.41)$$

where  $\phi_B$  = barrier height =  $(\phi_m - \chi_s + v_m)$

$v_m$  = maximum value of  $v(x)$

$\tau$  = effective transparency of the energy barrier to the thermionic emission

$$= 1 + \int_0^{q(v_c - v + v_m)/kT} \exp(\eta) / [1 + \exp(F(\eta))] a d\eta \quad (4.42)$$

$$a = |\eta|/\eta$$

In eqn. (4.42) the function  $F(\eta)$  is defined by,

$$F(\eta) = \frac{4\pi}{h} (2m_{xsc})^{\frac{1}{2}} \int_{x_1(\eta)}^{x_2(\eta)} -q[v_m - v(x) - \eta kT]^{\frac{1}{2}} dx \quad (4.43)$$

where  $x_1$  and  $x_2$  are the turning points where  $(v_m - v(x) - \frac{\eta kT}{q}) = 0$ .

It should be mentioned here that we have restricted our calculations to the range of doping density and applied



bias, where  $\tau$  is very close to unity. Thus confining the investigation to the metal-semiconductor contacts where the current transport is predominantly due to thermionic emission. This reduces eqn. (4.43) to the simple form,

$$I = SA^*T^2 \exp(-\phi_B/kT) [\exp(qV/kT) - 1] \quad (4.44)$$

This brings us to the end of the presentation of Pellegrini's results and in the next section we present the results of our investigation.

#### 4.3.2 Results and Discussion

In this section we present the results of our calculations, based on Heine-Pellegrini's model, on Au-nSi contacts. These calculations have been carried out to explore the possibility of finding  $T_0$  effect as a result of tunneling of metal-electron into the forbidden bandgap of the semiconductor. As already mentioned, to do this we require to obtain the  $\ln Q_{sc}$  versus  $\phi_B$ , and  $V_T$  versus  $\frac{kT}{q}$  plots, and check that,

- (i) the plot of  $\ln Q_{sc}$  versus  $\phi_B$  is a straight line,
- (ii) the slope of the  $\ln Q_{sc}$  versus  $\phi_B$  plot is a constant independent of temperature,
- (iii) in the case where (i) and (ii) are true, the  $V_T$  versus  $kT/q$  plots (as obtained from the forward I-V characteristics at different temperatures) exhibit  $T_0$  effect and

- (iv) in the case where (i) is not true, the  $V_T$  versus  $\frac{kT}{q}$  plot does not exhibit  $T_0$  effect.

(1)  $\ln Q_{sc} - \phi_B$  Plot:

The plots of  $\ln Q_{sc}$  versus  $\phi_B$ , evaluated from eqns. (4.35a) to (4.44) for a Au-nSi diode with the semiconductor doping  $N_D = 2 \times 10^{16}/\text{cm}^3$  are given in Fig. (4.5) for different temperatures with  $E'_T$  as a parameter. The parameter  $E'_T$  is the limit value of the electron energy in the semiconductor, perpendicular to direction of tunneling, beyond which the electron quantum penetration into the semiconductor is negligible [6]. A perusal of Pellegrini's results [6] show that  $E'_T$  varies from diode to diode for the same metal-semiconductor system. Based on this observation we have chosen  $E'_T$  as a variable parameter in our calculations. The following features of Fig. (4.5) are of interest:

- (i) The  $\ln Q_{sc}$  versus  $\phi_B$  plot is a straight line at all temperatures for  $E'_T > 0.03$  eV.
- (ii) The slope of the  $\ln Q_{sc}$  versus  $\phi_B$  plot for  $E'_T > 0.03$  eV is independent of temperature, thus satisfying Crowell's [2] criterion for  $T_0$  effect.

From these results, one concludes that according to Heine-Pellegrini's model, the  $T_0$  effect is expected to occur for  $E'_T > 0.03$  eV. Let us now look into the  $V_T$  versus  $T$  plot to investigate the existence of  $T_0$  effect in these diodes.

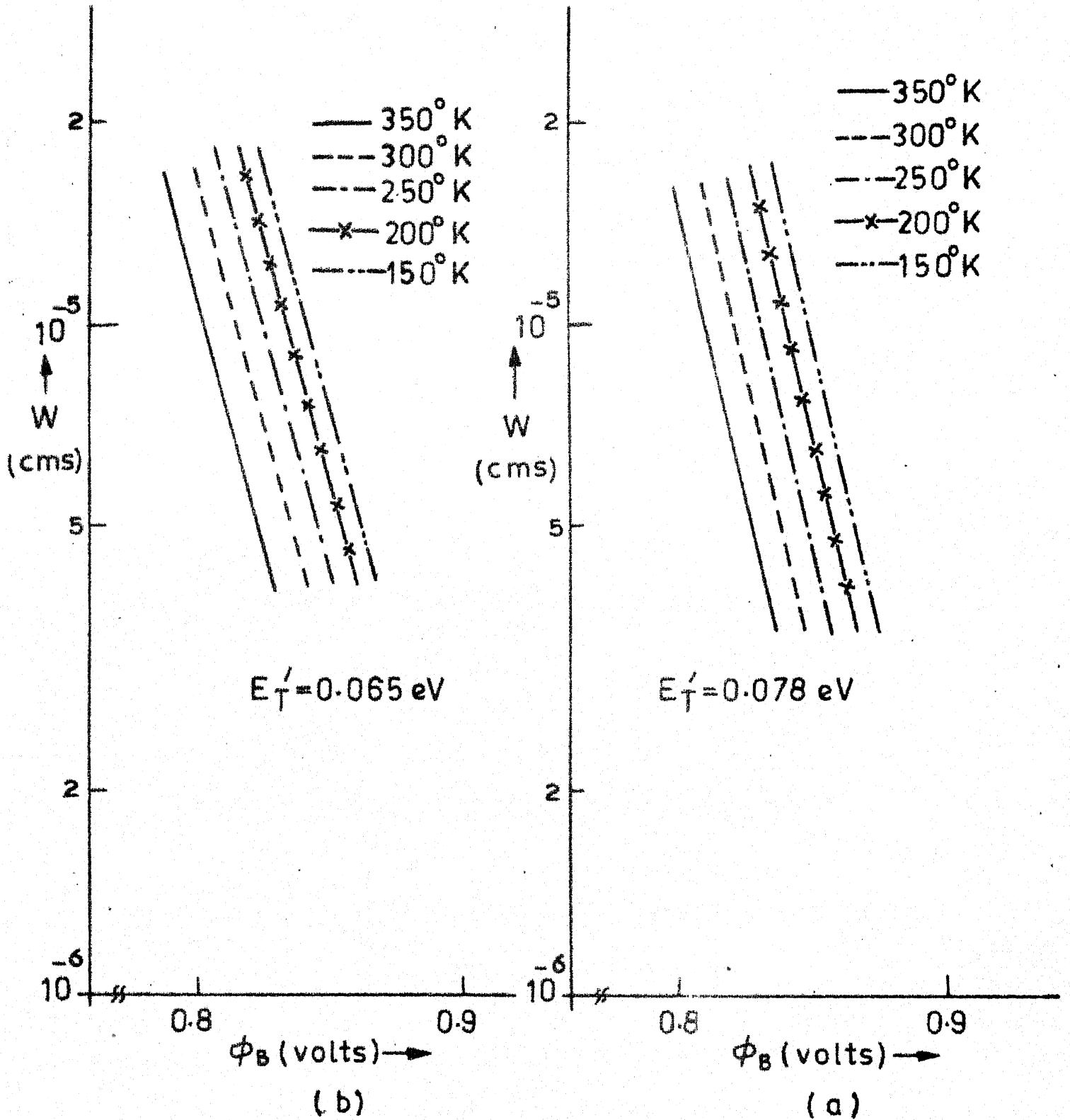


Fig.4.5 (a) Plot of  $\ln W$  versus  $\phi_B$  for  $E_T' = 0.078 \text{ eV}$ .  $W = Q_{sc}/qN_D$   
 (b) Plot of  $\ln W$  versus  $\phi_B$  for  $E_T' = 0.065 \text{ eV}$ .  $W = Q_{sc}/qN_D$

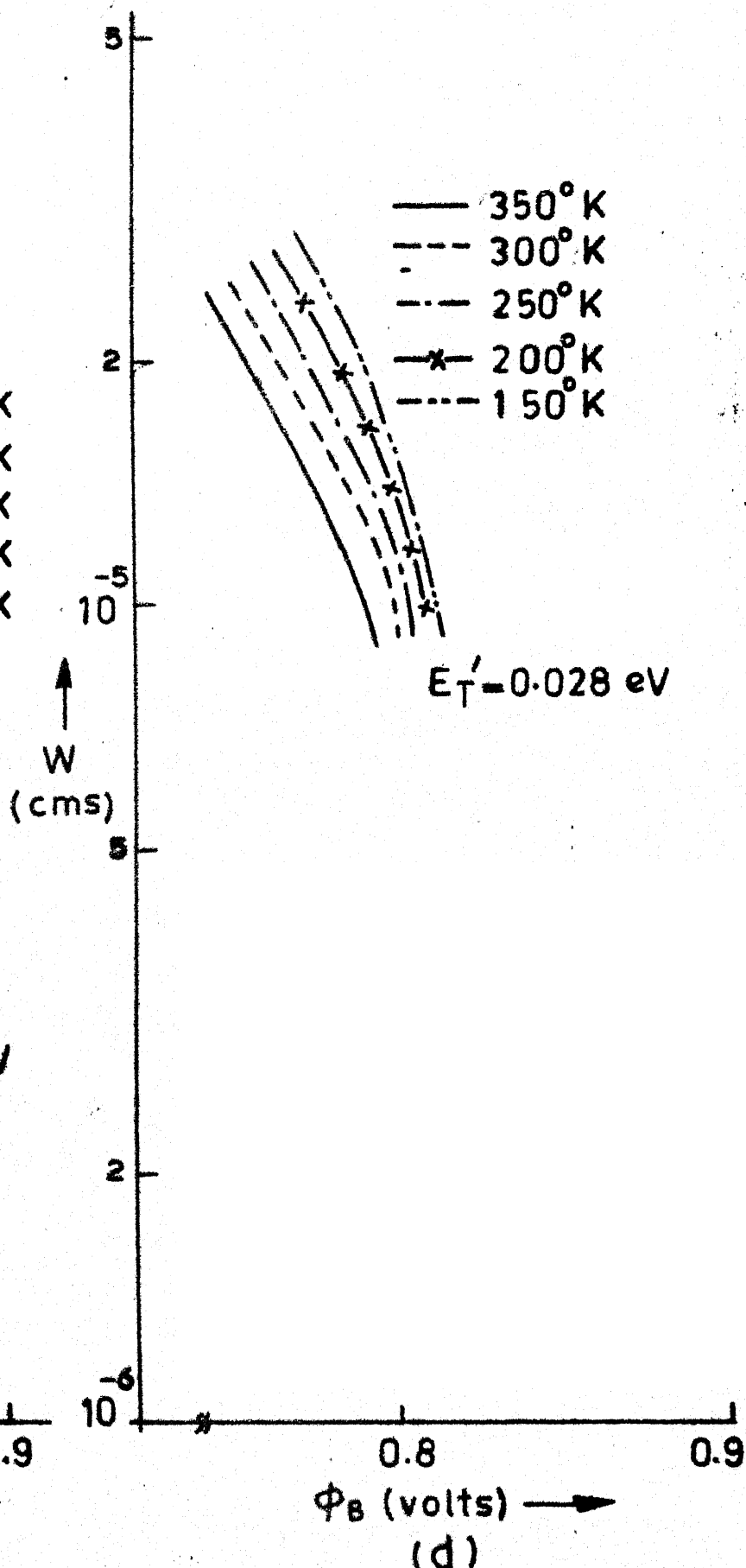
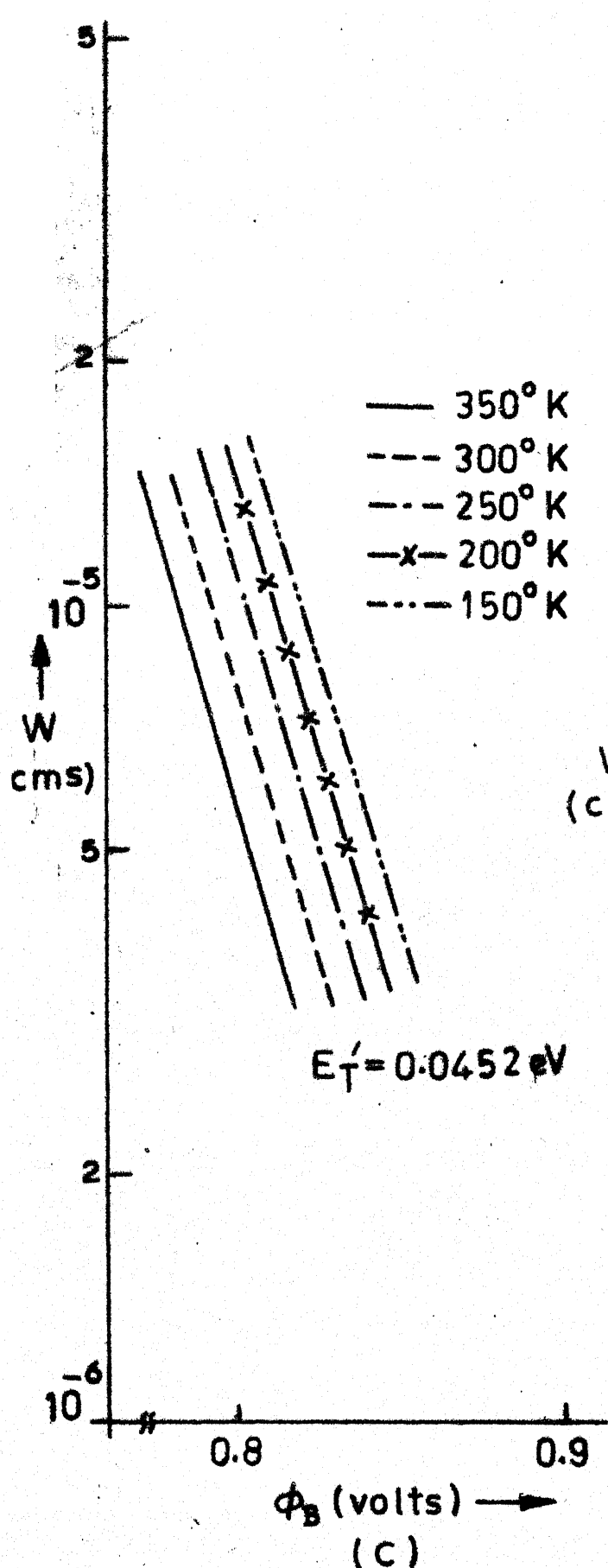


Fig. 4.5 (c) Plot of  $\ln W$  versus  $\phi_B$  for  $E_T' = 0.0452 \text{ eV}$ .  $W = Q_{sc}/qN_D$   
 (d) Plot of  $\ln W$  versus  $\phi_B$  for  $E_T' = 0.028 \text{ eV}$ .  $W = Q_{sc}/qN_D$

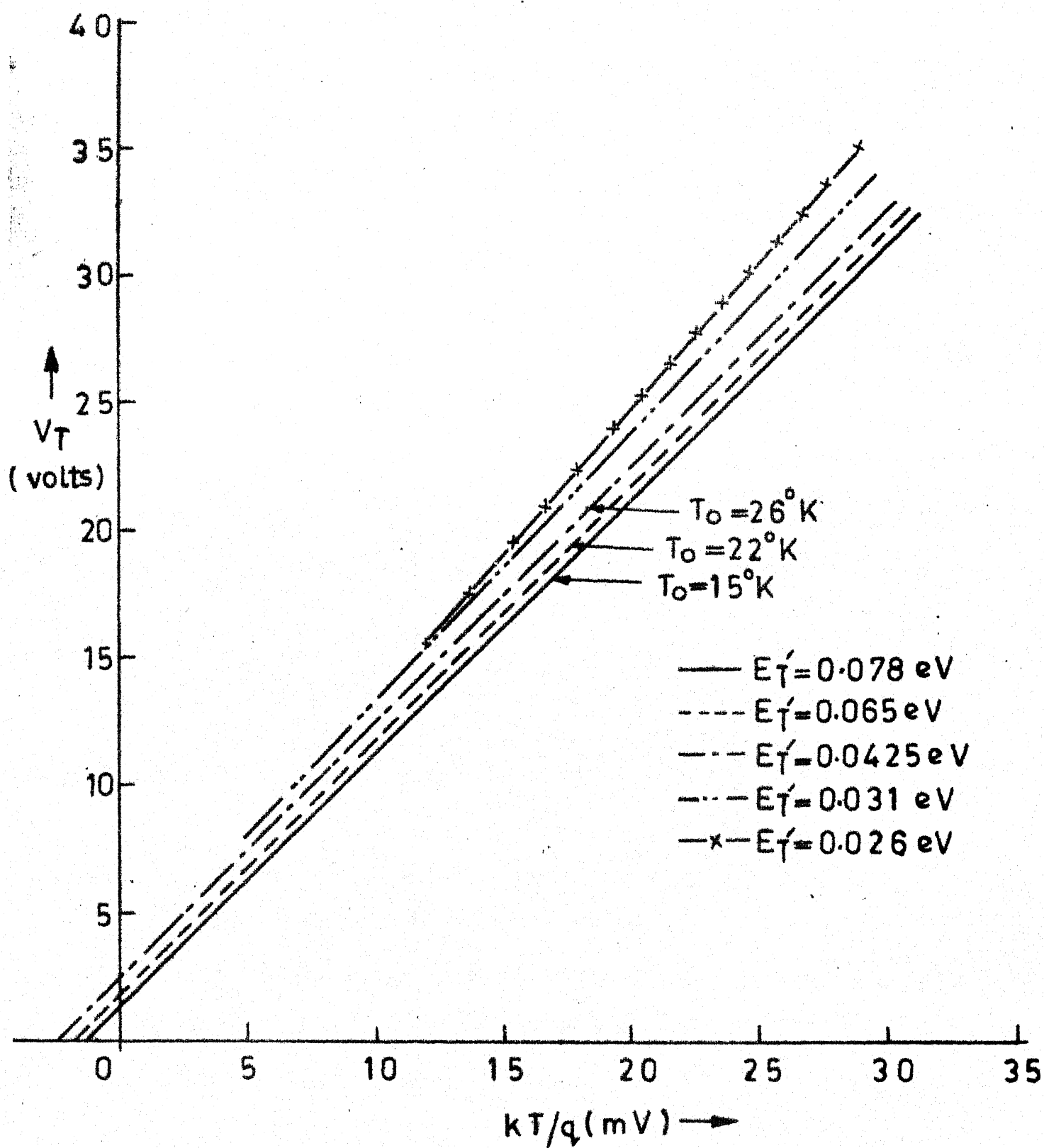


Fig.4.6 Plot of  $V_T$  versus  $kT/q$  for different  $E_T'$ .

(2)  $V_T$  versus  $T$  plot:

The  $V_T$  versus  $T$  plot for the diodes, whose  $\ln Q_{sc}$  versus  $\phi_B$  plot is given in Fig. 4.5, is given in Fig. 4.6. We note the following features of these diagrams:

- (i) For the diodes with  $E_T' > 0.03$  eV, the  $V_T$  versus  $T$  plot is a straight line, parallel to the unity ideality factor line but not passing through the origin. Thus, we see that Schottky barrier diodes in Heine-Pellegrini's model [6] exhibit  $T_0$  effect for certain values of  $E_T'$ .
- (ii) The value of  $T_0$  for different diodes, studied here, increases with a decrease in  $E_T'$ .
- (iii) For the diodes with  $E_T' < 0.03$  eV (for example, see plot for  $E_T' = .027$  eV in Fig. 4.5(d)) which do not satisfy Crowell's condition for  $T_0$  effect, the  $V_T$  versus  $T$  plot can be fitted to the form  $V_T = \frac{k}{q} (aT+b)$ , where the slope 'a' is greater than unity. Thus we see that in the case where  $\ln Q_{sc} - \phi_B$  plots are not a straight line of constant slope independent of temperature the diodes do not show  $T_0$  effect in the conventional sense.

Similar calculations were carried out for different doping densities and the following observations were made:

There is an upper and a lower limit on the range of doping densities, outside of which  $T_0$  effect is not observed. The upper limit is fixed by the doping density

beyond which the thermionic field emission current starts to be comparable to the thermionic emission current, and is found to be  $5 \times 10^{18}/\text{cm}^3$ . The lower limit arises due to the reduction in the ideality factor 'n' with the reduction in doping density. In our calculations we see that at a doping of about  $N_D = 10^{15}/\text{cm}^3$ , the ideality factor falls down to about 1.01.

The explanation for the decrease in 'n' with a decrease in the doping density is as follows:

It is well known that as the doping density  $N_D$  decreases the depletion charge  $Q_{sc} (= qN_D W)$  also decreases. Based on this, we see that in eqn. (D.13) (reproduced below for convenience), used to evaluate the potential at the metal semiconductor interface ( $v_0$ ),

$$\frac{e_m \cdot v_0}{\lambda_{TF}} = (qN_V \lambda_V - qN_D W) \quad (4.45)$$

the contribution of the  $qN_D W$  term decreases with decrease in the doping density  $N_D$ . This means that as the value of  $N_D$  is decreased, the value of  $v_0$  and hence the barrier height approaches the flat band barrier height. Thus, we see that as the doping density is reduced the barrier approaches the case of a strongly pinned barrier, wherein the barrier height changes very slowly with the applied bias, leading to an ideality factor close to unity [2].

To conclude, we observe that  $T_0$  effect can also be obtained when the surface states are due to the tunneling of metal-electron into the forbidden band gap of the semiconductor provided suitable value of  $E_T'$  and doping densities are chosen.

#### Conditions for Equivalence of $E_T'$ and $E_0$

The characteristic energy  $E_0$  in the exponentially distributed surface state model has been taken to be an empirical parameter. No attempt to link it with physical causes of surface state distribution has been made in Levine's work [1]. Having established that Heine-Pellegrini's model, under suitable constraints, can lead to  $T_0$  effect, and that the value of  $T_0$  is dependent on the value of  $E_T'$ , it becomes tempting to attempt a correlation between  $E_0$  and  $E_T'$ . If this succeeds, one would have succeeded in linking the phenomenological parameter  $E_0$  with a much more fundamental phenomenological parameter  $E_T'$ .

The first difficulty one faces in doing this is due to the observation that the surface states in Heine's model are distributed both in energy and space (near the metal-semiconductor interface) whereas in Levine's model these are distributed in energy but localised in space. The other difficulty arises from the observation that while Levine considers a zero charge on the metal, Heine's model considers



a finite charge on the metal. To see the correlation mentioned above, we integrate the surface state charge for the Heine-Pellegrini model, in space and add the charge on the metal and check for the relation [3],

$$Q_{sc} = Q_m + Q_{ss} = Q_f [\exp(-q(\phi^* - \phi_B)/E_0) - 1] \quad (4.46)$$

If the exponential relation of eqn. (4.46) is obtained then the correlation of  $E_T'$  and  $E_0$  can be easily established. We see that for the case of  $Q_f \ll Q_{sc}$  and by taking logarithm on both sides eqn. (4.46) reduces to:

$$\ln Q_{sc} = \ln Q_{sci} - \frac{q\phi_B}{E_0} \quad (4.47a)$$

$$\text{where } \ln Q_{sci} = \ln Q_f + \frac{q\phi^*}{E_0} = \ln Q_f + \frac{\Gamma E_g(T)}{E_0} \quad (4.47b)$$

Note that use has been made of the relation  $\phi^* = \Gamma E_g(T)$  which was developed in sec. 3.3.3 of Chapter III. Using the plot  $\ln Q_{sc}$  versus  $\phi_B$ ,  $\ln Q_{sci}$  at different temperatures can be obtained, which in turn is plotted as a function of  $E_g(T)$  to obtain the values of  $Q_f$  and  $\Gamma$ . Once  $\Gamma$  is known  $\phi^*$  is also obtained.

In Table 4.1 we have presented the values of  $E_0$ ,  $\phi^*$ ,  $Q_f$  and  $D_{so}$  ( $D_{so} = Q_f/E_0$ ) for different  $E_T'$  and  $N_D$ . Note that  $D_{so}$  represents the equivalent surface state density at an energy  $q\phi^*$  from the bottom of the conduction band. From the table we see that, (i) The values of  $\phi^*$  and  $D_{so}$  are

Table 4.1. Table showing a correlation between  $E_T'$  and  $E_o$  for three different values of the doping density.

Doping Density $N_D$ ( $\text{cm}^{-3}$ )	$E_T'$ (eV)	$E_o$ (eV)	$q\phi^{\#}$ (eV)	$D_{so}$ ( $\text{cm}^{-2} \text{eV}^{-1}$ )
$2.2 \times 10^{16}$	0.078	0.022	$.8 E_g(T)$	$4.94 \times 10^{11}$
	0.065	0.024	$.8 E_g(T)$	$4.92 \times 10^{11}$
	0.0452	0.036	$.79 E_g(T)$	$4.94 \times 10^{11}$
$6.3 \times 10^{16}$	0.078	0.031	$.81 E_g(T)$	$9.20 \times 10^{11}$
	0.065	0.035	$.8 E_g(T)$	$9.40 \times 10^{11}$
	0.0452	0.043	$.81 E_g(T)$	$9.40 \times 10^{11}$
$2.2 \times 10^{17}$	0.073	0.038	$.8 E_g(T)$	$2.30 \times 10^{12}$
	0.065	0.043	$.79 E_g(T)$	$2.10 \times 10^{12}$
	0.0452	0.047	$.79 E_g(T)$	$2.30 \times 10^{12}$

nearly independent of the value of  $E_T'$  for a given doping density. (ii) The value of  $E_0$  increases with a decrease in  $E_T'$ , and that the values of  $E_0$  can be fitted to the form,

$$E_0 = a + b, E_T'$$

$$\text{where } b = 0.00078 \text{ eV}^2 \quad (4.48)$$

$$a = [1 + \log(N_D/10^{16})] \times 0.014 \text{ eV}$$

Carrying out numerical calculations to evaluate the depletion charge  $Q_{sc}$  at zero bias, for  $E_T' = .03 \text{ eV}$ , using eqns.

(4.46) and (4.48), and the values of  $\phi^*$  and  $D_{so}$  for  $N_D = 2.2 \times 10^{16}/\text{cm}^3$  (given in Table 4.2), we see that in this case the condition that  $Q_{sc} \gg Q_f$  does not hold good. Since for the occurrence of  $T_0$  effect, we require  $Q_{sc} \gg Q_f$  [2], the observation mentioned above provides a reason for non-observance of  $T_0$  effect in cases where  $E_T' < 0.03 \text{ eV}$  for the values of other parameters as considered here.

To summarize the findings of this chapter, we briefly mention the main results that have been obtained.

- (1) It has been shown that  $T_0$  effect can also be obtained when the surface states are due to the tunneling of metal electrons into the forbidden bandgap of the semiconductor provided suitable values of  $E_T'$  and doping densities are chosen.

- (2) We have succeeded in linking the characteristic energy  $E_0$  in the exponential surface state model with  $E_T'$  in the Heine-Pellegrini model, through a linear relationship between  $E_0$  and  $1/E_T'$ .

## CHAPTER 5

### DETERMINATION OF DOPING DENSITY FROM THE FORWARD CURRENT-VOLTAGE CHARACTERISTICS

In the previous chapter, the interest has been to understand the mechanisms of current transport that constitute  $T_0$  effect in Schottky barrier diodes. In this chapter we present a novel method for determining the impurity concentration in a semiconductor wafer. The method requires the measurement of forward I-V characteristics of a Schottky barrier diode fabricated on the semiconductor wafer mentioned above. One more requirement of this method is that the Schottky barrier should exhibit  $T_0$  effect. Note that this requirement automatically puts a limitation on the application of this method.

Before presenting the method mentioned above, let us briefly go through some of the methods that are presently utilized to determine the impurity concentration of semiconductor wafers. The existing methods can be broadly classified into two categories. The first category consists of those methods (e.g., differential capacitance versus voltage method) which can determine the impurity concentration

in the wafer as a function of depth [1,2]. The second category consists of those methods which can determine the impurity concentration only when the doping density is independent of depth [2]. It is important to note, however, that the methods of category one are more versatile and can definitely do the job done by the methods of category two. The method evolved by us belongs to the second category and hence is useful only when the impurity concentration in the semiconductor wafer is independent of depth.

Thus we see that the method suggested in this chapter suffers from the following limitations:

- (1) It is applicable only when the Schottky barrier diode made on the wafers whose impurity concentration is to be measured exhibits a  $T_0$  effect, and
- (2) It is applicable only when the doping density is independent of the depth.

Note that the method being suggested here utilizes the I-V characteristics. The advantage of this method primarily ensues because of the ease of measurement of the forward I-V characteristics.

Perhaps the most popular of the existing methods of category two is the measurement of capacitance-voltage (C-V) characteristic of Schottky barriers made on wafers whose impurity concentration is to be determined. We consider this method in the next section.

### 5.1 Evaluation of Doping Density from the C-V Characteristics

The theoretical derivation leading to the use of C-V measurements as a profiling technique is based upon the validity of the depletion approximation. This assumes that the depletion region consists entirely of charge due to the ionised donors, (i.e.) the mobile carrier concentration is negligibly small compared to the fixed impurity concentration.

For a Schottky barrier diode under depletion approximation, the total charge  $Q_{sc}$  on the semiconductor at any bias  $V$  is given by,

$$Q_{sc} = \sqrt{2\epsilon_s q N_D (\phi_B - V - \phi_f - (kT/q))} \quad (5.1)$$

where  $N_D$  = the doping density

and  $\phi_B$  = barrier at a bias  $V$ .

Differentiating eqn. (5.1) with respect to the applied bias, we obtain the capacitance per unity area  $C'$  as,

$$C' = - \frac{dQ}{dV} = + \left\{ \frac{2}{q\epsilon_s N_D} (\phi_B - V - \phi_f - \frac{kT}{q}) \right\}^{-\frac{1}{2}} \left( 1 - \frac{\partial \phi_B}{\partial V} \right) \quad (5.2)$$

From eqn. (5.2) we observe that we require the voltage dependence of the barrier height to evaluate an expression for the capacitance as a function of the applied bias. Depending on the voltage dependence of the barrier height the diode can be classified either as an ideal diode with  $\partial \phi_B / \partial V = 0$

or a non-ideal (practical) diode, whose non-ideality is defined by an ideality factor  $n$ , given by,

$$n = [1 - \partial \phi_B / \partial V]^{-1} \quad (5.3)$$

Let us now look into each of these cases individually.

(1) Ideal diode:

For an ideal diode with  $\partial \phi_B / \partial V = 0$ , from eqn. (5.2) we get,

$$C' = \left[ \frac{2}{q \epsilon_s N_D} (\phi_B - V - \phi_f - \frac{kT}{q}) \right]^{-\frac{1}{2}} \quad (5.4)$$

$$\text{i.e.} \quad \frac{1}{C'^2} = \frac{2}{q \epsilon_s N_D} (\phi_B - V - \phi_f - \frac{kT}{q}) \quad (5.4a)$$

From eqn. (5.4a) we see that the doping density  $N_D$  can be obtained from the slope 'm' of the  $1/C'^2$ -V plot, using the relation,

$$N_D = \frac{2}{q \cdot \epsilon_s} \cdot \frac{1}{m} \quad (5.5)$$

(2) Non-ideal diode:

As has been seen in Chapter I, the class of non-ideal diodes can be classified into two categories depending on the temperature dependence of the ideality factor. These are,

(i) Diodes showing  $T_0$  effect, wherein the ideality factor  $n$  is given by the relation,

$$n = (1 + T_0/T) \quad (5.6)$$



where  $T_0$  is independent of temperature when measured under constant current condition. Note, at a given temperature  $T_0$  is voltage dependent.

(ii) Diodes showing 'n' independent of temperature and bias. These diodes have a thin insulating layer between the metal and semiconductor and are referred to as MIS diodes.

Let us look into the C-V characteristic and hence the evaluation of  $N_D$  in each of these cases,

(a) Diodes showing  $T_0$  effect:

For a diode showing  $T_0$  effect, using eqns. (5.6) and (5.3) in eqn. (5.2), we obtain,

$$C' = \left[ \frac{2}{q\epsilon_s N_D} (\phi_B - V - \phi_f - \frac{kT}{q}) \right]^{-\frac{1}{2}} (1 + T_0/T) \quad (5.7)$$

From eqn. (4.13) in Chapter IV, we have,

$$T_0 = \frac{q}{2k(\eta-1)} \cdot \frac{\partial \phi_B}{\partial \ln Q_{sc}} \quad (5.8a)$$

$$\text{where } \eta = \frac{q(\phi_B - V)}{kT} - q\phi_f/kT \quad (5.8b)$$

Using eqn. (5.8a) and (5.8b) along with the relation,

$$\frac{\partial \phi_B}{\partial \ln Q_{sc}} = \frac{E_0}{q} \quad (5.8c)$$

in eqn. (5.7) and squaring we obtain,

$$C'^2 = \left[ \frac{2}{\epsilon_s q N_D} \left( x + \frac{E_0}{q} + \frac{E_0^2}{4q^2 x} \right) \right] \quad (5.9a)$$

$$\text{i.e.} \quad \frac{1}{C'^2} = \frac{2}{\epsilon_s q N_D} \left( x + \frac{E_o}{q} + \frac{E_o^2}{4xq^2} \right) \quad (5.9b)$$

$$\text{where} \quad x = \left( \phi_B - V - \phi_f - \frac{kT}{q} \right)$$

For reverse bias when  $E_o^2/4xq^2 \ll (x + E_o/q)$  we have [3],

$$\frac{1}{C'^2} = \frac{2}{\epsilon_s q N_D} \cdot \left\{ \frac{1}{n_1} \left[ n_1 \left( \phi_B - \phi_f - \frac{kT}{q} \right) - V \right] \right\} \quad (5.10)$$

$$\text{where} \quad \phi_B = \phi_{BO} + \frac{\partial \phi_B}{\partial V} \cdot V = \phi_{BO} + \frac{T_o}{T+T_o} V$$

$$n_1 = (1 + T_o/T)$$

and  $\bar{T}_o$  = mean value of  $T_o$  in the voltage range of interest.

From eqn. (5.10) we observe that the doping density  $N_D$  can be obtained from the slope 'm' of the  $\frac{1}{C'^2} - V$  plot using the relation,

$$N_D = \frac{2}{\epsilon_s \cdot q} \cdot \frac{1}{m} \cdot \frac{1}{n_1} \quad (5.11)$$

(ii) MIS contacts:

For these contacts the ideality factor 'n' is both temperature and bias independent [4]. Thus using eqn. (5.1) in eqn. (5.2) we obtain,

$$\frac{1}{C'^2} = \frac{2}{q \epsilon_s N_D} \cdot n \left[ n \left( \phi_B - \phi_f - \frac{kT}{q} \right) - V \right] \quad (5.12)$$

From eqn. (5.12) we observe that the doping density can be obtained from the slope 'm' of the  $\frac{1}{C'^2} - V$  plot using the relation,

$$N_D = \frac{2}{q\epsilon_s} \cdot \frac{1}{m} \cdot n \quad (5.13)$$

From eqn. (5.11) and (5.13) we observe that to evaluate the doping density  $N_D$  from the  $\frac{1}{C^2} - V$  plot of a practical Schottky barrier diode requires a knowledge of the I-V characteristics also. Thus we see that it would be of interest to find a method to evaluate  $N_D$  from the forward I-V characteristic and hence reduce the number of measurements to be carried out.

Some of the other methods used to evaluate the doping density in a semiconductor wafer are (i) four point probe method and (ii) Van der Pauw method. Details of these methods are given in Appendix E.

## 5.2 Determination of Doping Density from the Forward I-V Characteristics

Although forward I-V characteristics are convenient to measure and are extensively used to characterize a Schottky barrier diode, to the best of our knowledge, there has been no method available so far to determine the impurity concentration from the I-V measurements. The method to be described in this section is based on the dependence of  $T_0$  (calculated from the slope of the forward I-V characteristics) on the current at which it is measured. For this we require a general relationship between  $T_0$  and I in the case of diodes showing  $T_0$  effect.

Referring to eqn. (5.8a), one can write the expression for  $T_o$  at a bias  $V$  as,

$$T_o = \frac{q}{2k(\eta-1)} \cdot \frac{\partial \phi_B}{\partial \ln Q_{sc}} \quad (5.13)$$

$$\begin{aligned} \text{where } \eta &= \frac{q(\phi_B - V)}{kT} - \ln(N_C/N_D) \\ &= \frac{q(\phi_B - V)}{kT} - b = -[\ln(I/SA^{\frac{1}{2}}T^2) + b] \end{aligned} \quad (5.13a)$$

$N_D$  = doping density in the semiconductor

$\phi_B$  = barrier height

and  $N_C$  = effective density of states in the conduction band of the semiconductor.

Using eqns. (5.13), (5.13a) and (5.8c), one obtains,

$$\frac{1}{T_o} = -\frac{2k}{qE_o} [\ln(I/SA^{\frac{1}{2}}T^2) + (b+1)] \quad (5.14)$$

From eqn. (5.14) one observes that a plot of  $1/T_o$  versus  $\ln(I/A^{\frac{1}{2}}T^2S)$  will be a straight line of slope  $t = -\frac{2k}{qE_o}$  and intercept with  $1/T_o = 0$  of,

$$\ln I' = -(b+1) + \ln(A^{\frac{1}{2}}T^2S) \quad (5.15)$$

$$\text{i.e., } -b = (1 + \ln I'/A^{\frac{1}{2}}T^2S) \quad (5.16)$$

Using the relation  $b = \ln(N_C/N_D) = -\ln(N_D/N_C)$  and eqn. (5.16), the expression for  $N_D$  is obtained as,

$$N_D = N_C \exp(-b) = N_C(I'/A^{\frac{1}{2}}T^2S) \cdot e \quad (5.17)$$

where  $e = 2.7183$ .

### 5.3 Results and Discussion

In Fig. (5.1) we present  $\frac{1}{T_0}$  versus  $\ln I$  plots at  $296^\circ\text{K}$  for three Au-nSi Schottky barrier diodes (EAu 110, EAu 120, EAu 130), which showed a  $T_0$  effect (see sec. 3.4, Chapter III). The doping density obtained from the slope of the  $\frac{1}{T_0}$  versus  $\ln I$  plot, using eqn. (5.11) for these three diodes is given in Table 5.1, along with the doping density obtained from the C-V method. The table also contains the values of doping density obtained for two more sets of Schottky barrier diodes. Note that for the set of diodes made on bulk silicon we have included the value of  $N_D$  obtained from four point probe and Van der Pauw measurements also.

From Table 5.1 it is observed that the value of doping density evaluated from the  $1/T_0$  versus  $\ln I$  plot matches well with the values obtained using the other methods.

To summarize, we have proposed a new method to determine the doping density from the forward I-V characteristics of a Schottky barrier diodes. With the proposal of a method to evaluate the doping density from the forward current-voltage (I-V) characteristics, one observes that this method along with the methods described in sec. 3.3 of Chapter III to evaluate  $E_0$ ,  $\phi^*$  and  $D_{so}$ , can be used to completely characterise a diode showing  $T_0$  effect, from the forward I-V

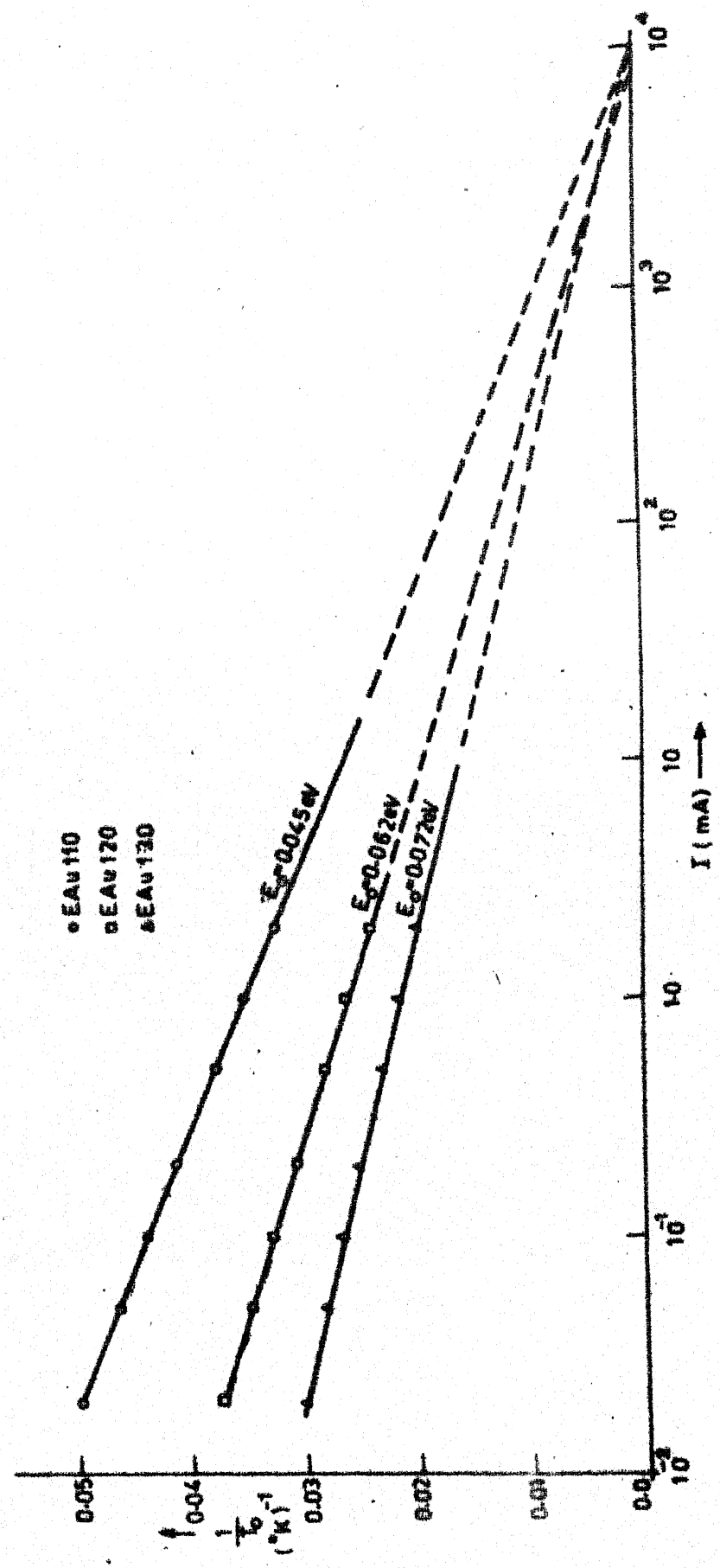


Fig. 5.1 Plot of  $\frac{1}{T_0}$  versus  $\ln I$  for three small area diodes EAu110, EAu120, EAu130.

Table 5.1. Values of doping densities calculated using different methods for three sets of diodes showing  $T_0$  effect.

Doping Density $N_D$ ( $\text{cm}^{-3}$ )					
Wafer used	Device	$1/T_0$ vs $\ln I$ plot	$1/c^2$ -V plot	Fourpoint probe	Van-der Pauw
$n^+$ -n Sili- con Epi wafer	EAu 110	$5.52 \times 10^{15}$	$5.3 \times 10^{15}$	-	-
	EAu 120	$5.35 \times 10^{15}$	$5.32 \times 10^{15}$	-	-
	EAu 130	$5.45 \times 10^{15}$	$5.52 \times 10^{15}$	-	-
$n^+$ -n Silicon Epi wafer	EAu 210	$5.0 \times 10^{15}$	$5.2 \times 10^{15}$	-	-
	EAu 220	$5.1 \times 10^{15}$	$5.16 \times 10^{15}$		
	EAu 230	$5.1 \times 10^{15}$	$5.05 \times 10^{15}$		
	EAu 240	$5.08 \times 10^{15}$	$5.17 \times 10^{15}$		
	EAu 250	$5.16 \times 10^{15}$	$5.4 \times 10^{15}$		
Bulk n-Si wafer	DAu 111	$2.35 \times 10^{15}$	$2.22 \times 10^{15}$	$2.4 \times 10^{15}$	$2.3 \times 10^{15}$
	DAu 121	$2.25 \times 10^{15}$	$2.25 \times 10^{15}$		
	DAu 131	$2.40 \times 10^{15}$	$2.3 \times 10^{15}$		
	DAu 141	$2.30 \times 10^{15}$	$2.1 \times 10^{15}$		

data alone. This means a reduction in the number of measurements to be carried out on the diode. Note,  $E_0$ ,  $\phi^*$  and  $D_{so}$  represent respectively, the characteristic energy, the neutral level at the surface and the density of surface states at the neutral level in an equivalent Levine's model [3] for a diode showing  $T_0$  anomaly.

Before concluding, we would like to reiterate that this method has the following limitations:

- (i) It can only be used if the Schottky barrier diode shows  $T_0$  anomaly, and
- (ii) It can only be used if the semiconductor wafer has a uniform doping profile.



## CHAPTER 6

### SUMMARY AND CONCLUSIONS

It has been observed by many workers that the ideality factor ( $n$ ) of rectifying metal-(low doped) silicon ( or GaAs etc.) contacts can either be independent of or dependent on temperature ( $T$ ) depending upon the processing and the nature of starting materials. The work in this thesis has mainly been concerned with those diodes which show a temperature dependent ideality factor. The main results are summarised below.

(i) We observed that a method has been suggested in literature to distinguish between the thermionic emission (TE), Thermionic field emission (TFE), and field emission (FE) as the mechanism of current transport in Schottky barrier diodes. The method consists of plotting  $nT$  versus  $T$  (obtained from the forward current-voltage ( $I$ - $V$ ) characteristics measured at different temperatures) where a linear plot corresponds to TE, a temperature independent plot corresponds to FE and the intermediate case corresponds to TFE. The work done here has pointed out that the above mentioned assignment is valid only in the case of homogeneous diodes (where there is no fluctuation in geometrical and material

parameters transverse to the metal-semiconductor interface) and is not valid for nonhomogeneous diodes. For example, it has been shown, both theoretically and experimentally (see Chapters I, II and III) that if  $T_0$  (where  $T_0$  is a temperature independent constant in the relation  $nT = T + T_0$ ) fluctuates the  $nT$  versus  $T$  plot would indicate the current transport to be due to field emission in the conventional sense when it is actually due to thermionic emission. Thus the present work emphasizes that caution must be exercised when inferring the mechanism of current transport from the nature of the  $nT$  versus  $T$  plots.

(ii) An attempt was made to correlate  $T_0$  with the material and geometrical parameters at the metal-semiconductor interface. In this regard it was noted that Levine (in 1971) had already proposed a model where an exponential energy distribution of interface states, characterized by a characteristic energy  $E_0$ , was shown to be the reason for the appearance of  $T_0$  effect in Schottky barrier diodes. Later in 1977, Crowell has pointed out that the choice of exponential energy distribution of interface states is not the only one which would give  $T_0$  effect, rather several other distributions of interface states could do it. For example, he has shown that it is possible to obtain  $T_0$  effect

in M-P(thin)-N diodes, provided suitable doping profile is chosen in the P-layer. We further noted that Heine (in 1965) has proposed a model of Schottky barrier where a potential profile similar to that of M-P(thin)-N diode appears due to the charge incorporated by metal electrons tunneling into the forbidden bandgap of the semiconductor. Prompted by these observations and the detailed calculations based on Heine's model as carried out by Pellegrini (in 1974), we set out to correlate a parameter  $E_T'$ , the limiting value of the transverse energy of the electrons tunneling from the metal into the forbidden bandgap of the semiconductor, with the  $T_0$  effect. The calculations have been done in two steps. The first step was to assume the correlation of  $T_0$  with  $E_0$  as given by Levine, and the second step was to correlate the intermediate phenomenological parameter  $E_0$ , with another phenomenological parameter  $E_T'$ . It has been observed, as shown in Chapter IV, that  $E_T'$  and  $E_0$  can be correlated provided  $E_T$  and the doping density of the substrate lie within a specified range. Thus, we note, that fluctuations which modify the  $nT$  versus  $T$  plots in the case of thermionic emission, so that apparently field emission seems to be the mechanism, may be due to fluctuations in  $E_T'$ . This provides at least one physical mechanism to explain the fluctuations in  $T_0$ .

The absence of the identification of a physical mechanism to explain the exponential energy distribution of surface states, and the identification of  $T_0$  effect in cases other than exponential surface states leads one to the question, whether Levine's model is only a mathematical representation of the actual conditions existing at the interface. A definite answer to this question would require an extensive study of the metal semiconductor interface and the formation of surface states. Accepting Heine-Pellegrini model to be the source of  $T_0$  effect, we would require the completion of the following studies to identify the cause of fluctuations in  $E_T'$  and hence  $T_0$ :

- (a) an experimental verification of the existence of  $T_0$  effect in Heine-Pellegrini model,
- (b) a theoretical evaluation or an independent experimental determination of  $E_T'$ , and
- (c) the modifications required in the Heine-Pellegrini model in the presence of a thin oxide layer between the metal and the semiconductor.

(iii) A method has been developed to determine the doping density of a semiconductor wafer using the dependence of  $T_0$  on the current at which it is measured. This method requires the measurement of only the forward I-V characteristics of a Schottky barrier diode, hence can be used

as a convenient method, if one does not want to use the conventional method of determination of doping profile from C-V measurements. The limitations of the method based on forward I-V characteristics are given in Chapter 5.

This brings us to the end of the present work, which was mainly concerned with the understanding of the mechanism of current transport in nonhomogeneous, rectifying metal-semiconductor junctions showing temperature dependent ideality factor.

## REFERENCES

1. F. Braun, Ann. Physik Chem., No. 1, 153, p. 556, 1974.
2. E. H. Rhoderick, 'Metal-Semiconductor Contacts', Clarendon Press, Oxford, 1978.
3. W. Schottky, R. Störmer and F. Warbel, Z. Hochfrequenztechnik, Vol. 37, p. 162, 1931.
4. A. H. Wilson, Proc. Roy. Soc. A, Vol. 136, p 487, 1932.
5. B. Davydov, J. Phys. U.S.S.R., Vol. 4, p 335, 1939.
6. F. A. Padovani and R. Stratton, Solid State Electron., Vol. 9, p 695, 1966.
7. C. R. Crowell and V. L. Rideout, Solidstate Electron., vol. 12, p 89, 1969.
8. E. Burstein and S. Lundquist, 'Tunneling Phenomenon in Solids', Plenum, New York, 1969.
9. C. B. Duke, 'Tunneling in Solids', Solid State Physics Supplement 10, Academic Press, New York and London, 1969.
10. W. Schottky, Naturwiss., Vol. 26, p 843, 1938.
11. N. F. Mott, Proc. Camb. Phil. Soc., Vol. 34, p 568, 1938.
12. H. A. Bethe, M.I.T. Radiation Laboratory, Report 43-12, 1943.
13. C. R. Crowell and S. M. Sze, Solid State Electron., Vol. 9, p 1035, 1966.
14. A. N. Saxena, Surface Science, Vol. 13, p 151, 1969.
15. W. E. Mayerhoff, Phys. Rev., Vol. 71, p 727, 1947.
16. J. Bardeen, Phys. Rev., Vol. 17, p 717, 1947.
17. A. M. Cowley and S. M. Sze, J. Appl. Phys., Vol. 36, p 3212, 1965.
18. H. C. Card and E. H. Rhoderick, J. Phys. D: Appl. Phys., Vol. 4, p 1589, 1971;  
H. C. Card and E. H. Rhoderick, J. Phys. D: Appl. Phys., Vol. 4, p 1602, 1971.

19. J. D. Levine, J. App. Phys., Vol. 42, p 3991, 1971.
20. C. A. Mead and W. G. Spitzer, Phys. Rev., Vol. 134, p A713, 1964.
21. J. O. McCaldin, T. C. McGill and C. A. Mead, Phys. Rev. Lett., Vol. 36, p 56, 1976.  
J. O. McCaldin, T. C. McGill and C. A. Mead, J. Vac. Sci. Technol., Vol. 13, p 802, 1976.
22. V. Heine, Phys. Rev., Vol. 138, p A1689, 1965.
23. G. H. Parker, T. C. McGill, C. A. Mead and D. Hoffman, Solid State Electron., Vol. 11, p 201, 1968.
24. B. Pellegrini, Phys. Rev., Vol. 7B, p 5299, 1973.  
B. Pellegrini, Solid State Electron., Vol. 17, p 217, 1974.
25. J. C. Inkson, J. Phy. C: Solid State, Vol. 6, p 1359, 1973.
26. S. M. Vernon and W. A. Anderson, Appl. Phys. Lett., Vol. 26, p 707, 1975.
27. C. R. Crowell, Solid State Electron., Vol. 20, p 171, 1977.
28. F. A. Padovani and G. G. Summer, J. Appl. Phys., Vol. 36, p 3744, 1965.
29. C. R. Crowell and M. Beguwala, Solid State Electron., Vol. 14, p 1149, 1971.
30. E. H. Rhoderick, J. Phys. D: Appl. Phys., Vol. 5, p 1920, 1972.
31. S. M. Sze, 'Physics of Semiconductor Devices', Wiley Interscience, New York, 1979.
32. F. A. Padovani, 'Semiconductors and Semimetals', Vol. 7, Part A, Eds. R. K. Willardson and A. C. Beer, Academic Press, New York, 1971.
33. F. J. Hovel, 'Solar Cells, Semiconductor and Semi-metals', Vol. 11, Eds. R. K. Willardson and A. C. Beer, Academic Press, New York, 1975.
34. D. Cooper, B. Bixby and L. Carver, Electron (U.S.A.), Vol. 49, p 85, 1976.
35. B. Bhaumik and R. Sharan, Appl. Phys. Lett., Vol. 29, p 257, 1976.
36. G. S. Visweswaran and R. Sharan, Proc. IEEE, Vol. 67, p 436, 1979.
37. E. C. Kemble, 'Fundamental Principles of Quantum Mechanics', Dover, New York, 1958 (p 575).

Chapter 2

1. H. C. Card and E. H. Rhoderick, J. Phys. D: Appl. Phys., Vol. 4, p 1539, 1971.
2. V. A. Johnson, R. N. Smith and H. J. Yearin, J. Appl. Phys., Vol 21, p 283, 1950.
3. A. M. Cowley and S. M. Sze, J. Appl. Phys., Vol. 36, p 3212, 1965.
4. H. C. Card, Appl. Phys. Lett., Vol. 29, p 52, 1976.
5. S. M. Sze, Physics of Semiconductor Devices, Wiley Interscience, New York, 1969.
6. L. Tessler and L. Eisenberg, Proc. IEEE, Vol. 60, p 737, 1972.
7. A. N. Saxena, Surface Science, Vol. 13, p 151, 1969.



Chapter 3

1. F. A. Padovani, 'Semiconductors and Semimetals', Vol. 7, Part A, Eds. R. K. Willardson and A. C. Beer, Academic Press, New York, 1975.
2. A. Y. C. Yu and E. H. Snow, IEEE Trans. Nucl. Sci. Vol. NS-16, p 220, 1969.
3. R. A. Zettler, and A. M. Cowley, IEEE Trans. Electron Devices, Vol. ED-16, p 58, 1969.
4. P. A. Tove, S. A. Hyder and G. Susila, Solid State Electron., Vol. 16, p 513, 1973.
5. A. Y. C. Yu and E. H. Snow, J. Appl. Phys., Vol. 39, 3008, 1968.
6. G. Kano, S. Fujiwara, M. Iizuka, H. Hasegawa and T. Sawaki, Appl. Phys. Lett., Vol. 15, p 138, 1969.
7. S. Kar, Solid State Electron., Vol. 18, p 169, 1975.
8. J. M. Borrego, R. J. Gutmann and S. Ashok, Solid State Electron., Vol. 20, p 125, 1977.
9. J. McKenna and E. Wasserstrom, B. S. T. J., Vol. 49, p 853, 1970.
10. J. D. Levine, J. Appl. Phys., Vol. 42, p 3991, 1971.
11. S. M. Sze, 'Physics of Semiconductor Devices', Wiley Interscience, New York, 1969.
12. H. C. Card and E. H. Rhoderick, J. Phys. D: Appl. Phys., Vol. 4, p 1589, 1971.

Chapter 4

1. J. D. Levine, J. Appl. Phys., Vol. 42, p 3991, 1971.
2. C. R. Crowell, Solid State Electron., Vol. 20, p 171, 1977.
3. E. H. Rhoderick, J. Appl. Phys., Vol. 46, p 2809, 1975.
4. V. Heine, Phys. Rev., Vol. 138, p A1689, 1965.
5. G. H. Parker, T. C. McGill, C. A. Mead and D. Hoffmann, Solid State Electron., Vol. 11, p 201, 1968.
6. B. Pellegrini, Solid State Electron., Vol. 17, p 217, 1974.
7. J. Bardeen, Phys. Rev., Vol. 17, p 717, 1947.
8. A. M. Cowley and S. M. Sze, J. Appl. Phys. Vol. 36, p 3212, 1965.
9. N. F. Mott, Proc. Camb. Phil. Soc., Vol. 34, p 568, 1938.
10. A. N. Saxena, Surface Science, Vol. 13, p 151, 1969.
11. S. M. Sze, 'Physics of Semiconductor Devices', Wiley Interscience, New York, 1969.
12. C. A. Mead, 'Tunneling Phenomena in Solids', Burstein and Lundquist, Eds., p. 128, Plenum Press, New York, 1969.
13. C. N. Krishnan, Ph.D. Thesis, I.I.T. Kanpur, 1977.

Chapter 5

1. J. Hilibrand and R. D. Gold, RCA Review, Vol. 21, p 245, 1969.
2. S. M. Sze, 'Physics of Semiconductor Devices', Wiley Interscience, New York, 1969.
3. J. D. Levin, J. Appl. Phys., Vol. 42, p 3991, 1971.
4. H. C. Card and E. H. Rhoderick, J. Phys. D: Appl. Phys., Vol. 4, p 1529, 1971.

# APPENDIX A

## EVALUATION OF $\phi_{BO}$ AND $n$ FOR AN MIS DIODE

In this appendix, expressions are derived for the zero bias barrier height  $\phi_{BO}$  and the ideality factor  $n$  for a metal-semiconductor contact with an interfacial oxide layer of thickness  $\delta$  and a constant energy distribution of surface states. Fig. (A.1) shows the energy band diagram for such a contact under (a) forward bias, (b) zero bias, and (c) reverse bias conditions.

The surface states are considered to be of two kinds, one controlled by the metal Fermi-level, where the surface state charge is given by,

$$Q_{ssa} = -q^2 D_{sa} \left( \frac{E_g}{q} - \phi_B - \phi_0 \right) \quad (A-1)$$

where  $D_{sa}$  = density of surface states controlled by metal-Fermi level in  $\text{cm}^{-2} \text{eV}^{-1}$ .

$q\phi_0$  = neutral level measured from the top of the valence band in eV.

$q\phi_B$  = barrier height in eV

and  $E_g$  = bandgap in eV.

and the other controlled by the semiconductor Fermi-level where the surface state charge is given by,

$$Q_{ssb} = -q^2 D_{sb} \left( \frac{E_g}{q} - \phi_B - \phi_0 + V \right) \quad (A-2)$$

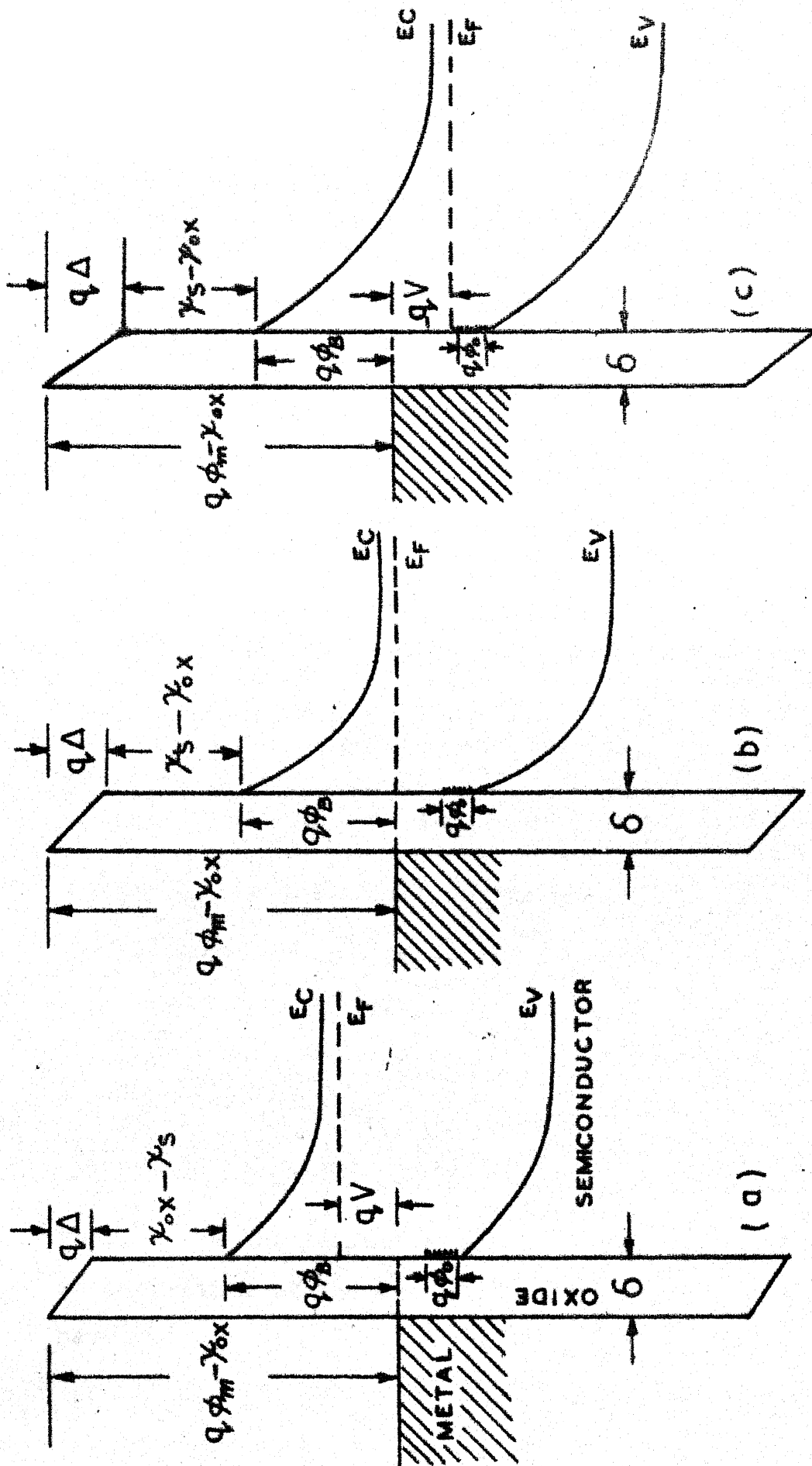


Fig.A.1 Energy band diagram of a Schottky barrier (MIS) contact under  
(a) Forward bias (b) Zero bias (c) Reverse bias.

where  $V$  is the applied bias with the proper sign. The total surface state charge is then given by,

$$Q_{ss} = Q_{ssa} + Q_{ssb} = -[q^2 D_{sa} \left( \frac{E_g}{q} - \phi_B - \phi_0 \right) + q^2 D_{sb} \left( \frac{E_g}{q} - \phi_B - \phi_0 + V \right)] \quad (A-3)$$

The space charge in the depletion layer of the semiconductor is given by,

$$Q_{sc} = \sqrt{2q\epsilon_s N_D (\phi_B - V - \phi_f - (kT/q))} \quad (A-4)$$

The total surface charge density on the semiconductor surface is given by the sum of eqn. (A-3) and (A-4) and for charge neutrality in the system we can write,

$$Q_m = -(Q_{ss} + Q_{sc}) \quad (A-5)$$

where  $Q_m$  is the charge on the metal.

Considering a potential drop  $\Delta$  across the interfacial layer, and the application of Gauss's law to the surface charge on the metal and semiconductor, the charge on the metal is obtained as,

$$Q_m = \frac{-\epsilon_i \Delta}{\delta} \quad (A-6)$$

where  $\epsilon_i$  is the permittivity of the interfacial layer. From an inspection of the energy band diagram of Fig. (A-1) we have,

$$q(\phi_m - \chi_{ox}) + q\Delta = q(\chi_s - \chi_{ox}) - q\phi_B$$

$$\text{i.e.} \quad \Delta = \phi_m - \chi_s - \phi_B \quad (\text{A-7})$$

Using eqns. (A-3), (A-4), (A-6) and (A-7) in eqn. (A-5), we obtain,

$$(\phi_m - \chi_s - \phi_B) = \sqrt{\frac{2q\epsilon_s N_d \delta^2}{\epsilon_i^2}} (\phi_B - V - \phi_f - \frac{kT}{q})$$

$$- [q^2 D_{sa} (\frac{E_g}{q} - \phi_B - \phi_0) + q^2 D_{sb} (\frac{E_g}{q} - \phi_B - \phi_0 + V)] \quad (\text{A-8})$$

The barrier height  $\phi_{B0}$  at zero bias can be obtained from eqn. (A-8) by putting  $V=0$  and solving for  $\phi_B$ . The solution for eqn. (A-8) with  $V=0$  is obtained as,

$$\phi_{B0} = [C_2 (\phi_m - \chi_s) + (1 - C_2) (\frac{E_g}{q} - \phi_0)]$$

$$+ \frac{C_2^2 C_1}{2} - C_2^{3/2} [C_1 (\phi_m - \chi_s) + (1 - C_2) (\frac{E_g}{q} - \phi_0)] \frac{C_1}{C_2}$$

$$- \frac{C_1}{C_2} (\phi_f + \frac{kT}{q}) + \frac{C_2 C_1^2}{4}]^{\frac{1}{2}} \quad (\text{A-9})$$

$$\text{where } C_1 = \frac{2q\epsilon_s N_d \delta^2}{\epsilon_i^2} ; \quad C_2 = \frac{\epsilon_i}{(\epsilon_i + q^2 \delta D_{ss})}$$

$$\text{and } D_{ss} = D_{sa} + D_{sb}.$$

Our interest now is to obtain the ideality factor  $n$ , which is given by the relation,

$$n = (1 - \frac{\partial \phi_B}{\partial V})^{-1} \quad (A-10)$$

Differentiating eqn. (A-8) with respect to V, we obtain,

$$- \frac{\partial \phi_B}{\partial V} = \frac{\delta}{\epsilon_i} \left[ \frac{\epsilon_s}{W} \left( \frac{\partial \phi_B}{\partial V} - 1 \right) + q^2 D_{sa} \frac{\partial \phi_B}{\partial V} + q^2 D_{sb} \left( \frac{\partial \phi_B}{\partial V} - 1 \right) \right] \quad (A-11)$$

$$\text{where } W = \text{depletion width} = \sqrt{\frac{2\epsilon_s}{qN_D} (\phi_B - V - \phi_f - \frac{kT}{q})}$$

Adding 1 to both sides of eqn. (A-11) we have,

$$(1 - \frac{\partial \phi_B}{\partial V}) = \frac{\delta}{\epsilon_i} \left( \frac{\partial \phi_B}{\partial V} - 1 \right) \left( \frac{\epsilon_s}{W} + q^2 D_{sa} + q^2 D_{sb} \right) + \frac{q^2 D_{sa} \delta}{\epsilon_i} + 1 \quad (A-12)$$

$$\therefore (1 - \frac{\partial \phi_B}{\partial V}) = \frac{1}{n}, \quad \text{eqn. (A-12) reduces to}$$

$$\frac{1}{n} = \frac{1 + q^2 D_{sa} \delta / \epsilon_i}{\left( \frac{\epsilon_s}{W} + q^2 D_{sa} + q^2 D_{sb} \right) \frac{\delta}{\epsilon_i} + 1}$$

$$\text{i.e. } n = 1 + \frac{(\epsilon_s/W + q^2 D_{sb}) \delta / \epsilon_i}{(1 + q^2 D_{sa} \delta / \epsilon_i)} \quad (A-13)$$

For  $\epsilon_s/W \ll q^2 D_{sb}$ , eqn. (A-13) reduces to

$$\begin{aligned} n &= 1 + \frac{q^2 D_{sb} \delta / \epsilon_i}{(1 + q^2 D_{sa} \delta / \epsilon_i)} \\ &= 1 + q^2 D'_{sb} \delta / \epsilon_i \end{aligned} \quad (A-14)$$

$$\text{where } D'_{sb} = \frac{D_{sb}}{(1 + q^2 D_{sa} \delta / \epsilon_i)}$$

Thus we see that eqn. (A-9) and (A-14) give us the relationship for  $\phi_{B0}$  and n in the presence of two kinds of surface states for an MIS diode.



# APPENDIX B

## AN ALGORITHM TO FIND THE SMALLEST ROOT OF A POLYNOMIAL

In this Appendix we present a method to evaluate the smallest root of a polynomial correct to two decimal places. The root finding algorithm is based upon the following theorem that was initially derived to yield an approximate root value in terms of all the coefficients of an arbitrary nth order polynomial (L. Tessler and L. Eisenberg, Proc. IEEE, Vol. 60, p 737, 1972).

Theorem: Given an nth order polynomial

$$P_N(x) = 1 + A_1x + A_2x^2 + \dots + A_Nx^N \quad (B-1)$$

the smallest magnitude root of (C-1) has an approximate value,

$$R = -1/(A_1 + U_1) \quad (B-2)$$

where

$$U_1 = \begin{vmatrix} -A_2 & 1 & 0 & 0 & \dots & 0 \\ -A_3 & A_1 & 1 & 0 & \dots & 0 \\ \vdots & \vdots & \vdots & \vdots & \vdots & \vdots \\ -A_N & A_{N-2} & \vdots & \vdots & \vdots & \vdots \end{vmatrix} W^{-1} \quad (B-3)$$

$$W = \begin{vmatrix} A_1 & 1 & 0 & 0 & \dots & 0 \\ A_2 & A_1 & 1 & 0 & \dots & 0 \\ \vdots & \vdots & \vdots & \vdots & \ddots & \vdots \\ \vdots & \vdots & \vdots & \vdots & \vdots & 0 \\ \vdots & \vdots & \vdots & \vdots & \vdots & 1 \\ A_{N-1} & A_{N-2} & \dots & \dots & \dots & A_1 \end{vmatrix} \quad (B-4)$$

Since the elements in eqns. (B-3) and (B-4) appear in a systematic manner, it is possible to construct an algorithm with very few arithmetic operations. Specifically if we define,

$$W_N = \begin{vmatrix} A_1 & 1 & \dots & \dots & \dots & 0 \\ A_2 & A_1 & 1 & \dots & \dots & 0 \\ \vdots & \vdots & \vdots & \ddots & \vdots & \vdots \\ \vdots & \vdots & \vdots & \vdots & \ddots & 0 \\ \vdots & \vdots & \vdots & \vdots & \vdots & 1 \\ A_N & A_{N-1} & \dots & \dots & \dots & A_1 \end{vmatrix} \quad (B-5)$$

and  $W_0 = 1$

then  $W_N$  can be calculated from the recursion relation,

$$W_N = \sum_{k=1}^N (-1)^{k-1} W_{N-k} A_k \quad (B-6)$$

Using eqns. (B-5), (B-3) and (B-4) in (B-2) one gets,

$$R = -1/(A_1 + U_1) = -\frac{W_{N-1}}{W_N} \quad (B-7)$$

In practice, we see that most of the polynomials are of the form

$$Q(x) = C_N x^N + C_{N-1} x^{N-1} + \dots + C_0, \quad C_0 \neq 1 \quad (\text{B-8})$$

For polynomials of this kind the determinant counterpart of  $W_N$  is

$$D_N = \begin{vmatrix} C_1 & C_0 & 0 & \dots & 0 \\ C_2 & C_1 & C_0 & \dots & 0 \\ \vdots & \vdots & \vdots & \ddots & \vdots \\ C_N & C_{N-1} & \dots & \dots & C_0 \end{vmatrix}$$

$$= C_0^N W_N$$

which reduces eqn. (B-6) to,

$$R = -\frac{W_{N-1}}{W_N} = -C_0 \frac{D_{N-1}}{D_N} \quad (\text{B-9})$$

It has been shown by L. Tessler and L. Eisenberg (Proc. IEEE, Vol. 60, p 737, 1972) that eqn. (B-9) gives the value of the smallest root correct to two decimals. Since we are not interested in very accurate values, we have chosen this algorithm to evaluate the root close to the origin in the cubic equation encountered in Chapter II.

### APPENDIX C

#### SOLUTION OF TWO DIMENSIONAL POISSON'S EQUATION FOR AN AUXILIARY SCHOTTKY BARRIER GUARD RING STRUCTURE

In this Appendix we give the details about the choice of the boundary and the boundary conditions for the solution of two dimensional Poisson's equation in a Schottky barrier diode with an auxiliary schottky barrier guard ring structure. The presentation is divided into two parts, viz. (a) the formulation of the problem and (b) the solution of the Poisson's equation.

(a) Formulation of the problem:

The Poisson's equation in two dimensions, considering the mobile carriers (majority carriers only) and the charge due to the ionised donors ( $N_D$ ) can be written as,

$$\frac{\partial^2 \Phi}{\partial X^2} + \frac{\partial^2 \Phi}{\partial Y^2} = - \frac{qN_D}{\epsilon_s} [1 - \exp(-q\Phi/kT)] \quad (C-1)$$

where  $\Phi$  is the potential at any point described by the co-ordinates  $X$  and  $Y$ . The next step now is to identify the boundary and the corresponding boundary conditions. From a perusal of Fig. (C.1), where we present a cross-sectional evaluation of a Schottky barrier diode, we see that the lines  $pp'$ ,  $pr$ ,  $ps$  get automatically chosen as the boundaries, whose  $pp'$  forms the line of symmetry, the line  $pr$  defines the



line of metal-semiconductor junction and  $ps$  defines the back contact. The fourth boundary is chosen as follows.

Let us consider the line  $qq'$  perpendicular to the junction and passing through the midpoint between the main and the auxiliary Schottky barrier diodes. It has been shown by McKenna and Wasserstrom (B.S.T.J., Vol. 49, p 853, 1970) that a metal strip of half width greater than thrice the depletion width ( $W$ ) under the metal can be considered to be semiinfinite for potential calculations. Based on this,  $qq'$  has been considered to be the fourth boundary (as a line of symmetry) assuming the radius of the main diode and the half width of the guard ring to be greater than  $3W$ . Thus, we note that the region for the solution of the Poisson's equation is  $pqq'p'$  in Fig. (C.1), and the boundary conditions can be written as follows (see Fig. C.1)

(i) Along  $pq$  ( $X=0$ )

$$\Phi(0, Y) = (\phi_B - V - \phi_f) = \phi_0 \quad 0 \leq Y \leq r \quad (\text{at the metal}) \quad (C.2a)$$

and using the criterion of continuity of potential and the normal component of the displacement vector

$$\begin{aligned} \eta \frac{\partial \Phi(0^+, Y)}{\partial X} &= \frac{\partial \Phi(0^-, Y)}{\partial X} \\ \Phi(0^+, Y) &= \Phi(0^-, Y) \end{aligned} \quad r < Y \leq (r+d/2) \quad (C.2b)$$

(ii) Along qq' (from symmetry condition)

$$\frac{\partial \Phi(X, r+d/2)}{\partial Y} = 0 \quad (C-3)$$

(iii) Along q'p' (back contact)

$$\Phi(t, Y) = 0 \quad (C-4)$$

(iv) Along pp' (symmetry condition)

$$\frac{\partial \Phi(X, 0)}{\partial Y} = 0 \quad (C-5)$$

For the above mentioned mixed boundary condition, the two dimensional nonlinear Poisson's equation given in (C-1) does not have an analytical solution and hence Numerical methods were resorted to for the solution of eqn. (C-1).

(b) Solution of the Poisson's equation:

For easier handling, let us first normalize the distances with respect to the depletion width  $W$ , the potential with respect to the band bending  $(\phi_B - V - \phi_f)$ , and the charge with respect to  $qN_D$ ,

$$\text{where } W = 2\lambda_D \sqrt{|\phi_s|}$$

$$\phi_s = \phi_0 / (kT/q) \quad (C-6)$$

and  $\lambda_D$  = Debye length.

Carrying out the normalization mentioned above eqn. (C-1) reduces to,

$$\frac{\partial^2 \phi}{\partial x^2} + \frac{\partial^2 \phi}{\partial y^2} = 2[1 - \exp(-|\phi_s| \phi)] = \bar{p} \quad (C-7)$$

The eqn. (C-7) is now numerically solved by replacing the differential equation by a five point difference equation and solving the resulting equation by the Newton-Gauss implicit scheme with a step size of  $h = 0.05$  and the relaxation factor  $w = 1.73$ . The differential equation then reduces to,

$$\begin{aligned} \phi_{ij} - \frac{1}{4} (\phi_{i+1,j} + \phi_{i-1,j} + \phi_{i,j+1} + \phi_{i,j-1}) \\ = -\frac{h^2}{2} [1 - \exp(-|\phi_s| \cdot \phi_{ij})] \end{aligned} \quad (C-8)$$

leading to an iterative relation,

$$\begin{aligned} \phi_{ij}^{(n+1)} - \frac{h^2}{2} \exp(-|\phi_s| \phi_{ij}^{(n+1)}) \\ = \frac{1}{4} [\phi_{i+1,j}^{(n)} + \phi_{i-1,j}^{(n+1)} + \phi_{i,j+1}^{(n)} + \phi_{i,j-1}^{(n+1)} - 2h^2] \end{aligned} \quad (C-9)$$

Let us now look into the boundary conditions and hence the iterative relation at the boundaries. Fig. (D.2) represents the given structure divided into mesh of dimension  $MXN$  with the mesh size equal to  $h$ .

(i) Since the two dimensional nature of the potential profile is restricted to within three times the depletion width from the edge of the metal (B.S.T.J., Vol. 49, p 853, 1970), beyond the line P'P we have,



$$\frac{\partial \phi}{\partial x} = 0 \quad (C-10)$$

Based on this observation we shift the boundary at pp' to PP' to reduce the number of mesh points. The iterative relation along the line PP' (i=0) can then be written as,

$$\phi(0, j) = \phi(2, j) \quad 1 \leq j \leq N \quad (C-11)$$

(2) Along the line qq' (i=M) we can write

$$\phi(M+1, j) = \phi(M-1, j) \quad 1 \leq j \leq N \quad (C-12)$$

(3) Along the line Pt, where the front metal is, we have,

$$\phi(i, 1) = 1.0 \quad 1 \leq i \leq M \quad (C-13)$$

The boundary condition along the line tq (see Fig. C.1) is in a little unwieldy form to be applied for the numerical calculations, for it would need a very small mesh size near the boundary and hence would lead to an unnecessarily large number of mesh points. To get over this one replaces the boundary condition (C-2b) by its equivalent integral form,

$$\int_G \epsilon \frac{\partial \phi}{\partial n^*} dl = \int_G \rho dx dy \quad (C-14)$$

where G is the path chosen by connecting the midpoints of the surrounding mesh (see Fig. C.2). This reduces numerically to,

$$\begin{aligned} \phi(i, 2) + \eta \phi(i, 2) + \left(\frac{1+\eta}{2}\right) (\phi(i+1, 1) + \phi(i-1, 1)) - 2(1+\eta) \phi(i, 1) \\ = h^2 [1 - \exp(-|\phi_p| \phi(i, 1))] \end{aligned} \quad (C-15)$$

Using this in the iterative relation we obtain

$$\begin{aligned}\phi_{i,1}^{(n+1)} &= h^2 \exp(-|\phi_s| \phi_{i,1}^{(n+1)}) / 2(1+\eta) \\ &= \frac{1}{4} [\phi_{i-1,1}^{(n+1)} + \phi_{i+1,1}^{(n)} + \phi_{i,2}^{(n)}] - \frac{1}{2(1+\eta)} \cdot h^2\end{aligned}\quad (C-16)$$

(4) The fourth boundary at the back contact is shifted to a distance of 3 times the depletion width from the metal-semiconductor junction. This has been done to reduce the number of mesh points. The boundary condition used is

$$\phi_{i,N} = \phi_{i,N+1} \quad 1 \leq i \leq M \quad (C-17)$$

and  $j=N$  represents the boundary.

With the boundary conditions outlined above, the Poisson's equation is solved using the scheme,

$$\phi_{i,j}^{(n+1)} = \phi_{i,j}^{(n)} - \frac{wF}{\Delta F} \quad (C-18)$$

$$\begin{aligned}\text{where } F &= \phi_{i+1,j}^{(n)} + \phi_{i,j+1}^{(n)} + \phi_{i-1,j}^{(n-1)} + \phi_{i,j-1}^{(n+1)} - 4\phi_{i,j}^{(n)} \\ &\quad - 2h^2[1 - \exp(-\phi_{i,j}^{(n)}|\phi_s|)]\end{aligned}\quad (C-19)$$

$$\Delta F = \frac{\partial F}{\partial \phi_{i,j}^{(n)}} = -[2h^2|\phi_s|\{\exp - \phi_{i,j}^{(n)}|\phi_s|\}] \quad (C-20)$$

$$w = \text{Relaxation factor} = 1.75.$$

and the convergence criterion,

$$\delta_{i,j} = \max [\phi_{i,j}^{(n+1)} - \phi_{i,j}^{(n)}] < 10^{-4} \quad (C-21)$$

$$\text{or } \bar{\delta}_{ij} = \sqrt{(\phi_{i,j}^{(n+1)} - \phi_{i,j}^{(n)})^2 / (MN + M + N)} < 10^{-5} \quad (C-22)$$

The mesh size chosen for our work was  $M = 101$ ,  $M1 = 61$   
and  $N=61$ .

# APPENDIX D

## EVALUATION OF THE POTENTIAL PROFILE IN THE HEINE-PELLEGRINI MODEL

In this Appendix, we present the method for evaluating the potential at the metal-semiconductor interface and hence the complete potential profile in the Heine-Pellegrini model. As seen in Chapter IV the Poisson's equation in a Schottky barrier diode can be written as,

$$\frac{d^2 V}{dx^2} = - \frac{q}{\epsilon_s} [N_V \exp(-x/\lambda_v) + N_c \exp(-x/\lambda_c) - N_D] \quad (D-1)$$

In (D-1) the densities of metal electron  $N_B$  tunneling close to the band B of the semiconductor and  $\lambda_B$  the corresponding penetration depth are given by (here  $B=c$  for conduction band  $B=v$  for valence band),

$$N_B = \frac{3N_M E_{osB}^{\frac{1}{2}} E_T' \mu_{xB} \mu_{TB}}{2E_M^{3/2}} \ln \left( \frac{1+A_{B2}}{1+A_{B1}} \right) \quad (D-2)$$

$$\lambda_B = \frac{\hbar \left\{ \arcsin \left( \frac{A_{B2}}{A_{B2}+1} \right) - \arcsin \left[ \frac{(1+1/A_{B2}) A_{B1}-1}{A_{B1}+1} \right] \right\}}{2[m_{xB} \mu_{xB} E_{osB} (1+\frac{1}{2}A_{B2})]^{\frac{1}{2}} \ln(1/A_{B2})/(1+A_{B1})]} \quad (D-3)$$

$$A_{C1} = (q(\phi_m - \chi_s - V_o) + E_T'/2)(\mu_{xc} E_{osc})$$

$$A_{C2} = \left( \frac{m_{xsv}}{m_{xsv} - m_{xsc}} + \frac{E_T'}{2} \right) / (\mu_{xc} E_{osc}) \quad (D-4)$$

in the conduction band and,

$$\begin{aligned}
 A_{v1} &= 0.0 \\
 A_{v2} &= \left( \frac{m_{xsc} E_g}{(m_{xsc} - m_{xsv})} + \frac{E_T'}{2} \right) / (|\mu_{xv}| E_{osv}) \quad (D-5)
 \end{aligned}$$

In equations (D-2) to (D-5) the symbols have the following meaning:  $h = 2\pi\hbar$  is the Plank constant,  $m_{DHB}$  is the electron effective mass in the band B of the material H ( $H \equiv m$  and  $H \equiv s$  in the metal and the semiconductor respectively) in the direction D (in obtaining (D-2) and (D-3) it is assumed that the constant energy surfaces are ellipsoids with the revolution diameter coinciding the x axis so that  $D \equiv X$  represents x direction and  $D \equiv T$  indicates a direction perpendicular to the x direction),  $\mu_{DB} = m_{DsB}/m_{Dmc}$ ,  $E_M$  is the metal Fermi-level evaluated from the bottom of the metal conduction band,  $\phi_m$  is the metal workfunction,  $\chi_s$  is the semiconductor electron affinity,  $E_g$  is the amplitude of the semiconductor forbidden energy gap,  $E_{osc} = E_c = E_m + q(\phi_m - \chi_s)$  and  $E_{osv} = E_v + E_c - E_g$ , are the electron energies at edges of the forbidden gap,  $v_0$  is the potential at the metal-semiconductor interface and  $E_T'$  is the limit value of the electron energy perpendicular to the x axis beyond which the quantum penetration into the forbidden energy bandgap of the semiconductor is negligible (B. Pellegrini, Solid State Electron., Vol. 17, p 217, 1974).

A closed form solution for eqn. (D-1) has been obtained by assuming that there exists a length  $w$  of a section of the

depletion region characterised by the inequalities,

$$v_c - V - v(w) \gg kT/q \quad (D-6)$$

$$\text{and } W \gg w \gg \lambda_c, \lambda_v$$

where  $v_c = (\phi_m - \chi_s) - \phi_f$  is the contact potential difference

$V$  = applied bias

$v(w)$  = the potential at a distance  $w$  from the metal-semiconductor interface

and  $W$  = depletion width.

Under this assumption the field  $\mathcal{E}(x)$ , and the potential  $v(x)$  at any point within the semiconductor, at a distance  $x$  from the metal-semiconductor interface can be written as,

$$\mathcal{E}(x) = -\frac{q}{\epsilon} [N_c \lambda_c \exp(-x/\lambda_c) + N_v \lambda_v \exp(-x/\lambda_v) - N_D(W-x)] \quad (D-7)$$

$$v(x) = v_o - \frac{qN_D x}{\epsilon_s} \left(W - \frac{x}{2}\right) + \frac{q}{\epsilon_s} [1 - \exp(-x/\lambda_c)] N_c \lambda_c^2 + \frac{q}{\epsilon_s} [1 - \exp(-x/\lambda_v)] N_v \lambda_v^2 \quad (D-8)$$

$$\text{where } W = \sqrt{\frac{2\epsilon_s}{qN_D} (v_b - V)}$$

$$v_b = (v_o + v_q - v_e)$$

$v_q$  = the contribution of the surface state charges to the built in potential

$$= \frac{q}{\epsilon_s} [N_c \lambda_c^2 + N_v \lambda_v^2] \quad (D-9)$$

$$\begin{aligned}
 v_e &= \text{the contribution of the electron tunneling from} \\
 &\quad \text{the conduction band into the forbidden bandgap} \\
 &= \frac{kT}{q}
 \end{aligned}$$

Our interest now is to obtain the value of  $v_0$  and hence the potential profile, and is done as given below.

Invoking the condition of continuity of electric flux at the interface, we have,

$$\epsilon_m \mathcal{E}(0^-) = \epsilon_s \mathcal{E}(0^+) \quad (\text{D-10})$$

where  $\mathcal{E}(0^-)$  is the field in the metal for  $x=0^-$  and  $\mathcal{E}(0^+)$  is the field in the semiconductor for  $x=0^+$ . If one neglects the positive charge induced by the band bending, the field  $\mathcal{E}(0^-)$  in the metal can be written as,

$$\mathcal{E}(0^-) = + \frac{v_0}{\lambda_{TF}} \quad (\text{D-11})$$

Using (D-11) in (D-10), we obtain the relation,

$$\frac{+\epsilon_m v_0}{\lambda_{TF}} = q [N_c \lambda_c + N_v \lambda_v - N_D W] \quad (\text{D-12})$$

It has been shown by Pellegrini (J. Phys. D: Appl. Phys., Vol. 19, p 55, 1976) that in most of the metal-semiconductor systems,  $N_c \approx 0$ , this reduces eqn. (D-12) to,

$$\frac{\epsilon_m v_0}{\lambda_{TF}} = (q N_v \lambda_v - q N_D W) \quad (\text{D-13})$$

Since  $W$  is a function of  $v_0$ , eqn. (D-13) is a transcendental equation and has been solved numerically by using iterative methods.

After having evaluated  $v_0$ , our next step has been to evaluate the potential profile and hence the barrier height  $\phi_B$ . In the cases considered by us we have  $\mathcal{E}(0^+) > 0$ , thus leading to a maxima in the  $v(x)$  profile. The maximum value of  $v(x) = v_m$  occurs at a distance  $x_m$  from the metal-semiconductor interface. The barrier height  $\phi_B$  is then given by,

$$\phi_B = (\phi_m - \chi_s) + v_m \quad (D-14)$$

The expression for  $x_m$  and hence  $v_m$  can be obtained as follows, At  $x = x_m$ , we have  $\mathcal{E}(x) = 0$ , hence from eqn. (D-7) for  $N_c = 0$  we have,

$$\mathcal{E}(x_m) = \frac{q}{\epsilon_s} [N_v \lambda_v \exp(-x_m/\lambda_v) - N_D(W - x_m)] = 0 \quad (D-15)$$

$$\text{i.e. } \frac{N_v \lambda_v}{N_D W} \exp(-x_m/\lambda_v) = (1 - x_m/W) \quad (D-16)$$

Taking natural logarithm on both sides series expanding  $\ln(1 - x_m/W)$  for  $x_m/W \ll 1$  we have,

$$\ln(N_v \lambda_v / N_D W) = -\frac{x_m}{W} + \frac{x_m}{\lambda_v}$$

$$\text{i.e. } x_m = \frac{\lambda_v W}{(\lambda_v - W)} \ln(N_v \lambda_v / N_D W) \quad (D-17)$$



Using eqn. (D-17) in eqn. (D-8) the potential  $v_m$  at  $x = x_m$  and hence the barrier height can be obtained.

In our calculations we have considered  $E_m$ , the metal Fermi level evaluated from the bottom of the metal conduction band, and  $N_m$ , the density of electrons in the metal conduction band, to be temperature independent. The temperature dependence of  $\phi_m$ , the metal workfunction,  $\chi_s$ , the electron affinity of the semiconductor and  $E_g$ , the bandgap of the semiconductor are given in Chapter II.

# APPENDIX E

## RESISTIVITY MEASUREMENT BY FOUR POINT PROBE AND VAN DER PAUW METHOD

In this Appendix we present the four point probe and the Van der Pauw methods to determine the resistivity of a semiconductor wafer.

### (a) Four point probe method:

A schematic of the dc circuit used with a four point probe is shown in Fig. (E.1).

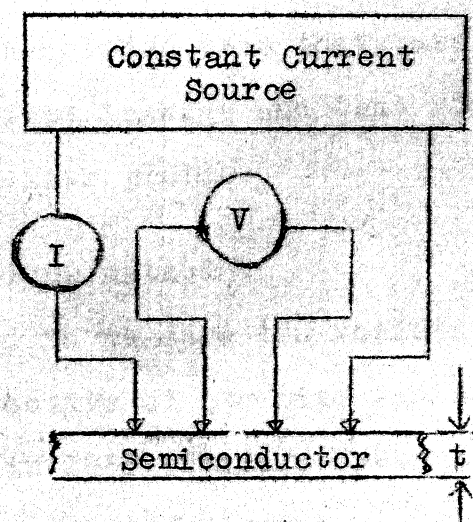


Fig. E.1. Schematic showing the dc circuit used with a four-point probe method.

The usual geometry is to place the probes in a line at equidistance from each other. Current ( $I$ ) is passed through the outer two probes and the potential ( $V$ ) is measured.

For a probe resting on a semiconductor with the nearest edge at a distance more than  $4s$  from any probe to the nearest edge, the resistivity is given by,

$$\rho = 2\pi s \cdot \frac{V}{I} \cdot F(t/s) \quad (E-1)$$

In eqn. (E-1)  $s$  represents the probe spacing and  $t$  the thickness of the sample, and  $F$  is a correction factor which depends on the  $(t/s)$  ratio. Normally the probe spacing is chosen to be about .16 cm, so that  $2\pi s = 1$ , and for a thickness  $t > 3s$ , eqn. (E-1) reduces to

$$\rho = \frac{V}{I} \text{ ohm-cm.} \quad (E-2)$$

It should be mentioned here that care must be taken to eliminate surface leakage and that good ohmic contact is made with all four probes.

(b) Van der Pauw method :

A method to measure the resistivity of a semiconductor wafer, irrespective of its size and shape was proposed by Van der Pauw in 1958 (Philips Research Report, Vol. 13, No. 1, p 1, 1958) and is as follows.

Fig. E.2 shows a sample of arbitrary shape used with the Van der Pauw method. The sample has four small contacts at the circumference of the sample. The resistivity  $\rho$  of the sample is given by,

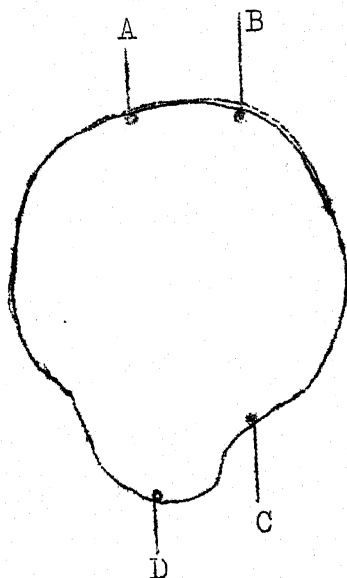


Fig. E.2. A sample of arbitrary shape used with the Van der Pauw method.

$$\rho = \frac{\pi d}{\ln 2} \cdot \frac{R_{AB,CD} + R_{BC,DA}}{2} \cdot f\left(\frac{R_{AB,CD}}{R_{BC,DA}}\right) \quad (E-3)$$

where  $f\left(\frac{R_{AB,CD}}{R_{BC,DA}}\right)$  is Van der Pauw's function. In Eqn. (E-3),  $R_{AB,CD}$  and  $R_{BC,DA}$  are given by,

$$R_{AB,CD} = \frac{V_{CD}}{I_{AB}} \quad (E-4a)$$

$$R_{BC,DA} = \frac{V_{DA}}{I_{BC}} \quad (E-4b)$$

In eqn. (E-4a)  $V_{CD}$  represents the voltage across the contacts C and D for a current  $I_{AB}$  through the contacts A and B. In eqn. (E-4b)  $V_{DA}$  represents the voltage across the contacts D and A for a current  $I_{BC}$  through the contacts B and C.

If the contacts are placed so that they are symmetrical about a line through any pair of nonadjacent contacts,

$R_{AB,CD}/R_{BC,DA} = 1$  and Van der Pauw's function also becomes

equal to 1. It should be noted that the sample for this method should be of uniform thickness.

Before concluding, we would like to mention that the methods mentioned in this Appendix are not applicable to  $n/n^+$  or  $p/p^+$  epitaxial wafers, since in these measurements the epitaxial layer gets shorted out by the heavily doped substrate.